DEUTSCHES ELEKTRONEN-SYNCHROTRON

DESY 93-001
January 1993

e^+e^- Linear Colliders: Physics Prospects

P. M. Zerwas

Deutsches Elektronen-Synchrotron DESY, Hamburg

ISSN 0418-9833

NOTKESTRASSE 85 · D-2000 HAMBURG 52

To be sure that your preprints are promptly included in the
HIGH ENERGY PHYSICS INDEX,
send them to (if possible by air mail):

DESY Bibliothek Notkestraße 85 W-2000 Hamburg 52 Germany	DESY-IfH Bibliothek Platanenallee 6 O-1615 Zeuthen Germany

ISSN 0418-9833

DESY 93-001
January 1993

e^+e^- Linear Colliders: Physics Prospects*

P.M. Zerwas
Deutsches Elektronen–Synchrotron DESY
D–2000 Hamburg 52, FRG

Abstract

This report describes the physics potential of e^+e^- linear colliders, expected in a first phase to operate in the energy range between 300 and 500 GeV. These machines will allow us to perform precision studies of the heavy particles in the Standard Model, the top quark and the electroweak bosons. They are ideal facilities for exploring the properties of Higgs particles in the intermediate mass range. New vector bosons and novel matter particles can be searched for and studied in detail. The machines provide unique opportunities for the investigation of supersymmetric extensions of the Standard Model, the SUSY Higgs spectrum and the supersymmetric partners of electroweak gauge/Higgs bosons and non-colored matter particles.

*Talk at LC92, Workshop on e^+e^- Linear Colliders, Garmisch-Partenkirchen (FRG), 1992.

1. Introduction and Synopsis

1.1 The Physical Basis

The e^+e^- colliders which have operated over the past two decades, have been outstandingly successful in searching for the fundamental constituents of matter, and in exploring their interactions. The charm quark and the τ lepton were established at SPEAR, completing the second family and opening up the third. The gluons were identified as the force quanta of the strong interactions at PETRA. Besides the discovery of these new particles, the copious production of quarks and leptons, including the b quarks, in a clean experimental environment has allowed precise studies of their electroweak properties. Likewise the properties of gluons and their basic interactions have been investigated in great detail. Crowning an exciting experimental evolution over many years, the present high–precision analysis of the Z boson and its decay modes at LEP has laid a solid base for both the electroweak as well as the strong sector of the Standard Model.

However, even within the Standard Model ($\mathcal{SM}$), a variety of fundamental problems remain to be solved.
(i) Symmetry arguments strongly support the existence of the top quark. By evaluating the radiative corrections to electroweak observables measured with very high precision at LEP and elsewhere, the top quark mass has been constrained to about 140 GeV. The t quark may be detected in $p\bar{p}$ collisions at the Tevatron soon. The high mass of this particle renders a thorough analysis of its electroweak properties mandatory. Since the mass is already close to the Fermi scale, the particle might hold important clues to the mechanism of the electroweak symmetry breaking.
(ii) The triple and quartic couplings of the electroweak gauge bosons, prescribed by the non–abelian gauge symmetry, and the related static properties of the W bosons (their electroweak charges, magnetic dipole and electric quadrupole moments), can be measured at existing machines only with large errors. The precision must be improved by one to two orders of magnitude to shed light on the nature of these fundamental particles and their interactions.
(iii) The Higgs particle is certainly the most mysterious particle in the Standard Model. Associated with the generation of masses for the fundamental particles, it is essential that no way of escape be left for this particle. If discovered, its properties must be determined. Besides the spin–parity assignments, the essential nature of the Higgs particle must be established by demonstrating that couplings to other particles grow with their masses.

Even though present experimental data support the Standard Model to unprecedented levels of accuracy, extensions can nevertheless be anticipated theoretically. Two directions are particularly important.
(i) The $\mathcal{SM}$ group $SU(3) \times SU(2) \times U(1)$ is expected to be embedded in a unifying group G at high energy scales. If this group is $SO(10)$, another set of gauge bosons $W_R^\pm$, Z_R with masses not much higher than the Fermi scale may exist, associated with the left–right symmetric subgroup $SU(2)_L \times SU(2)_R$. In addition, a right–handed neutrino is predicted, the mass of which could well be in the range of $\mathcal{O}(100$ GeV). Inspired by

superstring theories, the exceptional group $E(6)$ is another possible unification group of great interest. While just one additional neutral gauge boson Z' is expected at low energies in this scenario, the chiral $15plet$ of $\mathcal{SM}$ fermions is extended by a rich spectrum of vector–like leptons and quarks in each family.
(ii) A very attractive extension of the Standard Model is provided by supersymmetry ($\mathcal{SUSY}$). This symmetry stabilizes moderate masses of Higgs particles in the context of very high energy scales demanded by grand unified theories. Supersymmetry may even build up the physical basis for the Higgs phenomenon itself. Many new particles are predicted in this type of theory, in the Higgs sector a spectrum of several neutral and charged Higgs bosons, the mass of the lightest Higgs boson being probably less than ~ 130 GeV. The scalar partners of the $\mathcal{SM}$ leptons could well have masses in the range ~ 200 GeV, while squarks are expected to be heavier. The lightest $\mathcal{SUSY}$ states are likely to be the fermionic non–colored gaugino/Higgsino states with masses in the 100 GeV range. Searching for these states which are endowed with unique characteristics, will continue to be one of the most important tasks in experimental physics.

While new high mass vector bosons and particles carrying color quantum numbers can be searched for in hadron colliders, e^+e^- colliders are in many ways unique in their ability to detect and explore non–colored particles such as novel leptons and non-colored supersymmetric particles, sleptons and gauginos/Higgsinos. In addition, e^+e^- colliders are ideal machines for the search for Higgs particles in the intermediate mass range and the exploration of their characteristic properties. If new neutral gauge bosons were within the reach of the collider, the machine would naturally develop into a factory for these particles.

1.2 Characteristics of the Colliders

To avoid prohibitive synchrotron radiation losses, e^+e^- colliders beyond LEPII must be linear machines, a type of accelerator that has been pioneered by the SLC. The machines will probably be realized in two phases. In the first phase the energy range above LEPII up to ~ 500 GeV will be covered, in the second phase an energy of about 1 to 2 TeV will be reached. The physics potential of e^+e^- linear colliders in the first phase between 300 and 500 GeV is complementary to that of the high–energy proton colliders, covering areas in an ideal manner, which are very difficult to explore in hadron colliders. In the second phase the energy of the machines becomes effectively equivalent to the proton colliders.

The cross sections of most of the reactions which will be investigated at e^+e^- linear colliders, are of the order of the μ–pair cross section $e^+e^- \to \mu^+\mu^-$, Fig.1. Given a luminosity $\mathcal{L} = 10^{33}$ cm^{-2} sec^{-1} and an effective year of running time taken as 10^7 sec, the accumulated luminosity $\int \mathcal{L} = 10$ fb^{-1} leads to the production of about 5,000 μ pairs at a c.m. energy of 500 GeV. Such an integrated luminosity proves sufficient to allow for thorough data analyses, including cuts on the event samples and allowing for acceptance losses in the detectors. To generate the same number of events at higher e^+e^- energies, the luminosity must be scaled up as the square of the energy.

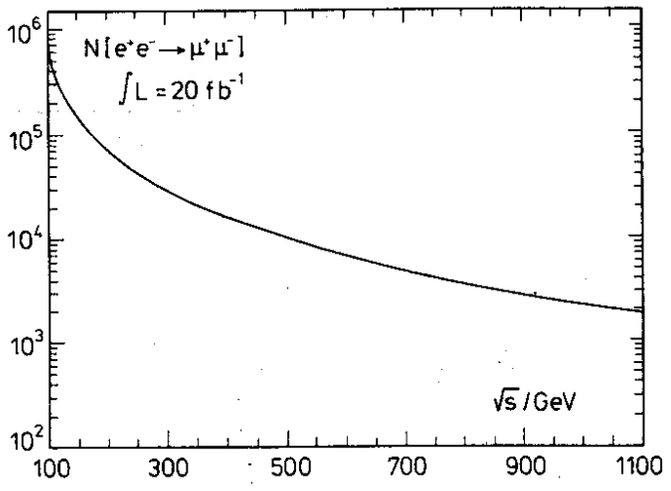

Fig. 1: *The μ–pair cross section $\sigma(e^+e^- \to \mu^+\mu^-)$ in the Standard Model, including γ and Z exchange contributions.*

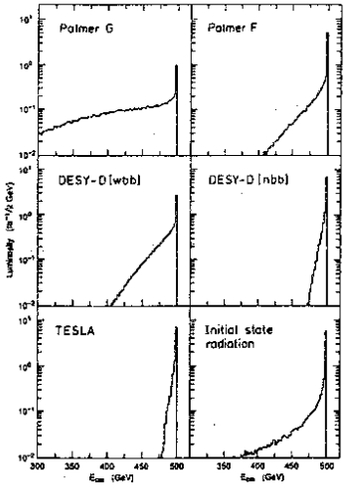

Fig. 2: *The smearing of e^+e^- luminosity spectra by beamstrahlung (a–d), compared with the smearing by initial–state photon radiation (f); from Ref.[3]*

The required high luminosity will be achieved by squeezing the electrons and positrons into bunches of extremely small transverse dimensions. Due to the large electromagnetic fields at these small distances, the trajectories of the electrons traversing the positron bunch – and vice versa – are bent so that the particles emit synchrotron light during the bunch collisions (beamstrahlung). As a result, a fraction of the electron and positron energy is lost and the initially sharp e^+e^- c.m. energy is smeared out. However, in narrow–band beam designs, Table 1, these effects can be reduced to a level of a percent and less, see Fig.2. The colliding beamstrahl photons produce background e^+e^- pairs, concentrated to cones of half–aperture $\sim 10^\circ$ about the beam pipe. The colliding photons will also produce hadrons, but at a level in narrow–band–beam designs that is of the same order as the rate induced by the ordinary γ bremsstrahlung. Only a very small fraction of e^+e^- annihilation events need eventually be discarded due to contamination by underlying $\gamma\gamma$ events.

	DLC	NLC	JLC	VLEPP	TESLA	CLIC
c.m. Energy [GeV]	500	500	500	500	500	500
Gradient [MV/m]	17	38	28	96	25	73/78
Active Length [km]	30	14	17	6.4	20	6.6
RF Frequency [GHz]	3	11.4	11.4	14	1.3	30
N/Bunch [10^{10}]	2.1	0.65	0.7	20	5.1	0.6
σ_x^*/σ_y^* [nm]	400/33	300/3	300/3	2000/4	640/100	90/8
σ_z [μm]	500	100	80	750	1000	170
Number of Bunches per Pulse	172	90	90	1	800	1/4
Repetition Rate [Hz]	50	180	150	300	10	1700
Luminosity [10^{33}cm^{-2}s^{-1}]	2.4	5.7	3.5	12	2.6	0.7/2.7
Υ	0.06	0.1	0.11	0.06	0.07	0.15
Bunch Separation [ns]	10.7	1.4	1.4		1000	0.33

Table 1: *Parameter list of design studies for 500 GeV e^+e^- linear colliders, presented at LC92; excerpt from a compilation in Ref. [4].*

By illuminating the incoming electron and positron bunches by laser light, hard Compton back–scattering of the laser photons off the electrons and positrons can be exploited to transform e^+e^- colliders into $e\gamma$ or $\gamma\gamma$ colliders. With the overall luminosity in size comparable to the original e^+e^- luminosity, the $e\gamma$ spectrum is strongly peaked at about 90% of the total e^+e^- energy. The distribution of the $\gamma\gamma$ invariant energies is broader, yet by using polarized beams it can be strongly enhanced near the maximum of 80% of the total e^+e^- energy. There is a broad spectrum of physics problems which can be addressed in $e\gamma$ and $\gamma\gamma$ colliders. Prominent examples are the measurement of the Higgs coupling to two photons, precision studies of the electromagnetic dipole and quadrupole moments of the W bosons, quartic gauge boson couplings, and the production of selectrons with masses beyond the $e^\pm$ beam energies.

1.3 Elements of the Physics Program

The main features of the physics program that can be studied at e^+e^- linear colliders, will be summarized in the following topics. In general we shall assume a c.m. energy of 300 to 500 GeV with an integrated luminosity of about $\int \mathcal{L} = 10$ fb^{-1} per year. Occasionally we will comment on areas that can be studied when the energy is raised to 1 to 2 TeV. Most of the material presented in this report, was elaborated in the Munich–Annecy–Hamburg 1990/91 Workshop [1], thoroughly compared with the results of other working groups at the Saariselkä Conference [2].

(a) Top and QCD

The mass of the top quark is apparently greater than that of the electroweak gauge bosons. Understanding the role of this particle in Nature is therefore an important goal for the future. A scan of the $t\bar{t}$ threshold region will allow the measurement of the top quark mass to better than 500 MeV. This is made possible by the steep rise of the cross section at the threshold, which is a remnant of the 1S ($t\bar{t}$) resonance smeared out by the rapidly increasing top quark width. Since the $t\bar{t}$ production process is restricted to distances of order 10^{-2} fm, the $t\bar{t}$ excitation curve can theoretically be predicted by perturbative QCD. The measurement of the top quark mass with high accuracy is a particularly desirable goal since we expect future theories of flavor dynamics to predict relations among the fermion masses in which the heavy top quark will play a key role. When combining all available measurements sensitive to electroweak parameters after LEP operations will be completed, the Higgs mass can be constrained with an accuracy of order 30%. Confronted with direct Higgs mass measurements, a most stringent test of the electroweak sector in the Standard Model will be provided.

Helicity analyses of the $t\bar{t}$ production vertex and the t decay vertex will lead to constraints of a few percent on the magnetic dipole moments of the top quark and the chirality of the charged (tb) decay current. The $\mathcal{CP}$ violating electric dipole moments can be bounded to less than 3×10^{-18} ecm. Given sufficiently large luminosities, the Higgs Yukawa coupling to top quarks can be measured. Depending on the value of the Higgs mass, this may provide a unique opportunity to check the fundamental Higgs–fermion couplings directly. Last but not least, the top quark may have unusual decay modes in extensions of the Standard Model, decays to charged Higgs bosons or top decays to stop. These decay modes are expected to be rare, yet frequent enough to be analyzed thoroughly at e^+e^- colliders.

Hadronic final states in high energy e^+e^- annihilation are an important testing ground for QCD. The large increase of the energies in linear colliders, compared to existing e^+e^- accelerators, motivates studies of the running coupling constant $\alpha_s(Q^2)$, providing a large lever arm for testing asymptotic freedom.

(b) Electroweak Gauge Bosons : $\mathcal{SM}$ and Extensions

To study the dynamics of the electroweak gauge bosons is another important task of high energy e^+e^- colliders. The form and the strength of the triple and quartic couplings of these particles are uniquely prescribed by the gauge symmetries in renormalizable theories. The triple gauge boson couplings define the electroweak charges, the magnetic dipole moments and the electric quadrupole moments of the W bosons in the static limit. By destroying the unitarity cancellations which in the Standard Model are associated with the longitudinal degrees of freedom of the gauge bosons, any small deviations from the $\mathcal{SM}$ values will be magnified with increasing energies, and the bounds will tighten.

The cross section for W pair production in e^+e^- colliders, $e^+e^- \to W^+W^-$, is large even after forward production is cut out. The clean environment of a 500 GeV e^+e^- collider allows for a high reconstruction efficiency of the gauge bosons, and makes such a machine competitive even with multi–TeV proton colliders. The analysis of the W polarization through the angular distribution of the decay products improves the bounds derived from the total cross sections significantly. If all parameters are allowed to vary freely, the anomalous magnetic dipole and electric quadrupole moments can be probed to less than about ± 0.02 (provided polarized electron beams are used). The precision improves by another order of magnitude if the number of free parameters is reduced by additional symmetry constraints.

It is physically plausible that the Standard Model, based on the gauge symmetry group $SU(3) \times SU(2) \times U(1)$, will be embedded into a grand–unified theory at very high energies $\sim 10^{16}$ GeV. The symmetry groups of these theories may be broken down to the $\mathcal{SM}$ group in several steps. In this case new gauge bosons are predicted with masses which may not be far away from the scale of electroweak symmetry breaking. For example, in $SO(10)$ a triplet $W_R^\pm$, Z_R of new gauge bosons may exist, remnant of an underlying left–right gauge symmetry; or in $E(6)$ a novel Z' gauge boson. If the e^+e^- energy can be raised high enough, the machine will operate as a Z_R or Z' factory. If the masses are above the maximum energy, the exchange of virtual Z_R or Z' particles affects the cross sections for μ and quark pairs. At 500 GeV, these observables are sensitive to Z_R, Z' exchange up to masses of order 3 to 4 TeV. The various models can be discriminated and their parameters can be measured with sufficiently high accuracy for boson masses up to ~ 2 TeV.

In most of the unifying groups additional new fermions are predicted with masses which may not be much larger than the Fermi scale. Among these novel leptons and quarks with exotic $\mathcal{SM}$ quantum numbers, heavy neutrinos, possibly of Majorana type, are a prominent example. These particles can either be produced pairwise or, if the mixing is strong enough, in association with ordinary chiral $\mathcal{SM}$ particles. While masses up to the beam energy are accessible in pair production, the total energy can be fully exploited in associated production of heavy new fermions with light $\mathcal{SM}$ fermions.

(c) Higgs Particles

e^+e^- colliders with an energy of 300 to 500 GeV are ideal instruments to search for Higgs particles throughout the mass range characterized by the electroweak symmetry breaking. The intermediate mass range below ~ 200 GeV is theoretically one of the most likely regions for Higgs masses. In this scenario Higgs particles remain weakly interacting up to the scale of the grand unification, providing a path for the renormalization of the electroweak mixing angle $\sin^2\vartheta_W$ from the GUT symmetry value 3/8 down to the obeserved value ~ 0.2 at low energies.

The Higgs mass range can be covered up to 70% of the total collider energy, irrespectively of the Higgs decay modes, in three independent production channels: the bremsstrahlung process $e^+e^- \to ZH$ and the WW/ZZ fusion processes $e^+e^- \to \overline{\nu}\nu H$ and $e^+e^- \to e^+e^-H$. The particles are easy to detect. Background events to the ZH channel from Z pair production $e^+e^- \to ZZ$ (for Higgs masses near the Z mass) can be suppressed efficiently by using μ–vertex detectors since Higgs particles with masses up to ~ 130 GeV decay mainly into $b\bar{b}$ pairs.

Once the Higgs particle is found, its properties must be investigated. The spin can be measured by analyzing the angular dependence of the ZH production process and of the Higgs decay processes. The Higgs coupling to the electroweak gauge bosons W and Z can be determined through the production rates, the couplings to heavy fermions through the Higgs decay branching ratios and, in some mass windows, Higgs radiation off top quarks.

A yet stronger case for e^+e^- linear colliders operating in the 300 to 500 GeV range is made by supersymmetric extensions of the Standard Model. A spectrum of at least five neutral and charged Higgs particles is predicted in such scenarios. The mass of the lightest neutral Higgs particle is bounded to typically less than ~ 130 GeV while the masses of the heavier particles could well be in the range below ~ 250 GeV. Since the neutral particles decay in general predominantly into $b\bar{b}$ jets, with a small fraction into $\tau^+\tau^-$ pairs, they can be detected at hadron colliders only through rare decay modes; charged Higgs particles appear to be accessible in these colliders only through top quark decays. In e^+e^- colliders, on the other hand, they can be produced either through the bremsstrahlung and the fusion mechanisms, or in pairs. It will be proved later that at least one neutral Higgs particle must be detected at such a collider, and that for large parts of the parameter space all three neutral Higgs particles can be observed. Charged Higgs particles can be detected with masses up to the kinematical limit.

(d) Supersymmetry

Supersymmetric theories are most appealing extensions of the Standard Model. These theories predict a greatly extended Higgs sector, scalar partners of the $\mathcal{SM}$ fermions as well as spin 1/2 partners to the gauge bosons and the Higgs particles. While the colored $\mathcal{SUSY}$ partners, squarks and gluinos, can be produced at high rates in hadron colliders,

e^+e^- colliders are ideal machines to search for the Higgs particles, the sleptons and the non–colored gauginos and Higgsinos. This has already been emphasized for the Higgs sector above. If R parity is conserved – an assumption which may be relaxed – sleptons and gauginos/Higgsinos are produced pairwise in e^+e^- collisions, $e^+e^- \to \tilde{\mu}^+\tilde{\mu}^-$ etc., so that mass spectra up to the beam energy can be covered. Selectrons in association with photinos may be generated also in $e\gamma \to \tilde{e}\tilde{\gamma}$ collisions; for light enough photinos the selectron masses which can be probed, can eventually exceed the $e^\pm$ beam energy. Besides the Higgs particles, gauginos and Higgsinos are expected to be the lightest among the $\mathcal{SUSY}$ particles, followed by the sleptons. The search for these $\mathcal{SUSY}$ states therefore provides one of the prime motivations for operating e^+e^- linear colliders.

1.4 Conclusions

e^+e^- linear colliders operating in the energy range of 300 to 500 GeV have a very high physics potential which is complementary to that of proton colliders in the multi–TeV regime.

High precision measurements in the top and the W, Z gauge boson sectors will not only lead to a deeper understanding of the Standard Model and its symmetry principles, but anomalous properties of these particles could hold important clues to the mechanism of electroweak symmetry breaking and to elements of the physics beyond the Standard Model. The intermediate mass range of the Higgs sector is covered at e^+e^- colliders in an ideal way.

An equally important *raison d'être* for high energy e^+e^- colliders can be derived from areas beyond the Standard Model. Extended gauge symmetries suggest new gauge bosons and novel leptons which can be explored in e^+e^- colliders very well. Last but not least, these colliders provide unique facilities to explore central aspects of supersymmetric extensions of the Standard Model, the Higgs spectrum and its properties, the gaugino/Higgsino sector and the supersymmetric partners of the leptons.

Extending the energy of the colliders in a second phase to a value between 1 and 2 TeV will allow us to study electroweak gauge bosons at a scale where they would interact strongly if Higgs bosons were not realized in Nature as light weakly coupled particles. In this phase the colliders will also greatly extend the discovery limits for new phenomena in the domains beyond the Standard Model.

The clarity of view given into the energy regime characterized by the scale of electroweak symmetry breaking, and the opportunities for exploring new physical phenomena beyond the Standard Model, make e^+e^- linear colliders unique facilities for addressing key issues at the frontier of fundamental physics.

2. Top and QCD

2.1 Basis of the Top Quark

Top quarks are the heaviest matter particles in the 3–family Standard Model ($\mathcal{SM}$). They have been introduced, together with the b quarks as weak isospin partners,

$$\begin{bmatrix}\nu_e\\ e^-\end{bmatrix}_L \; e_R^- \qquad \begin{bmatrix}\nu_\mu\\ \mu^-\end{bmatrix}_L \; \mu_R^- \qquad \begin{bmatrix}\nu_\tau\\ \tau^-\end{bmatrix}_L \; \tau_R^-$$

$$\begin{bmatrix}u\\ d\end{bmatrix}_L \; u_R \; d_R \qquad \begin{bmatrix}c\\ s\end{bmatrix}_L \; c_R \; s_R \qquad \begin{bmatrix}t\\ b\end{bmatrix}_L \; t_R \; b_R$$

to allow for $\mathcal{CP}$ violation in the left–handed charged–current sector of the $\mathcal{SM}$. While b quarks were discovered shortly after they had been suggested theoretically, the lower bound of the top quark mass has been shifted experimentally to a level comparable to the electroweak symmetry breaking scale. The t-quark may be discovered soon at the Tevatron.

The indirect evidence for the existence of top quarks is very strong. It is based on the $SU(3) \times SU(2) \times U(1)$ gauge symmetry principle of the Standard Model, which is supported by high precision measurements in the electroweak sector at e^+e^- colliders, in deep–inelastic lepton–nucleon scattering, high energy $p\bar{p}$ colliders and low energy atomic physics experiments. At a purely theoretical level, the requirement of the Standard Model to be anomaly free, i.e. to be renormalizable and mathematically well–defined, leads to the condition that the sum of all electric charges in a family be zero $\sum Q = 0$. Given the b quark, this condition is fulfilled only if there exists an up quark of charge $+2/3$ in the third family. The iso–multiplet structure of the third family can experimentally be investigated in several ways. Deviations from the doublet/singlet pattern of the first two families in the third family would lead to a breaking of the GIM mechanism and thus induce FCNC decays of B mesons at a level that is several orders above the observed bounds. The isospin quantum numbers of the b quarks can be measured directly through the Z–decay width to b quarks and the forward–backward asymmetry of b quarks on the Z at LEP. If combined with b data from PETRA/PEP and TRISTAN, a unique solution can be derived for the third isospin components of the left– and right–handed b quarks [5], Fig.3,

$$\begin{aligned} \{I_3^L(b)\}_{exp} &= -0.494^{+0.013}_{-0.010} \quad \to \quad I_3^L(b) = -1/2 \\ \{I_3^R(b)\}_{exp} &= -0.018^{+0.049}_{-0.068} \quad \to \quad I_3^R(b) = 0 \end{aligned}$$

which coincide with the isospin assignment of the Standard Model.

First indications of a large top mass can be traced back to the observation of high $B^0 - \overline{B}^0$ oscillation frequencies [6], which increase quadratically with m_t. Lower bounds

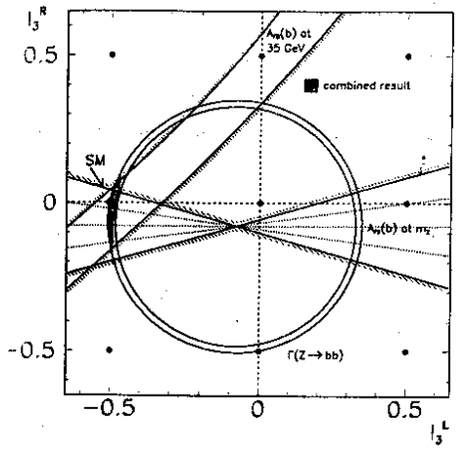

Fig. 3: *The weak isospins $I_3^L(b)$ and $I_3^R(b)$ of the left- and right-handed b quark components, extracted from the data on $\Gamma(Z \to b\bar{b})$ and $A_{FB}(b)$ at LEP, and PETRA/PEP and TRISTAN, Ref.[5].*

on the top mass have been set directly at various levels of assumptions on production mechanisms and decay modes. The non-observation of Z decays to top quark pairs raised the top mass to more than 45 GeV. The measured value of the leptonic W decay branching ratio can be exploited to extract a lower limit of 52 GeV as any contribution from $W \to t\bar{b}$ decays would reduce $BR_l(W)$ correspondingly. Both these methods depend only on the gauge group structure of the $\mathcal{SM}$ and they are independent of the specific top decay mechanism. The mass limit [7] of

$$m_t \geq 91 \text{ GeV}$$

from the direct search of top quarks in $p\bar{p} \to t$ collisions is based on the canonical branching ratio $BR(t \to bl\nu) \simeq 1/9$ as predicted for semileptonic top decays in the Standard Model. For top masses exceeding the W-boson mass, this assumption is rather mild as many extensions of the $\mathcal{SM}$ do not alter the branching ratio for the standard decay $t \to bW$ dramatically.

The top mass enters the ρ parameter, i.e. the relative strength between NC and CC processes, quadratically through radiative corrections. Within the framework of the Standard Model, the electroweak high-precision measurements allow us to estimate the value of the top mass [8],

$$m_t = 144^{+19+17}_{-21-19} \text{ GeV}$$

$$< 182 \text{ GeV [95\% CL]}$$

These limits on the top mass are fairly stable against possible extensions of the Standard

Model so that the true top mass value may be expected in the quoted bracket with some confidence.

Based on these estimates the hope is justified that the top quark will be discovered at the Tevatron. If $m_t < 140$ to 150 GeV, even soon. The future multi-TeV proton colliders LHC and SSC will produce 10^6 to 10^7 top quarks per year [9]. The accuracy with which the top quark mass can be measured in proton colliders is limited to about 4 GeV. Subtle effects in standard and possible non-standard decays will be very difficult to analyze in the multi-gluon jet environment of the $gg \to t\bar{t}$ production channel in these machines. e^+e^- linear colliders in the energy range below 500 GeV will provide a great step forward in exploring and understanding the properties of the top quark.

2.2 Profile of the Top Quark

If the top mass is fixed, all decay and interaction properties of the top quark can be predicted at the Born level in the 3-family Standard Model [10]. This holds true if QCD corrections are included, and only a weak dependence on the Higgs mass is introduced by one-loop electroweak corrections to the decay width. In the subsequent discussion we shall assume that the top mass exceeds the W-mass so that

$$t \to b + W^+$$

will be the dominant $\mathcal{SM}$ decay mode. The top quark width in the Standard Model grows very rapidly from small values above the W decay threshold to $\mathcal{O}(1 \text{ GeV})$ in the mass range $m_t \sim 150$ GeV. The top quark is a short-lived particle with $\tau_t \sim 10^{-24}$ sec. For still higher masses, the lifetime continues to drop as the third power of the mass.

In many extensions of the Standard Model that we shall discuss, non-standard decays are rare in the interesting range of model parameters, yet they are frequent enough to be observable in e^+e^- colliders. $\mathcal{SM}$ decays of one of the quarks in $t\bar{t}$ final states then serve as a useful tagging device while in the opposite hemisphere non-standard top decays may be searched for.

(a) Top Decay in the Standard Model

Soon above threshold the width for the dominant decay mode $t \to b + W^+$ is given by [10]

$$\Gamma(t \to b + W^+) = \frac{G_F m_t^3}{8\sqrt{2}\pi}\left[1 - \frac{m_W^2}{m_t^2}\right]^2\left[1 + 2\frac{m_W^2}{m_t^2}\right]$$

Asymptotically the width grows with the third power of the top mass, more specifically $\Gamma \simeq 175 \text{ MeV} \cdot [m_t/m_W]^3$. The rapid growth is expected from the equivalence theorem. Heavy t quarks decay into fast W bosons, the longitudinal component of which may be

identified with the charged Goldstone boson. Since the scalar coupling is proportional to the t mass, the width is proportional to m_t^3, the additional mass factor arising from wave functions and flux factors. By contrast, the couplings of the tranverse W degrees of freedom do not grow with the top mass so that for large top masses the longitudinal W mode is dominant, $\Gamma_L/\Gamma_T = m_t^2/2m_W^2$. The W helicity analysis can easily be carried out. The distribution of the fermion axis in the rest frame of the polarized W boson with respect to the W flight direction follows from $d\Gamma/d\cos\vartheta_* \sim \sin^2\vartheta_*$ and $(1 \pm \cos\vartheta_*)^2$ for longitudinal and transverse polarizations, respectively. Together with the top quark width, the degree of longitudinal polarization is shown in Fig.4.

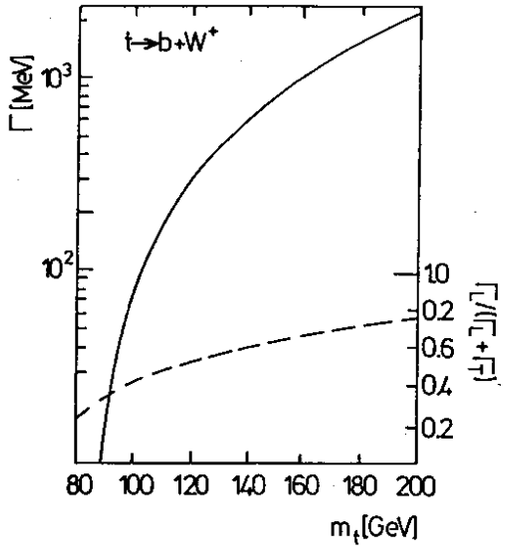

Fig. 4: *The top decay width Γ_t in the Standard Model (Born approximation), Ref. [10]. The degree of longitudinal W polarization is shown in the insert.*

It has been tacitly assumed in the preceding discussion that the Kobayashi–Maskawa matrix element V_{tb} is close to unity. This is indeed borne out by detailed analyses of the $\mathcal{CKM}$ matrix for the 3–family Standard Model. The branching ratios $\mathrm{BR}(t \to qW^+)$ for $q = b, s, d$ follow from

$$\begin{aligned} V_{tb} &= 0.9990 \pm 0.0005 \quad \to \quad \mathrm{BR}(b) \approx 1 \\ V_{ts} &= 0.042 \pm 0.012 \quad \to \quad \mathrm{BR}(s) \approx 0.2\% \\ V_{td} &= 0.010 \pm 0.007 \quad \to \quad \mathrm{BR}(d) \approx 0.01\% \end{aligned}$$

While the search for sW^+ final states, though difficult, may not be impossible, the t production rates will be too small to search for dW^+ decay products.

The width of the top quark is known to one–loop QCD and electroweak corrections. The QCD corrections include the one–loop vertex corrections and the gluon bremsstrahlung from the initial–state top and the final–state bottom quark [11]. The correction varies slowly from −8% down to −10% for top masses above 100 GeV. The electroweak one–loop corrections involve a large number of diagrams [12]. The numerical value of these corrections turns out to be small, $\approx +2\%$ for a Higgs mass of $\sim$ 100 GeV, and nearly independent of the top mass.

The measurement of the top quark width is very difficult. Two methods have been discussed in the literature. (i) The width of the remnant toponium $1S$ state is given by twice the top width, $\Gamma(1S(t\bar{t})) \approx 2\Gamma_t$, for top masses above $\sim$ 110 GeV. The actually observed width of the peak, however, is strongly affected by the smearing due to beamstrahlung. Nevertheless, the measurement of the width within a bracket of 50 to 80% appears feasible for top masses below $\sim$ 180 GeV, if a narrow–band beam design of the machine is realized [13,14]. (ii) The angular distribution of soft gluons emitted in $e^+e^- \to (t\bar{t}) \to b\bar{b}W^+W^- + g_{\mathrm{soft}}$ depends on the width of the top quark [15]. The non–zero lifetime of the top quark suppresses the radiation of soft, collinear gluons. However, the suppression is small for realistic values of the top quark width and it has not been demonstrated so far that the effect survives the complicated pattern [16] of parton hadronization in this process.

(b) Non–standard Top Decays

The theoretical study of non–standard top decays is motivated by the large top quark mass which could allow for exciting novel decay modes. A few illustrative, but characteristic examples will be discussed in some detail in the following chapters. They demonstrate the great potential of top production in e^+e^- collisions, even if the novel decay processes are fairly rare.

Charged Higgs Decays

Charged Higgs states $H^\pm$ appear in 2–doublet Higgs models in which out of the eight degrees of freedom three Goldstone bosons build up the longitudinal states of the vector bosons and three neutral and two charged states correspond to real physical particles. A strong motivation for this extended Higgs sector is provided by supersymmetry which requires the $\mathcal{SM}$ Higgs sector to be doubled in order to generate masses for the up and down–type fermions. In the minimal version of that model the masses of the charged Higgs particles are predicted to be larger than the W mass, mod. radiative corrections. Phenomenological constraints can eventually be derived from photonic B decays mediated by penguin diagrams to which charged Higgs bosons, charginos and other SUSY states can contribute [17].

If the charged Higgs mass is lighter than the top mass, the top quark may decay into

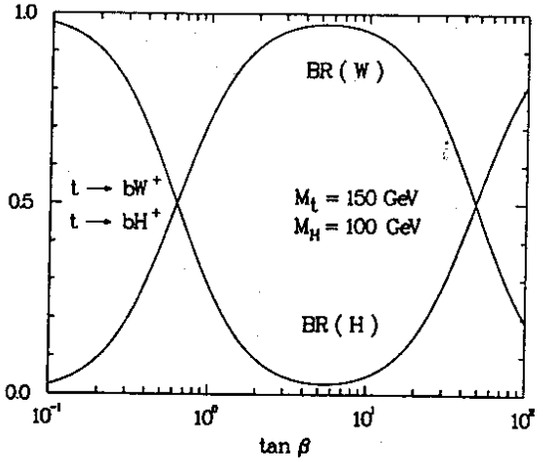

Fig. 5: **(a)** *Branching ratios for the decays $t \to bW^+$ and $t \to bH^+$ in two-doublet Higgs models.*

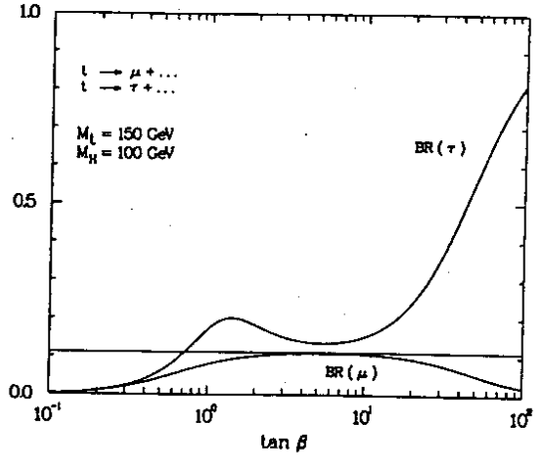

Fig. 5: **(b)** *Inclusive branching ratios for $t \to l + X$ in two-doublet Higgs models and the breaking of the lepton universality. The $\mathcal{SM}$ value $BR_l(t) = 1/9$ is indicated by the broken line.*

H^+ plus a b quark,

$$t \to b + H^+$$

The coupling of the charged Higgs to the scalar (t, b) current is defined by the quark masses and the parameter $\tan\beta$, the ratio of the vacuum expectation values of the Higgs fields giving masses to up and down-type fermions, respectively. For the sake of consistency, related to grand unification, we shall assume $\tan\beta$ to be bounded by $1 < \tan\beta < m_t/m_b \sim 30$. The width has a form quite similar to the $\mathcal{SM}$ decay mode,

$$\Gamma(t \to b + H^+) = \frac{G_F m_t^3}{8\sqrt{2}\pi}\left[1 - \frac{m_H^2}{m_t^2}\right]^2\left[\left(\frac{m_b}{m_t}\right)^2 \tan^2\beta + \cot^2\beta\right]$$

The branching ratio of this novel Higgs decay mode is compared with the W decay mode in Fig.5a. The W decay mode is in general dominant; the Higgs decay branching ratio in general small, yet large enough to be clearly observable. The detection of this scalar decay channel is facilitated by the characteristic decay pattern of the charged Higgs bosons, $H^+ \to \tau^+\nu_\tau$ and $c\bar{s}$. Since $H^\pm$ bosons couple preferentially to down-type fermions for $\tan\beta > 1$, the τ decay mode wins over the quark decay mode, thus providing a clear experimental signature. A first signal of top decays into charged Higgs particles would therefore be the breakdown of μ, e *vs.* τ universality in semileptonic top decays, Fig.5b.

Top Decay to Stop

Another exciting decay mode in supersymmetry models is the decay of the top to the $\mathcal{SUSY}$ scalar partner stop plus neutralinos, mixtures of neutral gauginos and higgsinos [18]. This possibility is intimately related to the large top mass which leads to novel phenomena induced by the strong Yukawa interactions. These effects do not occur in light-quark systems but are special to the top system.

The mass matrix of the scalar $\mathcal{SUSY}$ partners $(\tilde{t}_L, \tilde{t}_R)$ to the left- and right-handed top-quark components (t_L, t_R) is built-up by the elements

$$\mathcal{M}^2 = \begin{Vmatrix} m_{\tilde{t}_L}^2 + m_t^2 & \delta\tilde{m}_{LR}^2 \\ \delta\tilde{m}_{LR}^2 & m_{\tilde{t}_R}^2 + m_t^2 \end{Vmatrix}$$

Large Yukawa interactions lower the diagonal matrix elements $\sim -m_t^2$ with respect to the common squark mass value in supergravity models, and they mix the $\tilde{t}_L$ and $\tilde{t}_R$ states with the strength $\sim m_t$ to form the mass eigenstates $\tilde{t}_1, \tilde{t}_2$. Unlike the five light quark species, these Yukawa interactions of $\mathcal{O}(m_t)$ can be so large in the top sector that after diagonalizing the mass matrix, the smaller eigenvalue may fall below the top quark mass, $m_{\tilde{t}_1} < m_t$.

The decay modes

$$t \to \tilde{t} + \text{neutralinos}$$

compete with the ordinary W decay mode. Identifying the lightest $\mathcal{SUSY}$ particle with the photino $\tilde{\gamma}$, for example, the mass of which we neglect in this estimate,

$$\frac{\Gamma(t \to \tilde{t}\tilde{\gamma})}{\Gamma(t \to bW)} \approx \frac{8\sqrt{2}\pi\alpha}{9G_F m_t^2} \frac{[1 - m_{\tilde{t}}^2/m_t^2]^2}{[1 - m_W^2/m_t^2]^2[1 + 2m_W^2/m_t^2]}$$

This ratio is in general less than 10%. The subsequent $\tilde{t}$ decays, $\tilde{t} \to b\tilde{W}, \tilde{W} \to W\tilde{\gamma}$ or $l\tilde{\nu}$ *etc.*, and $\tilde{t} \to c\tilde{\gamma}$, lead to an overall softer charged lepton spectrum and, as a result of escaping photinos or sneutrinos, to an increase of the missing energy, the characteristic signature for $\mathcal{SUSY}$ induced phenomena [13].

Depending on the $\mathcal{SUSY}$ parameters however, stop decays could be enhanced if the top is heavy, so that decays to more strongly coupled, but fairly light higgsinos could frequently occur.

FCNC Decays

Within the Standard Model, FCNC decays like $t \to c\gamma$ are forbidden at the tree level by the GIM mechanism. However, they do occur in principle at the one–loop level, though strongly suppressed. The suppression is particularly strong for top decays since the quarks building up the loops, must be down–type quarks with m_b^2 setting the scale of the decay amplitude, $\Gamma_{FCNC} \sim \alpha G_F^2 m_b^4 m_t$. Branching ratios for $t \to c\gamma, cZ$, for example, are typically in the range of $\sim 10^{-12}$. At this level, no $\mathcal{SM}$ generated FCNC t decays can be observed. On the other hand, if these decay modes were detected, they would be an undisputed signal of new physics beyond the $\mathcal{SM}$. From such options we select one illustrative, though very speculative example for brutal GIM breaking. It is tied to the large top mass and may be observable even in low rate e^+e^- colliders.

The GIM mechanism requires all L and R quark components of the same electric charge in different families to carry identical isospin quantum numbers, respectively. This rule is broken by adding quarks in LR symmetric vector representations [19] to the "light" chiral representations or mirror quarks [20]:

$$\text{vector quarks:} \quad \cdots \quad \begin{bmatrix} t \\ b \end{bmatrix}_L \; t_R \quad b_R \qquad \begin{bmatrix} U \\ D \end{bmatrix}_L \begin{bmatrix} U \\ D \end{bmatrix}_R$$

$$\text{mirror quarks:} \quad \cdots \quad \begin{bmatrix} t \\ b \end{bmatrix}_L \; t_R \quad b_R \qquad U_L \quad D_L \qquad \begin{bmatrix} U \\ D \end{bmatrix}_R$$

Low energy phenomenology requires the masses M of the new U, D quarks to be larger than 300 GeV. Depending on the specific form of the mass matrix, mixing between the normal chiral states and the new states may occur at a level of $(m/M)^{1/2}$, so that FCNC

(t, c) couplings of the order $\sim (m_t m_c/M^2)^{1/2}$ can be induced. FCNC decays of top quarks, for example,

$$BR(t \to cZ) \sim \text{fraction of \%}$$

are therefore not excluded. Such branching ratios would be at the lower edge of the range accessible at e^+e^- colliders.

2.3 Top Production in e^+e^- Collisions

(a) The Annihilation Channel

The main production mechanism for top quarks in e^+e^- collisions is the annihilation channel

$$e^+e^- \xrightarrow{\gamma,Z} t\bar{t}$$

The cross section can be written in terms of the vectorial and axial contributions as [21]

$$\sigma = \beta\frac{3-\beta^2}{2}\sigma^{VV} + \beta^3\sigma^{AA}$$

with

$$\sigma^{VV} = \frac{4\pi\alpha^2(s)}{s}e_e^2e_t^2 + \frac{G_F\alpha(s)}{\sqrt{2}}e_e e_t v_e v_t \frac{m_Z^2}{s - m_Z^2} + \frac{G_F^2}{32\pi}(v_e^2 + a_e^2)v_t^2\frac{m_Z^4 s}{(s - m_Z^2)^2}$$

$$\sigma^{AA} = \frac{G_F^2}{32\pi}(v_e^2 + a_e^2)a_t^2\frac{m_Z^4 s}{(s - m_Z^2)^2}$$

The vector and axial–vector charges of the electron and top quark are given by $v_f = 2I_3^f - 4e_f \sin^2\vartheta_W$ and $a_f = 2I_3^f$ with $I_3^f = \pm 1/2$ for t, e. The running electromagnetic coupling can be set $\alpha(s) \approx 1/127$ in the energy range between 300 and 500 GeV. $\beta = (1 - 4m_t^2/s)^{1/2}$ is the velocity of the t quark. The cross section is shown in Fig.6 for three representative top mass values. About 85% of the cross section is due to γ exchange.

Most important are QCD corrections, the top vertex corrections and gluon bremsstrahlung off the final state quarks [21]. Near the threshold they are different for the vectorial and the axial t vertex. The QCD corrections may be summarized in the condensed form [22]

$$VV \to 1 + \frac{4\alpha_s}{3}\left[\frac{\pi}{2\beta} - \frac{3+\beta}{4}\left(\frac{\pi}{2} - \frac{3}{4\pi}\right)\right]$$

$$AA \to 1 + \frac{4\alpha_s}{3}\left[\frac{\pi}{2\beta} - \frac{19 - 44\beta + 35\beta^2}{10}\left(\frac{\pi}{2} - \frac{3}{4\pi}\right)\right]$$

with $\alpha_s = 12\pi/23\log(p_t^2/\Lambda^2)$. These formulae provide an accurate interpolation between the exact expressions of the one–gluon exchange for low β and in the asymptotic energy range where the QCD corrections approach the universal value α_s/π.

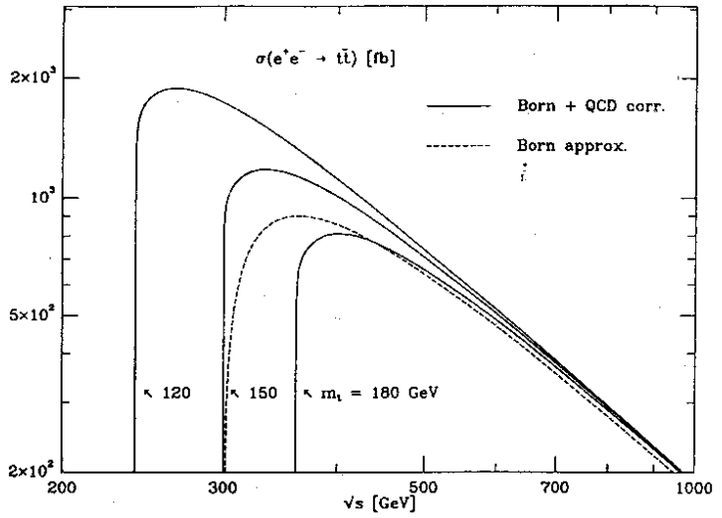

Fig. 6: *The cross section $\sigma(e^+e^- \to t\bar{t})$ [including QCD corrections] for three representative values of the top mass.*

Approaching the threshold, a Coulomb singularity develops which compensates the phase space suppression and leads to a non–zero cross section at the threshold: $VV, AA \sim \alpha_s/\beta$. Very close to the threshold the Coulombic one–gluon exchange diagrams have to be iterated, building up a ladder which gives rise to resonance formation. It can be shown by a detailed analysis that the loop–improved parton cross section accounts well for the properly smeared resonance excitation curve down to approximately 1 GeV above threshold if the argument in the running quark–gluon coupling is chosen to be the quark momentum p_t, $\alpha_s = \alpha_s(p_t)$ [22]. This is just a manifestation of the dual relationship between perturbative QCD based on the quark–gluon degrees of freedom and non–perturbative resonance phenomena. [The detailed discussion of the resonance region and their remnants for rapid top decays will be postponed to the next section.]

Above the threshold, the genuine electroweak [non–QED] corrections are small and depend only weakly on the top and the Higgs masses [23]. QED corrections, if restricted to infrared γ radiation, lower the cross section as usual. However, this effect is largely compensated by the radiation of hard photons.

The experimental analysis of charm and bottom fragmentation functions has clearly demonstrated that heavy quark fragmentation is hard in contrast to the fragmentation of light quarks. This is a consequence of the inertia of heavy particles, the momentum of which is not altered much if a light quark $\bar{q}$ is attached to the heavy quark Q in the fragmentation process to form a bound state $(Q\bar{q})$, see [24]. At the same time soft infrared gluon radiation is damped if the color source is heavy [10,15,16]. For top quarks

with mass $m_t < 100$ GeV the average energy loss due to perturbative gluon radiation and non–perturbative fragmentation can be estimated as

$$\delta_{PT} \approx 1 - \left[\frac{\alpha_s(E^2)}{\alpha_s(m_t^2)}\right]^{\frac{32}{3(33-2N_f)}}$$
$$\delta_{NP} \approx \tfrac{1}{2}\ \mathrm{GeV}/m_t$$

respectively. Only a small fraction of gluon energy is radiated off if the initial energy E is limited to several m_t. Likewise only a few soft pions/kaons are generated non–perturbatively in the wake–field of the top quark.

For $m_t \geq 100$ GeV the strong fragmentation process and the weak decay mechanism are intimately intertwined. The lifetime $\tau_* < \Lambda^{-1}$ becomes so short that the mesonic $(t\bar{q})$ and baryonic (tqq) bound states cannot be built–up any more. Depending on the initial top quark energy, even remnants of the t quark jet may not form any more [10]. Hadrons can be created in the string stretched between the t and the $\bar{t}$ only if the quarks are separated by about 1 fermi before they decay. If the flight path $\gamma\tau_* < 1/2$ fm, i.e.

$$E < \frac{1}{2}\frac{m_t^4}{m_W^3}$$

the length of the $t - \bar{t}$ string is too short to form hadrons and jets cannot develop any more along the flight direction of the top quarks.

The perturbative radiation of soft gluons, too, is interrupted by the t quark decay [15]. The angular distribution (Θ) and the energy distribution (ω) of the radiated gluons is approximately given by

$$dP_g = \frac{4\alpha_s}{3\pi}\frac{\Theta^2 d\Theta^2}{\left[\Theta^2 + \frac{1}{\gamma^2}\right]^2 + \left[\frac{\Gamma}{\gamma\omega}\right]^2}\frac{d\omega}{\omega}$$

for a short–lived radiation source accelerated to $\gamma = E_t/m_t$. The gluons accumulate on the surface of a cone with half–aperture $\Theta_c \sim \gamma^{-1}$ for a long–lived t, but $\sim \gamma^{-1}\sqrt{\gamma\Gamma/\omega}$ if the particle decays quickly. The energy spectrum rises from zero to a maximum at $\omega \sim \gamma\Gamma$ before falling off $\sim 1/\omega$ for large ω, if the width is greater than the confinement scale Λ. Top quarks are decelerated only by the early radiation of hard, non–collinear gluons. The non–zero t quark width Γ acts as an infrared cut–off for gluon radiation.

Neglecting the rare hard non–collinear gluon radiation, the flux tube forms between the b and $\bar{b}$ quarks after the decay of the top quarks, $e^+e^- \to t\bar{t} \to b\bar{b}W^+W^-$, if the top mass is so large that no t jet remnants are left–over. As a result, the light hadrons created in the flux tube, will be boosted into the $b\bar{b}$ hemisphere while the region opposite to the $b\bar{b}$ hemisphere will be depleted of particles [16].

(b) Static t Parameters

Because of the large t mass, deviations from the Standard Model may manifest themselves in the top quark sector first. Examples in which the large mass is crucial, are provided by

multi–Higgs doublet models, models of dynamical symmetry breaking and compositeness. These effects can globally be described by form factors parametrizing the electroweak $t\bar{t}$ production current ($a = \gamma, Z$) and the weak (t, b) decay current ($a = -$) [25–29],

$$j^a_\mu \sim F^a_{1L}\gamma_\mu P_L + F^a_{1R}\gamma_\mu P_R + \frac{i\sigma_{\mu\nu}q_\nu}{2m_t}[F^a_{2L}P_L + F^a_{2R}P_R]$$

[$P_{L,R}$ project on the left and right chirality components of the wave functions.] In the $\mathcal{SM}$, $F^-_{1L} = 1$ while all other F^-_i vanish; $F^\gamma_{1L} = F^\gamma_{1R} = 1$ and $F^\gamma_{2L} = F^\gamma_{2R} = 0$, analogously for the Z current. $\mathcal{CP}$ invariance requires $F^{\gamma,Z}_{2L} = F^{\gamma,Z}_{2R}$ in the $t\bar{t}$ production current, and equal phases for F^-_{1L} and F^-_{2R} *etc.* in the decay current. The static values of the form factors $F^{\gamma,Z}_2$ are the anomalous magnetic and electric dipole moments of the top quark.

The form factors are determined experimentally by measuring the angular distribution of the $t\bar{t}$ decay products, $e^+e^- \to t\bar{t}, t \to bW^+, W^+ \to f\bar{f}'$ *etc.* The corresponding helicity amplitudes have been given in Refs.[25–27] at the quark level. This requires the top quark to be treated as a free particle, the polarization of which not being affected by non–perturbative hadronic binding effects. This assumption is justified by the short lifetime of the top quark as discussed earlier. While the general helicity analysis can be found in the literature, we shall focus here on a few physically interesting specific examples.

Anomalous magnetic dipole moments of the top quark

If the electrons in $e^+e^- \to t\bar{t}$ are left–handedly polarized, the top quarks are preferentially produced as left–handed particles in the forward direction and only a small fraction is produced as right–handed particles in the backward direction. As a consequence of this $\mathcal{SM}$ prediction, the backward direction is most sensitive to small anomalous magnetic moments of the top quarks. This is demonstrated quantitatively in Fig.7 where the angular distribution of the top quarks is broken down to the various helicity contributions. It is apparent that the anomalous magnetic moments can be bounded to a few percent through the measurement of the angular dependence of the t quark cross section.

Electric dipole moments of the top quark

A term $\sim F_2\sigma_{\mu\nu}q_\nu\gamma_5$ can only be generated in a $\mathcal{CP}$ non–invariant γ or Z interaction [25,28,29]. The static limit $d^{\gamma,Z}$ of F_2 is the electric dipole moment of the top quark. Independently of the $\mathcal{CP}$ properties of the $t \to bW$ decay amplitude, such a contribution would be signalled by a non–zero expectation value of the $\mathcal{CP}$ odd momentum tensor [28] $T_{ij} \sim (q_+ - q_-)_i(q_+ \times q_-)_j$. The greatest sensitivity is achieved by choosing the unit momentum vectors of the charged W–decay leptons for $q_\pm$, $\langle T_{ij}\rangle \sim c_\gamma d^\gamma + c_Z d^Z$, where the coefficient c_γ, for instance, falls rapidly from zero at threshold to ~ -0.4 at $\sqrt{s} = 500$ GeV for $m_t = 150$ GeV. Correlations between $q_+ \times q_-$ and the initial e^+e^- beam direction can be exploited to disentangle d^γ from d^Z. Sensitivity limits to the electric dipole moments

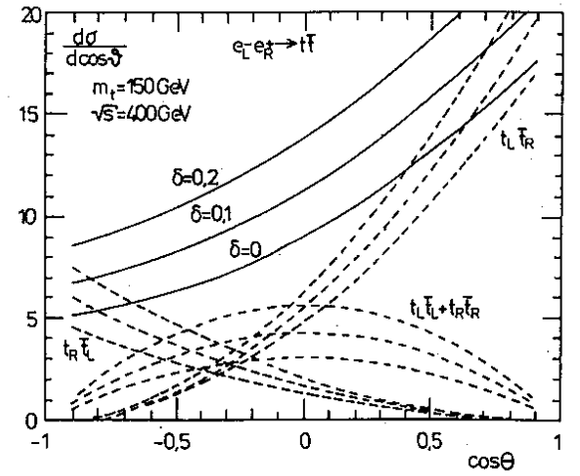

Fig. 7: *Angular distributions of the t production cross sections for fixed t and $\bar{t}$ helicities in polarized $e^-_L e^+_R$ annihilation. The parameter δ measures the anomalous magnetic (γ, Z) dipole moment of the top quark. From Ref.[26].*

are listed in the following table for a top mass $m_t = 150$ GeV and the integrated luminosity $\int \mathcal{L} = 10$ fb^{-1}:

$\sqrt{s}$	$d^{\gamma,Z}$
310 GeV	$< 7.0 \times 10^{-18}$ e cm
500 GeV	$< 2.8 \times 10^{-18}$ e cm

Other correlations, like $q_{e^+}[q_{e^+} \times q_b - q_{e^-} \times q_{\bar{b}}]$, and energy asymmetries can be defined that are sensitive to $\mathcal{CP}$ violation in the decay current [28] (see also Ref.[25]).

Chirality of the (t, b) decay current

The precise determination of the weak isospin quantum numbers of the b quark does not allow for large deviations of the (t, b) decay current from the left–handed $\mathcal{SM}$ prescription. Nevertheless, since $V + A$ admixtures may grow with the masses of the quarks involved [through mixing with heavy mirror quarks, for instance], it is necessary to check the chirality of the decay current directly. The l^+ energy distribution in the semileptonic

decay $t \to bW^+ \to l^+\nu_l$ depends sensitively on the chirality of the current:

$$\frac{d\Gamma}{dx_l} \sim \begin{cases} x_l(1-x_l) & \text{for } V-A \\ (x_l-\mu^2)(1-x_l+\mu^2) & \text{for } V+A \end{cases}$$

where $\mu^2 = m_W^2/m_t^2$ and $\mu^2 < x_l = 2E_l/m_t < 1$ denotes the scaled l^+ energy. Since the b–quark mass has been neglected, the two distributions add up incoherently, weighted by the probabilities for the $V \mp A$ mixture. Any deviation from the standard $V-A$ current would lead to a stiffening of the l^+ energy spectrum and, in particular, to a non–zero value at the upper end–point of the energy distribution.

(c) Higgs–Top Yukawa Coupling

The Higgs mechanism is one of the key points in the theory of the electroweak interactions. The fundamental particles acquire masses through the interaction with the ground–state Higgs field. The scale for the coupling of the physical Higgs boson to fermions and gauge bosons is therefore set by the masses of these particles. The fundamental nature of the mass generation demands this picture to be scrutinized experimentally in all facets. While the measurement of the Higgs coupling to W, Z bosons appears straightforward, the experimental check of the coupling to fermions is surprisingly difficult. In a small window of the intermediate mass range, the b, c, τ couplings can be measured directly. An indirect access to the Higgs–top coupling is provided by the $H\gamma\gamma$ and Hgg vertices which are built–up [partly] by top–quark loops. The bremsstrahlung of Higgs particles from top quarks produced in gluon–gluon fusion processes at pp colliders is difficult to disentangle from the background as the Higgs boson must be tagged through the rare $\gamma\gamma$ decay channel.

A direct way to determine the Yukawa coupling of the intermediate mass Higgs boson to the top quark in the range $m_H < 120$ GeV is provided by the bremsstrahl process

$$e^+e^- \to t\bar{t}H$$

in high energy e^+e^- colliders [30]. For large Higgs masses above the $t\bar{t}$ threshold, the decay channel $H \to t\bar{t}$ increases the cross section [31] for $e^+e^- \to Zt\bar{t}$ through the reaction

$$e^+e^- \to ZH, H \to t\bar{t}$$

Without the Higgs decay to the top quarks, the final state $Zt\bar{t}$ is produced mainly through virtual photons and Z bosons coupled to the $t\bar{t}$ pair, $e^+e^- \to Z + (\gamma^*, Z^*)(\to t\bar{t})$.

The $t\bar{t}H$ final state is generated almost exclusively through Higgs bremsstrahlung off the top quarks. Additional contributions from Higgs particles emitted by the Z line, are very small. The integrated cross sections, proportional to $g_{ttH}^2 = \sqrt{2}G_F m_t^2$, are shown for various values of the top mass in Fig.8. as a function of the Higgs mass. While for light Higgs masses the cross sections increase with the top mass as a result of the rising Yukawa coupling, this trend is reversed for heavy Higgs particles by the reduction

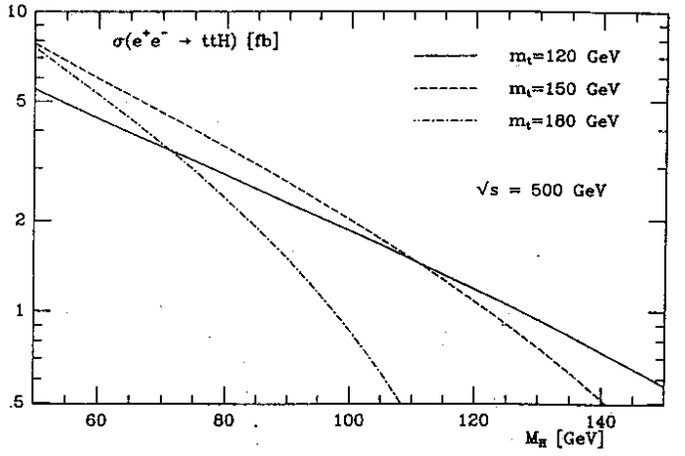

Fig. 8: *The cross section $\sigma(e^+e^- \to t\bar{t}H)$ in the Standard Model at $\sqrt{s} = 500$ GeV as a function of the Higgs mass for three different top mass values; from Ref.[30].*

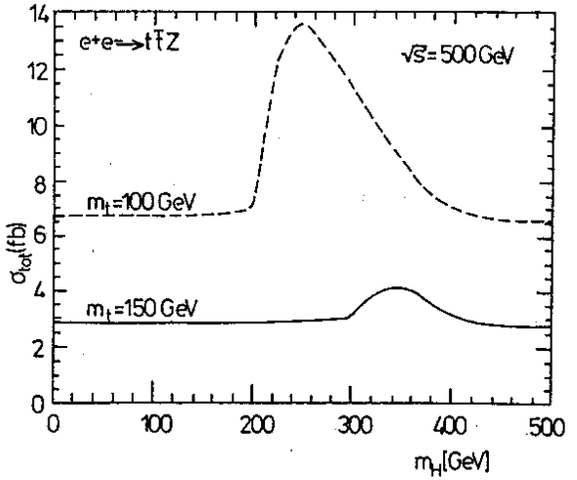

Fig. 9: *The cross section $\sigma(e^+e^- \to t\bar{t}Z)$ for two top mass values at $\sqrt{s} = 500$ GeV as a function of the Higgs mass; from Ref.[31].*

of the available phase space. For an integrated luminosity of $\int \mathcal{L} = 20$ fb^{-1}, some 100 events can be expected at Higgs masses of order 60 GeV, falling to 20 events at 120 GeV. Taking acceptance losses into account, this appears to be the upper limit at which the ttH coupling in the intermediate mass range can be measured directly in the course of a few years. Since the signature of the process $e^+e^- \to t\bar{t}H \to WWbbbb$ is spectacular, the hope is justified to isolate these events experimentally despite the low rates. The large number of b quarks together with the mass constraints $m(b\bar{b}) = m(H)$ and $m(Wb) = m(t)$ will be crucial in rejecting background events. QCD initiated $t\bar{t}b\bar{b}$ final states are suppressed strongly, $\sigma_{QCD} < 0.1$ fb, if the $b\bar{b}$ invariant mass is assumed to be larger than 50 GeV. [The case of $\mathcal{SUSY}$ Higgs particles is discussed in Ref.[30].]

The Higgs contribution to $e^+e^- \to t\bar{t}Z$ is important only if the Higgs boson is produced as a real particle, with a mass large enough to allow the decay into a top quark pair. The effect on the cross sections, Fig.9, is most pronounced for Higgs masses not far above the top decay threshold [31]. For large Higgs masses the partial width

$$\Gamma(H \to t\bar{t}) = \frac{3G_F m_t^2 m_H}{4\sqrt{2}\pi}\beta^3$$

rises linearly with the Higgs mass while the decay widths to W and Z bosons grow as the third power, thus suppressing the branching ratio to top quark pairs. For a top mass of 100 GeV the cross section $\sigma(e^+e^- \to t\bar{t}Z)$ increases by almost a factor two for a Higgs mass of 250 GeV. The analysis of the Z recoil spectrum will help to isolate the Higgs signal events. Since for Higgs masses of order 250 GeV the width is still narrow, the recoiling Z is approximately monoenergetic. The Z boson in $e^+e^- \to (\gamma^*, Z^*) + Z$ is emitted preferentially along the beam pipe so that an angular cut reduces this background with high efficiency. For high energies the Z boson produced together with the Higgs particle is longitudinally polarized and the helicity states of the signal are given by $F_H = [t_L\bar{t}_L + t_R\bar{t}_R]Z_L$. By contrast, the particles from the dominant background process are produced in the helicity states $F_V = [t_L\bar{t}_R + t_R\bar{t}_L]Z_T$ with transversely polarized Z bosons. Given a sufficiently large number of events, the measurement of the helicities can eventually be exploited to suppress the background.

Even though both reactions, Higgs bremsstrahlung off top quarks and Higgs decay to top quark pairs, are not easy to handle experimentally in view of the small cross sections, they nevertheless deserve attention as they may provide the only opportunity to measure the Higgs–fermion coupling directly.

2.4 The Threshold Region

Quark–antiquark production near the threshold in e^+e^- annihilation is of exceptional interest. The long time during which the particles stay close together, allows the strong interactions to build up rich structures of bound states and resonances, adequately described as a non–relativistic two–body system for large quark masses. This picture, familiar from the c, b quark complex, applies, *cum grano salis*, to top quarks up to the mass

range of $\sim$ 130 GeV [32]. Beyond this value, however, the rapid top decay changes the picture quite dramatically: The decay time of the states becomes shorter than the revolution time even in the $1S$ state so that toponium resonances cannot be formed any more [10,33]. For a while, remnants of the $1S$ state still lead to a peak in the excitation curve, yet it disappears gradually for t masses up to 180 GeV. Nevertheless, across this range the resonance remnants induce a steep rise of the cross section near the threshold. Since the rapid t decay restricts the interaction region to small distances, the excitation curve can be predicted in perturbative QCD [34] and is thus well under control [35]. From measurements of the cross section near the threshold one can, first of all, extract the Balmer top mass very accurately. Conservative estimates of residual theoretical uncertainties and experimental errors, including the smearing of beam energies and bremsstrahlung, lead us to expect an error Δm_t of less than 500 MeV on the top mass – improving jet mass measurements in proton colliders [9] by an order of magnitude [13,14].

Such a high accuracy is physically desirable since the top quark is expected to play a key role in a future theory of flavor dynamics. The precise measurement of the top mass will also help to refine tests of the electroweak Standard Model at the quantum level [36], Fig.10.

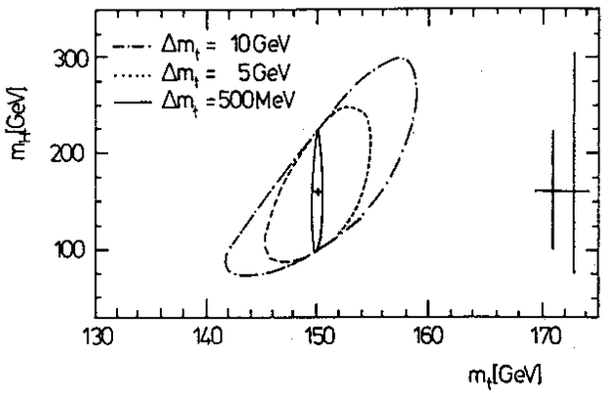

Fig. 10: *Constraints on the Higgs mass for a central value of 150 GeV from final data of LEPI, direct W–mass measurements and the left–right e^+e^- polarization asymmetry, if the t mass is determined externally with large or small error [36].*

The height of the excitation curve is sensitive to the value of the strong coupling constant α_s and, within a restricted range of the mass parameters, to the exchange of Higgs particles between the t and $\bar{t}$ quark [37,38]. If the top mass and the strong coupling constant α_s are measured through the analysis of the excitation curve, their errors are strongly correlated. This problem can be solved by measuring the momentum spectrum of the top quarks [39] which provides an orthogonal access to these parameters so that a

high precision measurement of the top quark mass can finally be performed that is largely independent of the uncertainties in α_s [40].

(a) Excitation Curve in QCD

The non–relativistic motion of heavy quarks in the lowest bound states is a self–consistent notion in QCD. The Bohr radius $a_0 = (\frac{2}{3}m_t\alpha_s)^{-1}$ and the velocity $\sim \frac{4}{3}\alpha_s$ in the ground state of the QCD Coulomb potential correspond to a non–relativistic system with small diameter for heavy quarks — justifying, in a self–consistent way, the primary assumption that the force is generated by the [perturbative] one–gluon exchange. For higher excitations the radius grows linearly with the quantum number n while the velocity drops $\sim 1/\sqrt{n}$.

The time needed to build up such a state can be estimated by the revolution time within the $t\bar{t}$ dipole, for the ground state $t_R \sim (\frac{2}{3}m_t\alpha_s^2)^{-1}$. Since the weak decay time of the resonance, on the other hand, decreases with the third power of the top mass, $t_D \sim 4\pi\sqrt{2}/G_F m_t^3$, the ground state cannot form any more if $m_t > 130$ GeV. [For higher excitations the critical top mass value decreases $\sim 1/n^{3/4}$.] At this mass value the width of the toponium state becomes larger than the $1S-2S$ level spacing and the quarkonium level structure dissolves. When the lifetime becomes still shorter, the distance the t quark travels before it decays, is limited to

$$d \sim \frac{1}{\sqrt{m_t\Gamma}} \sim \frac{350 \text{ fm}}{(m_t[\text{GeV}])^2}$$

This corresponds to less than $\sim 10^{-2}$ fm for $m_t > 130$ GeV so that top production in the threshold region is truly a short distance phenomenon in the realm of perturbative QCD.

The static interquark potential at short distances is given by a Coulomb type form

$$V(R) = -\frac{4}{3}\frac{\alpha_s(R)}{R}$$

where the strong coupling constant [in the two–loop approximation] varies with the distance R according to $\alpha_s(R) = 4\pi/[b_0 \log(\Lambda_{pot}R)^{-2} + b_1/b_0 \log\log(\Lambda_{pot}R)^{-2}]$ with $b_0 = 11 - \frac{2}{3}N_f$ and $b_1 = 102 - \frac{38}{3}N_f$. Based on the $Q\overline{Q}$ interaction energy including gluon and light quark loops the scale parameter Λ_{pot} can be related to the familiar $\overline{MS}$ parameter through [35] $\Lambda \approx 2.43\,\Lambda_{\overline{MS}}$ for $N_F = 5$ light quark degrees of freedom [appropriate to distances R between m_t^{-1} and $(\frac{2}{3}\alpha_s m_t)^{-1}$]. Thus the static interquark potential is completely specified at small distances by perturbation theory.

With rising R the perturbative part of the potential has to be connected with the expected non–perturbative linear behavior KR at large distances. However, after regularizing the artificial singularity in α_s outside the perturbative domain through the substitution $\Lambda R \to a\tanh(\Lambda R/a)$ with $a \approx 0.3$ and matching the potential to the shape required by $b\bar{b}$ and $c\bar{c}$ bound state spectra, the results do not strongly depend on a nor

on the matching procedure within wide areas of the phenomenological parameters [35]. Other prescriptions [32] for the interpolation at intermediate distances give essentially identical results. The excitation curve for heavy quarks is sensitive only to the small distance part of the interquark potential.

The excitation curve for top quarks near the threshold is built–up by the superposition of all nS states,

$$\sigma = \frac{96\pi^3\alpha^2\kappa}{s^2}\left[1 - \frac{16}{3}\frac{\alpha_s}{\pi}\right]\sum_n \Psi_n^2(0)\delta_\Gamma(E - m_n)$$

κ accounts for the [small] correction of the Z exchange in addition to the photon exchange,

$$\kappa = \left|e_e e_t + \frac{v_e v_t}{y^2}\frac{s}{s - m_Z^2}\right|^2 + \left|\frac{a_e v_t}{y^2}\frac{s}{s - m_Z^2}\right|^2$$

with $y = 4\sin\vartheta_W\cos\vartheta_W$; the square bracket describes the hard, transverse gluon correction at the $\gamma(Z)tt$ vertex that is not accounted for by the interquark potential generated by Coulombic gluons. The function $\delta_\Gamma = \Gamma_R/2\pi[(E-m_n)^2 + (\Gamma_R/2)^2]$ finally describes the Breit–Wigner form of the resonance excitation with $\Gamma_R = 2\Gamma$ being the universal width of the $t\bar{t}$ states.

For small top masses $m_t < 130$ GeV the excitation curve is built–up by the formation of individual resonances [32] properly smeared over the width of the states.

For top masses beyond 130 GeV, summing up the individual resonance contributions becomes quite cumbersome. A much more elegant method exploits the fact that the sum over the states in the cross section can be interpreted [34] as the imaginary part of the non–relativistic Green's function G at the origin for the complex energy $E + i\Gamma$, $\Im m\, G(0,0; E + i\Gamma) = \pi\sum_n \Psi_n^2(0)\delta_\Gamma(E - m_n)$. The Green's function is a solution of the Schrödinger equation with point–like source term. This equation has been solved analytically for the Coulomb potential with fixed coupling [34] and numerically for the QCD potential [35]. The cross sections [in units of the standard electromagnetic μ–pair cross section] are shown for a representative range of top masses, $m_t = 120, 150$ and 180 GeV, in Fig.11. The sequence demonstrates clearly how the increasing top quark width levels off all resonance peaks with increasing t mass. However, the cross sections continue to rise steeply within a very narrow energy interval, leading to a high sensitivity on the top mass. Notice also the sensitivity on the strong coupling constant α_s which is reparametrized to the value at the Z mass.

Even though the peaks are reduced considerably by the energy smearing of the beams, the sensitivity on m_t is not reduced much as has been demonstrated in detailed experimental simulations [13,14]. The measured t-mass value is positively correlated with the the value of α_s. Increasing the value of α_s [so that the $1S$ level would be lowered] can be compensated by increasing m_t. The one–standard deviation error in the measurement of m_t varies for $m_t = 150$ GeV between 400 and 600 MeV for narrow–band beam designs and $\delta\alpha_s = 0.005$. The error depends on m_t; for 120 GeV the error is reduced by a factor 2, for 180 GeV it is larger by a factor 2.

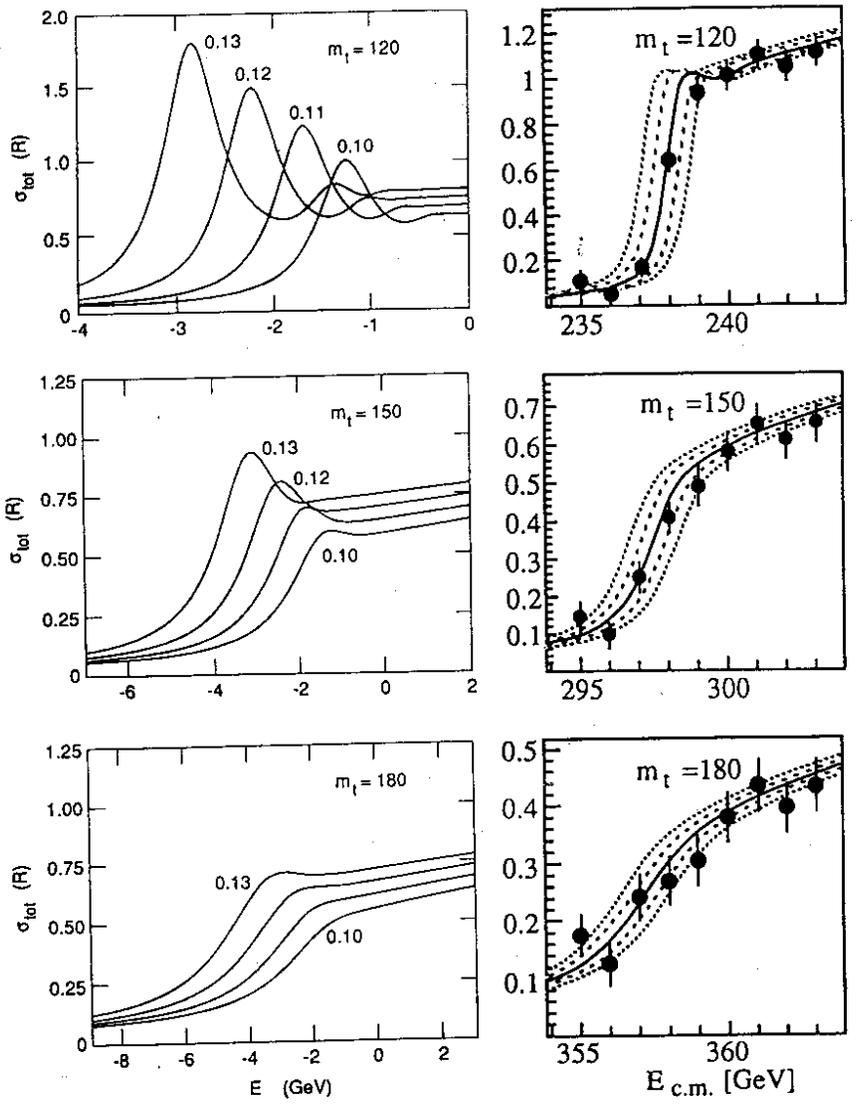

Fig. 11: *Excitation curves for t quarks near the threshold for three representative top mass values. The labels at the curves denote the α_s value at the Z mass. From Ref.[35]. On the right–hand side the excitation curves are shown after convoluting the cross sections with the TESLA luminosity function which includes beamstrahlung [13].*

(b) The Momentum Spectrum of the top–Quark

Top quarks confined by the QCD potential within the Bohr orbit, will have an average momentum of order $\langle p \rangle \sim \alpha_s m_t$, corresponding to about 15 GeV. The momentum distribution can be analyzed by measuring the momenta of the t–decay products. Since the spectrum depends on m_t and α_s, it provides another method to determine the top mass [39]. Since, on average, the product $\alpha_s m_t$ is fixed, the two parameters are not positively correlated any more so that this measurement is orthogonal to the analysis of the excitation curve [40].

(c) Higgs Exchange

For large top masses the Higgs exchange between the quarks becomes an important contribution [37,38] which affects the threshold behavior of the excitation curve. Depending on the Higgs mass value, two different approaches must be pursued to account for these effects.

For light Higgs bosons $m_H \ll m_t$ retardation can be neglected and the Higgs exchange can effectively be described by a static Yukawa potential between the t and $\bar{t}$ quarks,

$$V_H = -\frac{\sqrt{2} G_F m_t^2}{4\pi} \frac{e^{-m_H R}}{R}$$

This potential reinforces the attractive QCD potential. Hence, the Higgs exchange increases the top production cross section by increasing the wave function at the origin. For $m_H \ll a_0^{-1}$ the Higgs exchange can be incorporated in the Coulomb potential with an appropriate change of the coupling strength [35]. In the range $a_0^{-1} \ll m_H \ll m_t$, the Higgs exchange corrects the $\gamma(Z)tt$ vertex locally and it can be interpreted as enhancement of the vectorial form factor [38]

$$\Delta F_1 = \frac{\sqrt{2} G_F}{4\pi} \frac{m_t^3}{m_H} \left[1 + \frac{2}{\pi} \frac{m_H}{m_t} \log \frac{m_H}{m_t} + \cdots \right]$$

The $1/m_H$ behavior is reminiscent of the $1/\beta$ enhancement of the QCD form factor cut–off by the non–zero Higgs mass.

For Higgs masses not much below the top mass, retardation effects play an important role and the full set of electroweak corrections must be calculated. The Higgs vertex corrections are the dominant corrections only for light Higgs particles and heavy top masses. For realistic values like $m_t = 150$ GeV and $m_H = 100$ GeV they are small, about 5%, and of a size comparable to the remaining non–Higgs contributions to the weak corrections.

2.5 The QCD Coupling Constant

The experimental analysis of the $t\bar{t}$ threshold region will allow us to measure the QCD coupling constant with an error of about 0.005. An independent measurement of α_s can be performed by measuring the annihilation cross section into jets [41]. The 3–jet fraction is directly proportional to α_s. The prospects for measuring the 3–jet fraction at $\sqrt{s} = 500$ GeV are shown in Fig.12. The analysis will provide a clear and stringent test of asymptotic freedom down to distances of order 10^{-3} fermi.

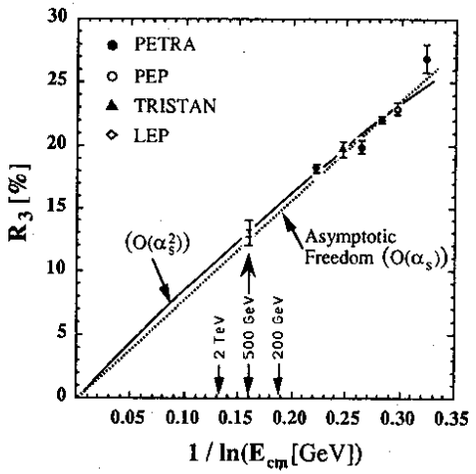

Fig. 12: *Energy dependence of the QCD coupling constant, as extracted from the 3–jet fraction in e^+e^- annihilation to hadrons [light quarks].*

3. Electroweak Gauge Bosons : Standard Model and Extensions

3.1 W, Z Bosons in the Standard Model

The fundamental electroweak and strong forces appear to be of gauge theoretical origin. This is one of the outstanding results of theoretical and experimental analyses in the past decades. While the non–abelian gauge theoretical nature of QCD has been succesfully demonstrated by evaluating the distribution of hadronic jets in Z decays, only indirect evidence has been claimed so far for the electroweak $W^\pm$, Z, γ sector, based on loop–corrections to low–energy parameters and Z observables. HERA, LEP200 and the Tevatron can shed light, for the first time directly, on the triple couplings of the electroweak gauge bosons as prescribed by the gauge symmetries [42]. Since deviations from the gauge symmetry prescriptions manifest themselves in experimental observables with coefficients $(\beta\gamma)^2$, only the very high energies of future pp end e^+e^- colliders will allow for stringent direct tests of the self-couplings of the electroweak gauge bosons. The high efficiency of reconstructing W, Z bosons in the clean environment of e^+e^- collisions makes a 500 GeV collider competitive even with the SSC [43–45].

The gauge symmetries of the Standard Model determine the form and the strength of the self–interactions of the electroweak bosons, triple couplings $WW\gamma, WWZ$ and quartic couplings $WWWW, WWZZ$ and $WW\gamma\gamma$. Deviations from the gauge symmetry values of these vertices, as well as novel couplings like ZZZ or $ZZ\gamma\gamma$ in addition to the canonical $\mathcal{SM}$ couplings could be expected in more general scenarios. In models with composite W, Z bosons for instance, corrections could alter the vertices to order $M_W/\Lambda_{\rm comp}$ and induce new types of couplings. Other examples are provided by models in which the W, Z bosons are generated dynamically or interact strongly with each other. While the experimental analysis of the self–couplings of the electroweak bosons can be carried out at collider energies of 500 GeV with high accuracy [43,44,45], WW scattering can only be studied at energies in the TeV range [46,47,45]. This is a very important process to be investigated if light Higgs particles do not exist and W bosons become strongly interacting particles at high energies. We shall discuss this alternative to the canonical $\mathcal{SM}$ briefly at the end of this section.

A large number of W^+W^- pairs will be produced in e^+e^- collisions at high energies. The reaction is mediated by neutrino exchange in the t–channel and γ, Z exchange in the s–channel. For an integrated luminosity of $\int \mathcal{L} = 10$ fb^{-1}, the cross section [48]

$$\begin{aligned}\sigma(e^+e^- \to W^+W^-) = \frac{G_F^2 M_W^4 \beta}{\pi s}\Bigg\{&\left[1 + 2\gamma^{-2} + 2\gamma^{-4}\right]\frac{1}{\beta}\log\frac{1+\beta}{1-\beta} - \frac{5}{4} \\ &+ \frac{M_Z^2(1 - 2\sin^2\vartheta_W)}{s - M_Z^2}\left[2(2\gamma^{-2} + \gamma^{-4})\frac{1}{\beta}\log\frac{1+\beta}{1-\beta} - \frac{\gamma^2}{12} - \frac{5}{3} - \gamma^{-2}\right] \\ &+ \frac{M_Z^4(8\sin^4\vartheta_W - 4\sin^2\vartheta_W + 1)}{48(s - M_Z^2)^2}\beta^2\left[\gamma^4 + 20\gamma^2 + 12\right]\Bigg\}\end{aligned}$$

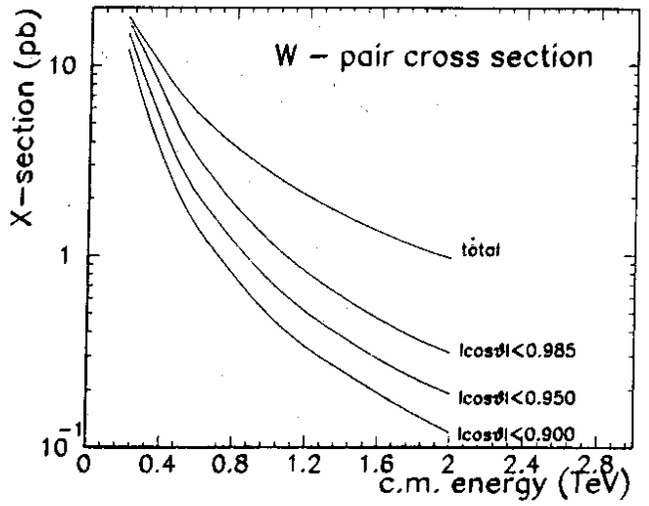

Fig. 13: *W–pair production cross section for c.m. energies between 200 GeV and 2 TeV. Also shown is the reduction of the cross sections for limited experimental acceptance near the beam pipe; from Ref.[49].*

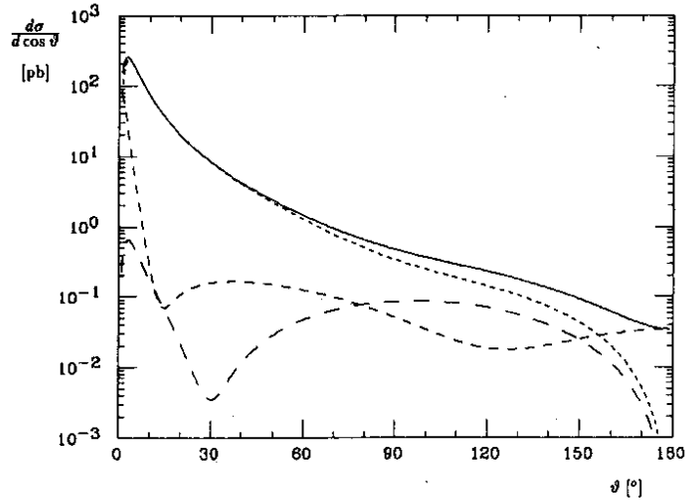

Fig. 14: *Differential cross section for unpolarized electrons at 500 GeV. The solid curve corresponds to unpolarized W's, the dashed curves, in order of increasing dash length, correspond to transverse, mixed and longitudinal W polarizations. From Ref.[43].*

(where β denotes the velocity of the W bosons and $\gamma = E/M_W$ leads to the large number of $\sim 10^5$ events at $\sqrt{s} = 500$ GeV, Fig.13. Most of the W^- bosons are produced in the direction of the incoming electron. This is shown in Fig.14 in which the differential cross section is broken down to the transverse, mixed transverse–longitudinal and longitudinal W helicities.

(a) The Triple Gauge Boson Couplings

The couplings $W^+W^-\gamma$ and W^+W^-Z are, in general, described by seven parameters each. Assuming $\mathcal{C}, \mathcal{P}$ and $\mathcal{T}$ invariance in the pure boson sector, the number of parameters can be reduced to three, which may be defined as

$$\mathcal{L}_\gamma/g_\gamma = ig^1_\gamma W^+_{\mu\nu}W^\mu A^\nu + \text{h.c.} \; + \; i\kappa_\gamma W^+_\mu W^-_\nu F_{\mu\nu} \; + \; i\frac{\lambda_\gamma}{M_W^2}W^+_{\rho\nu}W_{\mu\nu}F_{\nu\rho}$$

$$\mathcal{L}_Z/g_Z = ig^1_Z W^+_{\mu\nu}W^\mu Z^\nu + \text{h.c.} \; + \; i\kappa_Z W^+_\mu W^-_\nu Z_{\mu\nu} \; + \; i\frac{\lambda_Z}{M_W^2}W^+_{\rho\nu}W_{\mu\nu}Z_{\nu\rho}$$

While g^1_γ and g^1_Z are the electric and Z charges of the W bosons, the coefficients $\kappa_{\gamma,Z}$ and $\lambda_{\gamma,Z}$ are related to the corresponding magnetic dipole moments and electric quadrupole moments of the W bosons,

$$\mu_\gamma = \frac{e}{2M_W}(1 + \kappa_\gamma + \lambda_\gamma) \quad \text{and} \quad [\gamma \to Z]$$

$$Q_\gamma = -\frac{e}{M_W^2}(\kappa_\gamma - \lambda_\gamma) \qquad \text{and} \quad [\gamma \to Z]$$

The gauge symmetries of the $\mathcal{SM}$ demand $g_{\gamma,Z} = 1$ for the charges, and $\kappa_{\gamma,Z} = 1$ and $\lambda_{\gamma,Z} = 0$ for the anomalous moments at tree level.

Symmetries of the underlying dynamical interactions may constrain the generalized couplings. For example [50],

- (A) custodial/local SU(2)$_I$ symmetry : $\lambda_\gamma = \lambda_Z = \lambda$ and $\kappa_\gamma = \kappa_Z = 1$
- (B) no intrinsic SU(2)$_I$ violation and no quadratic energy terms : $\kappa_\gamma \neq 1$ and $g^1_\gamma = 1, \lambda_\gamma = \lambda_Z = 0, \kappa_Z = 1 - (\kappa_\gamma - 1)\text{tg}\theta_W, g^1_Z = -\text{tg}^2\theta_W + \kappa_\gamma/\cos^2\theta_W$

Bounds on the anomalous moments can be derived from high–precision measurements of electroweak observables which are affected by W–loop corrections [51]. These effects have been discussed for the Z boson parameters and for atomic parity violation. While some aspects can be studied very well, blind directions prevent a general and comprehensive analysis.

The magnetic dipole and the electric quadrupole moments can be measured *directly* through the production of electroweak bosons at $p\bar{p}/pp$ and e^+e^- colliders. Modifications of the self–coupling vertices destroy the unitarity cancellations in the $\mathcal{SM}$ between interfering boson and fermion exchange amplitudes for longitudinal gauge boson production.

As a result, small deviations of the moments from their $\mathcal{SM}$ values are magnified by a coefficient $(\beta\gamma)^2$, so that a 500 GeV e^+e^- collider will have a sensitivity more than one order of magnitude greater than LEP200.

The analysis of $W\gamma$ final states at $p\bar{p}$ colliders led to bounds of $\mathcal{O}(1)$ for the anomalous photonic couplings. From the $W\gamma$ production cross sections at the future proton colliders LHC/SSC, bounds of order $|\lambda_\gamma| \leq 0.02$ and $|\kappa_\gamma - 1| \leq 0.1$ are expected [52], while information on λ_Z and κ_Z may be extracted from WZ final states.

High energy e^+e^- colliders are ideal machines for probing the self-interactions of the electroweak gauge bosons. The main reaction to be exploited is W pair production

$$e^+e^- \longrightarrow W^+W^-$$

Additional and complementary information can be obtained from the WW fusion to Z bosons [53]

$$e^+e^- \to \bar{\nu}\nu\,(WW) \to \bar{\nu}\nu Z$$

and, in particular if laser induced γ beams are available, from [54]

$$e^-\gamma \to \nu W^- \qquad \text{and} \qquad \gamma\gamma \to W^+W^-$$

These processes are sensitive separately to γ and Z couplings so that they can help to disentangle $\kappa_\gamma, \lambda_\gamma$ from κ_Z, λ_Z. Very tight bounds on the anomalous moments can be obtained [50,49] if deviations from the $\mathcal{SM}$ values are constrained by the symmetry requirements (A) and (B) introduced above

$$\begin{aligned} (A)\quad & \lambda_\gamma = \lambda_Z = -0.010 \;\to\; +0.002 \\ (B)\quad & \kappa_\gamma - 1 \;= -0.014 \;\to\; +0.000 \end{aligned}$$

If all κ_i and λ_i are allowed to vary freely, the anomalous moments can be probed [45] to an accuracy of

$$|\kappa_\gamma - 1|\,,\ |\kappa_Z - 1|\,,\ |\lambda_\gamma|\,,\ |\lambda_Z| \quad \leq 0.02$$

These bounds, Fig. 15a, follow from the combined analysis of the W pair production cross section and the angular distributions of the W decay products which allow to separate the various W helicity components. To disentangle γ from Z couplings in this reaction, longitudinal beam polarization is essential. With beamstrahlung included properly, the bounds are based on an integrated luminosity of 10 fb^{-1}.

The bounds on $|\kappa_\gamma - 1|$ and $|\lambda_\gamma|$ that can be reached at e^+e^- linear colliders are compared with the values expected at the SSC from the measurement of the $W\gamma$ cross section in Fig. 15b. The e^+e^- linear colliders, even at $\sqrt{s} = 500$ GeV, are apparently at least as powerful as the multi-TeV pp colliders, a result of the high efficiency for reconstructing W bosons.

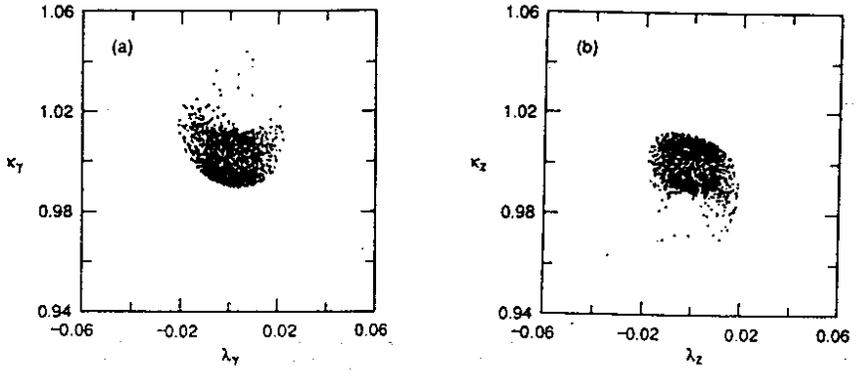

Fig. 15: (a) *Projections onto the $(\kappa_\gamma, \lambda_\gamma)$ and (κ_Z, λ_Z) planes of the 95% CL joint probability ellipsoid for a four parameter fit. $\sqrt{s} = 500$ GeV and $\int \mathcal{L} = 10$ fb^{-1} are assumed. From Ref. [45].*

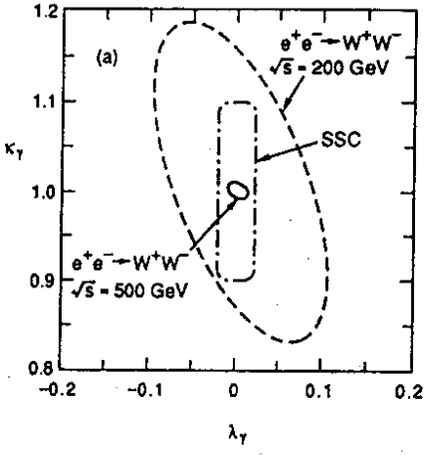

Fig. 15: (b) *Projections onto the $(\kappa_\gamma, \lambda_\gamma)$ plane of the 95% CL joint probability ellipsoid. $\mathcal{SM}$ values are assumed for (κ_Z, λ_Z) in the e^+e^- analysis; this assumption can be avoided at the expense of slightly larger integrated luminosities. Luminosities of $\int \mathcal{L} = 10$ fb^{-1} at $\sqrt{s} = 500$ GeV, $\int \mathcal{L} = 1.3$ fb^{-1} at $\sqrt{s} = 200$ GeV and $\int \mathcal{L} = 10$ fb^{-1} at the SSC are assumed. From Ref. [45].*

(b) Quartic Couplings

While the measurements of the triple couplings probe possible deviations from the non-abelian gauge symmetries due to novel interactions, the quartic couplings can provide a window to mechanisms of the electroweak symmetry breaking other than the light Higgs scenario of the $\mathcal{SM}$. New $WWWW$ couplings, for instance, can be induced by the exchange of heavy scalar particles.

The analysis of quartic couplings is still in the first phase of theoretical-phenomenological estimates [55]. Possible deviations from the quartic couplings prescribed by the gauge symmetries, are in general restricted to globally $SU(2)_W$ invariant interactions. For example,

$$(A)\ \dim = 4\ :\ \mathcal{L}_4^0 = \frac{1}{4} g_0 g_W^2 (\vec{W}_\mu \vec{W}_\mu)^2\ ,\ \mathcal{L}_4^c = \frac{1}{4} g_c g_W^2 (\vec{W}_\mu \vec{W}_\nu)^2$$

These interactions give rise to $WWWW, WWZZ$ and $ZZZZ$ couplings which can be probed in the reactions

$$e^+e^- \longrightarrow W^+W^-Z \text{ and } ZZZ$$

Since these 3–particle cross sections are much smaller than those for W pair production, the bounds on quartic anomalies are correspondingly weaker, $|g_0| \leq 0.2$ and $|g_c| \leq 0.3$.

$$(B)\ \dim = 6\ :\ \mathcal{L}_6^0 = -\frac{\pi\alpha}{4\Lambda^2} a_0 \vec{W}_\mu^2 F_{\nu\rho}^2\ ,\ \mathcal{L}_6^c = -\frac{\pi\alpha}{4\Lambda^2} a_c (\vec{W}_\mu F_{\mu\rho})^2$$

[F is the electromagnetic field]. These anomalous couplings can be measured in reactions such as

$$e^+e^- \to W^+W^-\gamma \text{ and } ZZ\gamma$$

The highest sensitivity however, can be achieved in the colliding $\gamma\gamma$ process

$$\gamma\gamma \to ZZ$$

[which is forbidden in the $\mathcal{SM}$ at tree level]: $|a_0| < 3 \times 10^{-3}$ and $|a_c| < 6 \times 10^{-3}$ for $\Lambda = M_W$. The energy scale which can effectively be probed, $M_W/\sqrt{a}$, is of the order of a TeV.

(c) Strongly Interacting W, Z Bosons

If the scenario in which W, Z, Higgs bosons are weakly interacting up to the GUT scale [requiring a Higgs mass of less than 200 GeV] is not realized in Nature, the next possible scenario is a strongly interacting W, Z sector. Without a light Higgs of less than about 1 TeV, the electroweak bosons must become strongly interacting at energies of about 1.2 TeV [56] to fulfill the requirements of unitarity. New strong interactions may build up the longitudinal degrees of freedom of the massive vector bosons in technicolor theories, for instance. In such a case, new types of resonances could be realized in the $\mathcal{O}(1$ TeV) range; however, the formation of resonances in W_LW_L scattering could also be delayed until several TeV [47,57].

In the strongly interacting vector boson scenario, W_LW_L scattering must be studied at $\mathcal{O}(1$ TeV) energies which requires the highest energies possible beyond 1 TeV at e^+e^- colliders. (Quasi)elastic WW scattering can be investigated by using W's radiated off the $e^\pm$ beams [47], or by exploiting final state interactions in e^+e^- annihilation to W pairs [46]. All possible (isospin, angular momentum) combinations in WW scattering

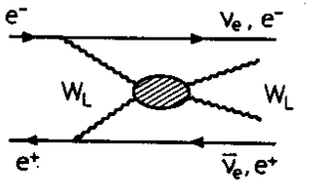

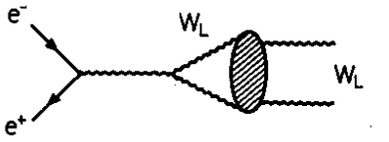

e^+e^-: $W^+W^- \to W^+W^-, ZZ$
$W^\pm Z \to W^\pm Z\ ,\ ZZ \to ZZ$
e^-e^-: $W^-W^- \to W^-W^-$

$e^+e^- \to W^+W^- \to W^+W^-$

amplitudes a_{IJ} can be realized in the first process. The cross sections however are small as long as no resonances are formed. Since the invariant WW energy is distributed continuously and energy is lost in the bremsstrahl process $e \to W$, the backgrounds, in particular $\gamma\gamma \to WW$, are difficult to suppress. A complementary method is the rescattering method in e^+e^- annihilation to W^+W^- pairs in which the $(I,J) = (1,1)$ WW scattering phase shift enters through the Omnès factor [46],

$$a_{11} = a_{11}^{(0)} \exp\left[\frac{s}{\pi}\int \frac{ds'\delta_{11}(s')}{s'(s'-s)}\right]$$

Building up the vector boson masses through spontaneous breaking of the electroweak symmetries, the longitudinal degrees of freedom of the vector bosons can be identified at high energies with the Goldstone bosons associated with the spontaneous symmetry breaking. In analogy to the $\pi\pi$ low–energy theorems, the first terms in the energy expansion of the WW scattering amplitudes are determined independently of dynamical details [47],

$$a_{00} = +\frac{s}{16\pi v^2} \qquad \text{attractive}$$

$$a_{11} = +\frac{s}{96\pi v^2} \qquad \text{attractive}$$
$$a_{20} = -\frac{s}{32\pi v^2} \qquad \text{repulsive}$$

where $v = 246$ GeV. The attractive $I = 0$ and 1 channels may form Higgs and ρ–type resonances at high energies.

While "H, ρ" resonances would alter the scattering amplitudes dramatically compared with the predictions in a light–Higgs scenario, the low–energy theorems nevertheless affect the cross sections significantly. For $\sqrt{s} = 1.5$ TeV and $\sqrt{s_{WW}} > 500$ GeV, the predictions in the weak scenario with a light Higgs mass are confronted with the strong scenario in the following table [47]:

σ [fb]	Weak Scenario	Strong Scenario
$e^+e^- \to \overline{\nu}\nu WW$	0.45	0.68
$e^+e^- \to \overline{\nu}\nu ZZ$	0.37	0.74

Similar effects would also be observed in $\sigma(e^+e^- \to W^+W^-)$ [46]. $(I, J) = (1, 1)$ resonance effects would be noticeable at $\sqrt{s} = 1$ TeV up to resonance masses of about 5 TeV in angular distributions of the W decay final states [45].

3.2 Extended Gauge Theories*

Despite of its tremendous success in describing the experimental data within the range of energies available today, the Standard Model based on the gauge symmetry SU(3) × SU(2) × U(1) is widely believed not to be the *ultima ratio*. Besides the fact that it has too many parameters which are merely incorporated by hand, the $\mathcal{SM}$ does not unify the electroweak and strong forces in a satisfactory way since the coupling constants of these interactions are different and appear to be independent. Therefore one would expect that a more fundamental theory exists which describes the three forces within the context of a single gauge group and hence, with only one coupling constant. This grand unified theory will be based on a gauge group containing SU(3) × SU(2) × U(1) as a subgroup and it will be reduced to this symmetry at low energies.

Two predictions of grand unified theories can have dramatic phenomenological consequences in the energy range of a few hundred GeV:

(i) The unifying group must be spontaneously broken at the unification scale, $\Lambda_{GUT} > 10^{15}$ GeV in order to be compatible with the experimental bounds on the proton lifetime. However, it is possible that the breaking to the $\mathcal{SM}$ group occurs in several steps and

*in collaboration with A. Djouadi

that some subgroups remain unbroken down to a scale of order 1 TeV. In this case the surviving group factors allow for new gauge bosons with masses not far from the scale of electroweak symmetry breaking.

(ii) The grand unified groups incorporate fermion representations in which a complete generation of $\mathcal{SM}$ quarks and leptons can be naturally embedded. In most of the cases these representations are large enough to accomodate additional new fermions which are needed to have anomaly–free theories. It is conceivable that these new fermions [if they are protected by symmetries, for instance] acquire masses not much larger than the Fermi scale. This is very likely, and even necessary if the predicted new gauge bosons are relatively light.

The direct search for these new fermions and gauge bosons and tests of indirect effects will be a major goal of the next generation of accelerators [58].

Besides the SU(5) group which has no room for "light" new gauge bosons or new fermions [the simplest Lie group containing SU(3)×SU(2)×U(1) as a subgroup and two representations to accomodate the 15 $\mathcal{SM}$ fermions], two other unifying groups have received much attention in recent years, SO(10) and the exceptional group E_6.

SO(10) is the simplest group in which the 15 Weyl spinors of each $\mathcal{SM}$ generation of fermions can be embedded into a single multiplet. This representation has dimension **16** and contains a right–handed neutrino

$$\begin{bmatrix}\nu_e\\ e\end{bmatrix}_L \quad e_R \quad \begin{bmatrix}u\\ d\end{bmatrix}_L \quad \begin{matrix}u_R\\ d_R\end{matrix} \quad ; \quad \nu_{eR}$$

The gauge group can be spontaneously broken to the $\mathcal{SM}$ group at an intermediate scale, two interesting chains of breaking patterns being via SU(5)×U(1) or SU(4)× SU(2)×SU(2), leading to the intermediate symmetries

$$\begin{aligned} \mathrm{SO(10)} \to \quad & \mathrm{SU(3) \times SU(2) \times U(1) \times U(1)_\chi} \quad \to \mathrm{SU(3) \times SU(2) \times U(1)} \\ \to \ & \mathrm{SU(3)_C \times SU(2)_L \times SU(2)_R \times U(1)_{B-L}} \to \mathrm{SU(3) \times SU(2) \times U(1)} \end{aligned}$$

These chains would induce new right–handed charged currents and/or neutral currents which could eventually be studied at TeV energies.

Another popular unifying group is E_6. It contains SU(5) and SO(10) as subgroups and is the next anomaly–free choice after SO(10). The interest in this group is mainly due to the fact that superstring theories, which attempt to unify all fundamental forces including gravity, suggest this theory as a possible four dimensional field theoretic limit. In E_6, each quark–lepton generation lies in a representation of dimension **27**. To complete this representation, twelve new fields are needed in addition to the $\mathcal{SM}$ fermion fields. For each family one has two additional isodoublets of leptons, two isosinglet neutrinos and an isosinglet quark with charge $-1/3$,

$$\begin{bmatrix}\nu_E\\ E\end{bmatrix}_L \quad \begin{bmatrix}\nu_E\\ E\end{bmatrix}_R \quad n \quad n' \quad D_L \quad D_R$$

In the breaking of E_6 down to the $\mathcal{SM}$ gauge group, two additional U(1) symmetry factors may survive at low energies

$$E_6 \to SO(10) \times U(1)_\psi \to SU(5) \times U(1)_\chi \times U(1)_\psi$$
$$\to SU(3) \times SU(2) \times U(1) \times U(1)_\chi \times U(1)_\psi$$

leading to two new neutral gauge bosons. Assuming that only one of them is light, the relevant neutral gauge boson would be $Z' = Z_\chi \cos\beta + Z_\psi \sin\beta$, where β=0 and $\pi/2$ correspond to pure Z_χ and Z_ψ while $\beta = \text{arctg}(-\sqrt{5/3})$ corresponds to the model η in which E_6 is directly broken to a rank–5 group at the unification scale in superstring models.

Several other gauge groups have been considered, based on various theoretical motivations. For instance, schemes of grand unification built on large orthogonal groups have been proposed to explain the origin of parity violation in weak interactions. In these models, weak interactions are $\mathcal{P}$ invariant but fermions with left–handed and right–handed couplings acquire different masses. They predict a new spectrum of fermions, mirror fermions [59], which have chiral properties opposite to the ordinary particles. In the simplest version of these models, the gauge symmetry and the symmetry breaking pattern are the same as in the Standard Model; three families of heavy fermions with opposite chiralities are simply added to the $\mathcal{SM}$ spectrum

$$\begin{bmatrix} N_R \\ E_R \end{bmatrix} \quad N_L \quad \begin{bmatrix} U_R \\ D_R \end{bmatrix} \quad U_L \quad D_L$$

Theoretical arguments based on [weak coupling] unitarity suggest that the masses of these mirror fermions should not exceed a few hundred GeV.

(a) New Gauge Bosons

The existence of an extra neutral gauge boson with a mass below the maximal energy of the e^+e^- collider will provide a new resonance which will increase the e^+e^- annihilation cross section by several orders of magnitude. In this case, an e^+e^- collider operating at the resonance peak would be a "Z' factory" allowing to measure the couplings of the Z' to other conventional and new particles with very high precision, a situation comparable to the LEP experiments exploring the Z peak. High–energy e^+e^- colliders would then be ideal instruments to study the properties of the new gauge bosons.

Even if a new vector boson is too heavy to be produced as a resonance, it could give rise to virtual effects which are measurable. Indeed, besides mixing with the Z, a new heavy Z' will participate in the production process of ordinary fermions [60,61]

$$e^+e^- \longrightarrow \gamma, Z, Z' \longrightarrow f\bar{f}$$

and it will affect the cross sections and the various asymmetries through its propagator effects. The clean environment of e^+e^- colliders allows to probe these virtual effects

with high precision and therefore provides a sensitivity to Z' masses considerably higher than the available center of mass energy. In addition, because of the large number of observables which can be measured precisely, a detailed investigation of the properties of the new Z' boson can be performed and its origin can be identified.

The virtual effects of a new Z' associated with the most general effective theories which arise from breaking E_6, $SU(3) \times SU(2) \times U(1) \times U(1)_{Y'}$ and $SU(2)_L \times SU(2)_R \times U(1)$, have been investigated in Ref. [61]. Assuming that the Z' is heavier than the c.m. energy, its propagator effects on various observables of the process $e^+e^- \to f\bar{f}$ have been studied. The leptonic cross section and the forward–backward asymmetry σ^{lep} and A_{FB}^{lep}, the ratio of the hadronic and leptonic cross section $R = \sigma^{\text{had}}/\sigma^{\text{lep}}$ as well as the polarization asymmetries A_{LR}^{had} and A_{LR}^{lep} were shown to be best suited to probe high Z' masses and to discriminate between various models.

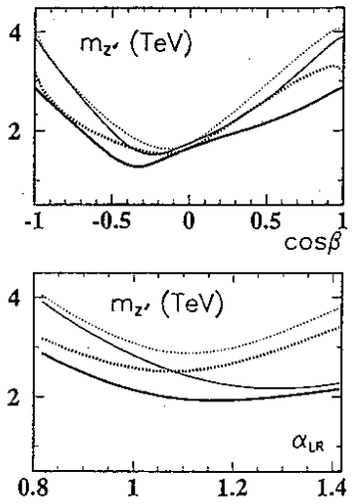

Fig. 16: (a) *Z' mass limits in models with an extra U(1) and left–right models. Solid (dotted) lines: without (with) polarization.*

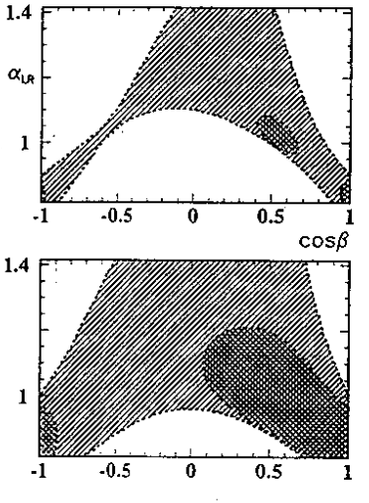

Fig. 16: (b) *Distinction between models with an extra U(1) and left–right models. Top (bottom): $M_{Z'}$ =1.5 (2) TeV.*

Assuming an integrated luminosity of 20 fb^{-1} and a cut on the final state fermion energy $\Delta = 0.7$, Fig. 16a demonstrates that when combining the measurements of σ^{lep}, A_{FB}^{lep} and $R = \sigma^{\text{had}}/\sigma^{\text{lep}}$, the effects of the new Z' can be probed for masses up to 3 TeV at the 95% confidence level without polarization [thick solid curve]. Assuming that longitudinal polarization is available, this value can be extended up to 3.5 TeV for certain values of the model parameters [thick dotted curve]. In the ideal case of vanishing systematic errors [thin curves], Z' masses up to 4 TeV can be probed for certain parameter values. An excellent distinction between extra U(1) and left–right models can be obtained for Z'

masses below 1.5 TeV. Fig. 16b shows that only a small confusion region [the hatched area] remains in this case. The increase of the sensitivy if polarization is available, is very important since in this case the confusion region [cross hatched area] becomes much smaller. Finally, the determination of the model parameters themselves is also possible up to masses of similar size.

At pp colliders, Z' discovery limits range up to 3–5 TeV at the LHC and up to 5–6 TeV at the SSC. However, due to the difficult environment, the identification of the origin of the Z' will probably be limited to masses below 1 to 2 TeV. If a new Z' with such a mass is found at LHC/SSC, a 500 GeV e^+e^- collider would give valuable complementary information on its detailed properties.

(b) New Fermions

The new leptons and quarks will mix with the ordinary fermions of the Standard Model. The mixing will give rise to new currents which determine to a large extent their decay properties, and allow for new production mechanisms [62]. LEP data restrict the mixing angles to values smaller than $\mathcal{O}(10^{-1})$ [63] and the masses of new states [except for the singlet neutrinos] to values larger $M_Z/2$. For mixing angles close to the upper limit, the mass range between $M_Z/2$ and M_Z is also excluded. [This range will also be probed through pair production at LEP200.]

If the new particles have non–zero electromagnetic and weak charges, they can be pair produced if their masses are smaller than the beam energy of the e^+e^- collider [62,64,65]. In general, the reactions are built–up by a superposition of γ and Z exchange, but additional contributions could come from the extra neutral bosons if their masses are not much larger than the c.m. energy. At a 500 GeV collider, the cross sections are fairly large [64,65], up to phase space suppression factors, of the order of the point–like QED cross section $\sigma(e^+e^- \to F\bar{F}) \sim \sigma_0 \simeq 400$ fb. This leads to samples of several thousands events. The large number of events allows to probe masses up to the kinematical limit of 250 GeV. In some cases, the singlet neutrinos can be produced with sufficient rates if a Z' boson with a mass below 1 TeV exists. The cross sections for E_6 lepton pair production at $\sqrt{s} = 500$ GeV are shown in Fig. 17a in units of σ_0, $R_L = \sigma(e^+e^- \to L\bar{L})/\sigma_0$; the solid lines are the predictions in the limit of a very heavy Z' [the cross sections for mirror leptons are of similar size] while the dashed lines include the contribution of the extra SO(10) Z' with a mass of 700 GeV. For a heavy Z', the zero–values of the forward–backward asymmetries of E_6 leptons clearly indicate the vectorial nature of their couplings; the forward–backward asymmetries of mirror leptons are of opposite sign to those of fourth generation leptons.

Fermion mixing allows an additional production mechanism for the new fermions: single production in association with their light partners. In this case, masses very close to the total energy of the e^+e^- collider can be reached. For the second and third generation of leptons [if inter–generational mixing is neglected] and for quarks, the process proceeds only through s–channel Z exchange and leads to relatively small cross sections. But in

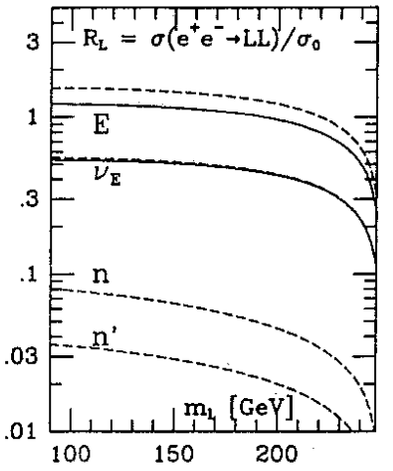

Fig. 17: (a) *Cross sections for the pair production of E_6 leptons in units of σ_0. The solid (dashed) lines correspond to $M_{Z'} = \infty$ ($M_{Z'} = 700$ GeV).*

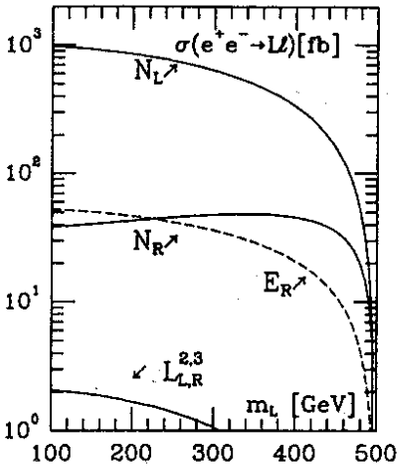

Fig. 17: (b) *Cross sections for the single production of E_6 leptons. N standards generically for ν_E, n and n'.*

the case of the first generation leptons, additional t–channel exchanges [W exchange for neutral leptons and Z exchange for charged leptons] are present, increasing the cross sections by several orders of magnitude. The cross sections [64] are shown in Fig. 17b for E_6 leptons at $\sqrt{s} = 500$ GeV, with the left and right–handed mixing angles set to $\zeta_L, \zeta_R = 0.1$ i.e. close to the upper limits. In the case of the first generation neutral and charged leptons, the important contributions of the t–channel Z or W exchanges result in large production cross sections, allowing the discovery of these particles up to masses close to 500 GeV. The production cross sections for the leptons of the second and third generations $L^{2,3}$ [and for quarks] are much smaller; they could nevertheless provide direct information, for the first time, on the mixing angles in these families.

For masses larger than M_Z, the new fermions will decay into ordinary fermions and on–shell weak bosons. At e^+e^- colliders, the signals are clear and rather easy to separate from backgrounds due to conventional processes. Once these particles have been found, the clean environment allows the detailed investigation of their properties: measurement of their masses, determination of their couplings and quantum numbers. Angular distributions and the polarization of the heavy final states can be exploited to discriminate between particles of different nature [e.g. Majorana or Dirac neutrinos] or with different couplings [e.g. vector or standard chiral couplings in pair production, or with left or right–handed mixing in single production].

4. HIGGS PARTICLES

The Higgs mechanism is a cornerstone in the electroweak sector of the Standard Model. The fundamental particles, leptons, quarks and weak gauge bosons, acquire their masses through the interaction with a scalar field. The self–interaction of the scalar field leads to a non–zero field strength in the ground state, inducing the spontaneous breaking of the electroweak SU(2)×U(1) symmetry down to the electromagnetic U(1) symmetry.

To accomodate the well–established electromagnetic and weak phenomena, this mechanism for generating particle masses requires the existence of at least one weak iso–doublet scalar field. The three Goldstone bosons among the four degrees of freedom are absorbed to build up the longitudinal polarization states of the massive $W^{\pm}, Z$ gauge bosons. One degree of freedom is left–over, corresponding to a real physical scalar particle. The discovery of this Higgs particle is the *experimentum crucis* for the standard formulation of the electroweak interactions.

The only unknown parameter in the $\mathcal{SM}$ Higgs sector is the mass of the Higgs particle. Even though the value of the Higgs mass cannot be predicted in the Standard Model, interesting constraints can be derived from assumptions on the energy range within which the model be valid before perturbation theory breaks down at a scale Λ and new dynamical phenomena would emerge.

(*i*) If the Higgs mass were larger than $\sim$ 1 TeV, gauge bosons would interact strongly with each other to ensure unitarity in the scattering of the massive gauge bosons at high energies [66]. Residual final state interactions in $e^+e^- \to W^+W^-$ would be too small to be observable in the 500 GeV energy range. This scenario which can eventually be studied at proton colliders in an exploratory way, would require machines operating at energies well beyond the 1 TeV range.

(*ii*) The strength of the Higgs self–interaction is determined by the Higgs mass itself at the scale M_H. Increasing the scale, the quartic self–coupling of the Higgs field grows logarithmically with the energy scale [67,68], similarly to the electromagnetic coupling in QED. If the Higgs mass is small, the energy cut–off Λ is large at which the coupling grows beyond any bound and new phenomena may be observed; conversely, if the Higgs mass is large, the cut–off Λ is small. The condition $M_H < \Lambda$ sets an upper limit on the Higgs mass in the Standard Model. Thorough analyses of the non–perturbative regime near the cut–off lead to an estimate of about 630 GeV for the upper limit of M_H. However, if the Higgs mass is less than 180 to 200 GeV, the Standard Model can be extended up to the GUT scale $\Lambda_{\rm GUT} \sim 10^{15}$ GeV with weakly interacting particles. Including the effect of t–quark loops on the running coupling, a detailed analysis predicts the area of the allowed (m_t, M_H) values shown in Fig. 18 for several values of the cut–off parameter Λ.

On quite general grounds, the hypothesis that interactions between W, Z bosons and Higgs particles remain weak up to the GUT scale, is an attractive idea and may play a key rôle in the explanation of the experimental value of the electroweak mixing parameter $\sin^2\theta_W$. Based on the $\mathcal{SM}$ particle spectrum, the mixing parameter evolves from the

symmetry value 3/8 at the GUT scale down to ~ 0.2 at $\mathcal{O}(100$ GeV) [69]. Even though additional degrees of freedom are needed [70] to account for the small discrepancy to the experimentally observed value 0.23, the hypothesis that the particle interactions remain weak up to the GUT scale, is nevertheless qualitatively supported by this result.

(*iii*) Top–quark quantum corrections to the quartic Higgs coupling are negative, driving the coupling for large t masses to negative values for which the vacuum becomes instable. The boundary on the right hand side of the allowed domain in the (m_t, M_H) plane corresponds to the values where the quartic coupling vanishes. For top masses larger than about 100 GeV, this leads to a lower limit on the Higgs mass. [The (m_t, M_H) mass pairs are attracted by the line connecting the tips of the allowed areas if the theory evolves from the cut–off energies Λ down to the $\mathcal{O}(100$ GeV) range [71].]

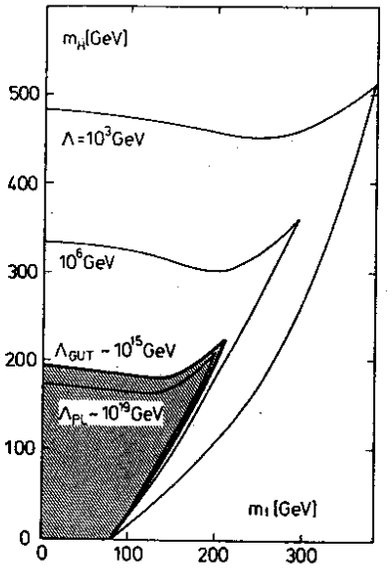

Fig. 18: *Allowed values of the top and Higgs masses if the Standard Model can be extended up to the scale Λ; from Ref. [68]. The dashed area follows from the assumption that the Standard Model can be extended up to the GUT scale. The lower bound is derived from vacuum stability.*

From the requirement of vacuum stability and from the assumption that the Standard Model can be continued up to the GUT scale, upper and lower bounds on the Higgs mass can be derived. Based on these arguments, the Higgs mass could well be expected in the window $100 < M_H < 180$ GeV for a top mass value of 140 GeV. It must however be stressed again that the upper limit is based on assumptions which are backed only *qualitatively* by the measured value of the electroweak mixing angle. The important range of M_H between M_Z and $2M_Z \simeq 180$ GeV is generally referred to as the intermediate Higgs mass range.

Once the Higgs mass is fixed, the triple and quartic self–couplings of the $\mathcal{SM}$ Higgs particle are uniquely determined. The scale of the Higgs couplings to massive gauge bosons and quarks/leptons is set by the masses of these particles. Hence, the profile of the Higgs particle can be predicted completely for a given value of the Higgs mass: the decay properties are fixed and the production mechanisms and the production rates can be determined.

The width of the Higgs particle increases from very small values of $\mathcal{O}$(1 MeV) in the 50 GeV mass range to $\mathcal{O}$(300 MeV) near the WW decay threshold. Once the WW and ZZ decay channels are open, the width grows as the third power of the mass and reaches rapidly very large values, extending up to several hundred GeV in the upper Higgs mass range. The dominant decay mode for masses in the intermediate range below $\sim$ 140 GeV is the $b\bar{b}$ decay channel. For higher mass values, the WW and ZZ decays become dominant, one of the vector bosons being virtual below the threshold for two real bosons. Other decay modes $[\tau^+\tau^-, c\bar{c}, gg]$ occur at a level of several percent in the lower part of the intermediate mass range.

A large variety of channels can be exploited to search for Higgs particles in the bremsstrahl and fusion processes. In the bremsstrahl process, missing–mass techniques can be applied in events with leptonic Z decays and the Higgs particle may be reconstructed in $H \to b\bar{b}$ directly. [Missing–mass techniques of course call for collider designs in which the beamstrahlung is minimal.] These techniques can be applied for Higgs masses $>$ 100 GeV; below this value, flavor tagging through vertex detection must be used to separate the ZH signal from the ZZ background. The WW fusion process requires the reconstruction of the Higgs particle, while missing–mass techniques can also be used in ZZ fusion. Background events from single W and Z production restrict these experimental search techniques in the fusion channels to Higgs masses above 100 GeV.

Once the Higgs boson has been found, it will be of great importance to explore its properties. This is possible at great detail in the clean environment of e^+e^- colliders. The zero–spin of the Higgs particle is reflected in the angular distribution of the bremsstrahl process which asymptotically must follow the $\sin^2\theta$ law [corresponding to the predominantly longitudinal polarization of the accompanying Z boson]. Of tantamount importance is the measurement of the couplings to gauge bosons and matter particles. The strength of the couplings to Z and W is reflected in the magnitude of the production cross sections. The relative strength of the couplings to fermions is accessible through the decay branching ratios. The absolute magnitude is difficult to measure directly. [Indirect access to the top–Higgs coupling is provided by top–loop mediated photonic and gluonic decays.] The direct measurement is possible in a small mass window where the Higgs decays to $b\bar{b}$ and WW^* compete with each other. Else, Higgs bremsstrahlung off top quarks or Higgs decays to $t\bar{t}$ pairs offer opportunities to measure the ttH coupling in limited ranges of the Higgs mass.

From the preceding discussion we conclude that e^+e^- linear colliders with energies in the range of 300 to 500 GeV are ideal instruments to search for Higgs particles in the intermediate mass range [and beyond] which, *a priori*, may be considered as a very important part in the entire range of possible Higgs mass values. The search for Higgs

particles can be carried out in a highly redundant variety of channels. In the same way, the properties of the Higgs particle can be investigated thoroughly. This is possible throughout the intermediate mass range [and extending, in fact, up to Higgs mass values of order 350 GeV].

An even stronger case for linear colliders in the 300 to 500 GeV energy range is made by supersymmetric extensions of the $\mathcal{SM}$. In particular, the Minimal Supersymmetric extension of the Standard Model ($\mathcal{MSSM}$) [72] provides a Higgs scenario which, beyond any doubt, can best be explored in e^+e^- colliders. Even though the $\mathcal{MSSM}$ is a specific realization of $\mathcal{SUSY}$, some of the key features are expected to be realized in more general $\mathcal{SUSY}$ models too, so that the analysis can be considered as representative for a wide class of models.

The $\mathcal{MSSM}$ requires the existence of two iso–doublets of scalar fields, giving mass separately to up and down–type fermions. Three neutral $[h^0/H^0(\mathcal{CP}=+), A^0(\mathcal{CP}=-)]$ and a pair of charged scalar particles $[H^\pm]$ are introduced by this extension of the Higgs sector. At tree level, the mass of the lightest Higgs boson h^0 is smaller than the Z mass. Radiative corrections [73] however, which grow as the fourth power of the top quark mass, can shift the upper bound from M_Z to $\sim$ 130 GeV. Beyond $\sim$ 90 GeV, Higgs particles are not accessible anymore at LEP200 and higher energies are required to produce them. The masses of the heavy neutral and charged Higgs particles can be expected, with a high probability, in the range of the electroweak symmetry breaking scale so that a large part of the mass parameter space can be covered at an e^+e^- collider with an energy of 500 GeV.

Apart from cascade decays in some corners of the parameter space, the main decay modes of the neutral Higgs particles are in general $b\bar{b}$ decays [$\sim$ 90%] and $\tau^+\tau^-$ decays [$\sim$ 10%] which are easy to tag experimentally. The gold–plated ZZ decays of the $\mathcal{SM}$ Higgs above 140 GeV play a minor rôle in the $\mathcal{SUSY}$ Higgs sector – and in large parts of the parameter space even a negligible rôle. Charged Higgs particles decay into $\tau\nu_\tau$ pairs and into $t\bar{b}$ pairs [primarily into the latter channel, if kinematically allowed]. The total width of the states remains small, $< \mathcal{O}$ (1 GeV) anywhere in the intermediate mass range.

$\mathcal{SUSY}$ Higgs particles can be created through a variety of mechanisms. Besides the classical bremsstrahl and fusion processes, neutral and charged Higgs particles can also be produced in pairs. The cross sections for light h^0 and heavy H^0 $\mathcal{CP}$–even neutral Higgs bosons add up to the $\mathcal{SM}$ cross section while their relative weights can vary between wide margins [74,75]. Nevertheless, combining all production channels at least the lightest of the neutral Higgs particles must be found at the linear collider. If not, the minimal supersymmetric extension of the Standard Model is ruled out. Furthermore, in a large part of the parameter space *all* the neutral Higgs particles and the charged Higgs particles can be found, thus enabling us to confirm experimentally the two–doublet structure of the Higgs sector. The detailed comparison of branching ratios and production cross sections with the predictions of the $\mathcal{MSSM}$ will eventually shed light on the physical origin of the extended Higgs sector.

Even though the minimal supersymmetric extension of the Standard Model provides

only one example for possible scenarios of extended Higgs sectors, it clearly demonstrates the power of e^+e^- linear colliders for exploring the intermediate mass range [and some range beyond]. In this domain, which is a very attractive range for Higgs particles on general grounds, e^+e^- colliders are truly unique accelerators the potential of which cannot be matched by any other facility in this field.

4.1 Higgs in the Standard Model

(a) Decays of the Higgs Particle

The profile of the Higgs particle in the Standard Model is uniquely determined if the Higgs mass is fixed. The strength of the Yukawa couplings of the Higgs boson to fermions is set by the fermion masses m_f, and the coupling to the electroweak gauge bosons $V = W, Z$ by their masses M_V, $g_{ffH} = \left[\sqrt{2}G_F\right]^{1/2} m_f$ and $g_{VVH} = 2\left[\sqrt{2}G_F\right]^{1/2} M_V^2$. The decay width, the branching ratios and the production cross sections are given by these parameters.

For Higgs particles in the intermediate mass range $M_Z \leq M_H \leq 2M_Z$ the main decay modes are decays into $b\bar{b}$ pairs and WW, ZZ pairs with one of the gauge bosons being virtual below the respective threshold. Above the WW threshold, the Higgs particles decay almost exclusively into these channels. Below 140 GeV, the decays $H \to \tau^+\tau^-, c\bar{c}$ and gg are also of significance besides the dominating $b\bar{b}$ channel.

In the Born approximation the partial width of the Higgs decay into lepton pairs is given by [76]

$$\Gamma(H \to l^+l^-) = \frac{G_F m_l^2}{4\sqrt{2}\pi}\, M_H\, \beta^3$$

with $\beta = (1 - 4m_l^2/M_H^2)^{1/2}$ being the velocity of the leptons in the final state. For the decay widths into quark pairs, QCD corrections must be included,

$$\Gamma(H \to q\bar{q}) = \frac{3G_F}{4\sqrt{2}\pi}\, m_q^2(M_H^2)\, M_H$$

The bulk of the QCD corrections, which are very important for these decays, can be absorbed into the running quark masses evaluated at the scale $\mu = M_H$ [77] $m_q(M_H^2) = m_q(m_q^2)\left[\alpha_s(M_H^2)/\alpha_s(m_q^2)\right]^{12/(33-2N_F)}$. For $M_H = 120$ GeV, the b and c quark masses $m_b(m_b^2) = 4.2$ GeV and $m_c(m_c^2) = 1.35$ GeV have dropped to the effective values $m_b(M_H^2) = 3$ GeV and $m_c(M_H^2) = 0.77$ GeV, respectively.

Above the WW and ZZ decay threshold, the partial width into massive gauge boson pairs may be written as [66]

$$\Gamma(H \to VV) = \delta_V \frac{\sqrt{2}G_F}{32\pi}\, M_H^3\, (1 - 4x + 12x^2)\, \beta$$

where $x = M_V^2/M_H^2$ and $\delta_V = 2(1)$ for $V = W(Z)$. For large Higgs masses, the vector bosons are longitudinally polarized. Since these wave–functions are linear in the energy, the width grows with the third power of the Higgs mass. Below the threshold for two real bosons, the Higgs particles can decay into VV^* pairs, one of the vector bosons being virtual. The partial decay width is given by [78]

$$\Gamma(H \to VV^*) = \frac{3G_F^2 M_V^4}{16\pi^3}\, M_H\, R(x)\, \delta_V'$$

where $\delta_W' = 1, \delta_Z' = 7/12 - 10s_W^2/9 + 40s_W^4/27$ and

$$R(x) = \frac{3(1 - 8x + 20x^2)}{(4x-1)^{1/2}} \arccos\left(\frac{3x-1}{2x^{3/2}}\right) - \frac{1-x}{2x}(2 - 13x + 47x^2) - \frac{3}{2}(1 - 6x + 4x^2)\log x$$

In the Standard Model, gluonic Higgs decays $H \to gg$ are mediated by top quark loops. Since this decay mode is significant only for Higgs masses far below the top threshold, the gluonic width can be cast into the approximate form [79]

$$\Gamma(H \to gg) = \frac{G_F \alpha_s^2(M_H^2)}{36\sqrt{2}\pi^3}\, M_H^3 \left[1 + \left(\frac{95}{4} - \frac{7}{6}N_F\right)\frac{\alpha_s(M_H^2)}{\pi}\right]$$

The QCD radiative corrections which include ggg and $gq\bar{q}$ final states are very important; they increase the partial width by $\sim 65\%$.

The branching ratios for the $H \to \gamma\gamma$ and $H \to Z\gamma$ decays are so small $\mathcal{O}(10^{-3})$ that they cannot play a significant rôle in e^+e^- colliders. With less than 10 events, large background problems associated with radiative corrections to standard processes like $e^+e^- \to Z\gamma\gamma$, would be very difficult to overcome. [However, since all these decays are built–up by loops, their strength can be sensitive to energy scales far beyond the Higgs mass.]

By adding up all possible decay channels, we obtain the total Higgs decay width shown in Fig. 19a for $m_t = 150$ GeV. Up to masses of 140 GeV, the Higgs particle is very narrow, $\Gamma(H) \leq 10$ MeV. After opening the [virtual] gauge boson channels, the state becomes rapidly wider, reaching ~ 1 GeV at the ZZ threshold. The width cannot be measured directly in the intermediate mass range. Only above $M_H \geq 250$ GeV it becomes wide enough to be resolved experimentally. The branching ratios of the main decay modes are displayed in Fig. 19b. A large variety of channels will be accessible for Higgs masses below 140 GeV. The dominant mode are $b\bar{b}$ decays, yet $c\bar{c}$, $\tau^+\tau^-$ and gg still occur at a level of several percent. [At $M_H = 120$ GeV for instance , the branching ratios are 68% for $b\bar{b}$, 4.6% for $c\bar{c}$, 6.6% for $\tau^+\tau^-$ and 6% for gg.] Above this mass value, the Higgs decay into W's becomes dominant, overwhelming all other channels if the decay mode into two real W's is kinematically possible.

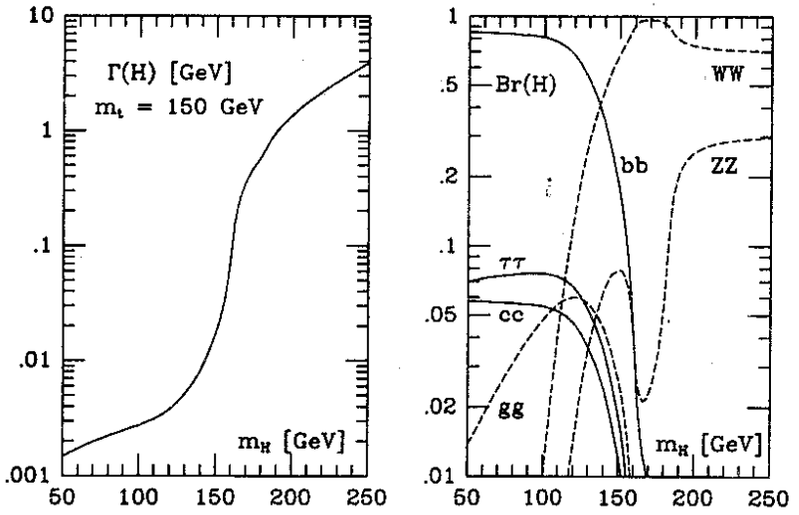

Fig. 19: *(a) Decay width and (b) decay branching ratios of the Higgs particle in the Standard Model.*

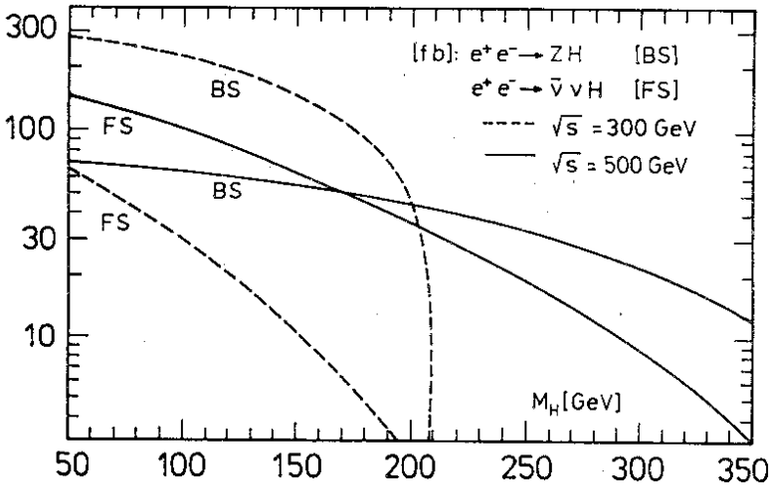

Fig. 20: *Production cross sections for Higgs bremsstrahlung and fusion in the Standard Model.*

(b) Higgs Production

The main production mechanisms for Higgs particles in e^+e^- collisions are Higgs bremsstrahlung off the Z boson line [80,66,81]

$$e^+e^- \longrightarrow (Z) \longrightarrow Z + H$$

and the fusion processes [82]

$$e^+e^- \longrightarrow \bar{\nu}\nu\,(WW) \longrightarrow \bar{\nu}\,\nu + H$$
$$e^+e^- \longrightarrow e^+e^-(ZZ) \longrightarrow e^+e^- + H$$

with the [virtual] vector bosons radiated off the initial electrons and positrons.

Higgs Bremsstrahlung

The cross section for the bremsstrahl process can be presented in a compact form

$$\sigma(e^+e^- \to ZH) = \frac{G_F^2 M_Z^4}{96\pi s}(v_e^2 + a_e^2)\ \lambda^{1/2}\frac{\lambda + 12M_Z^2/s}{(1 - M_Z^2/s)^2}$$

where $a_e = -1$ and $v_e = -1 + 4s_W^2$ are the Z charges of the electron and $\lambda = (1 - M_H^2/s - M_Z^2/s)^2 - 4M_H^2M_Z^2/s^2$ is the usual two–particle phase space function. The cross section is shown in Fig. 20 for two energy values $\sqrt{s} = 300$ and 500 GeV as a function of the Higgs mass. With $\sigma \sim 200$ fb, a rate of $\sim 2,000$ Higgs particles in the intermediate mass range is produced at an energy $\sqrt{s} = 300$ GeV and an integrated luminosity of $\int \mathcal{L} = 10$ fb^{-1}. Asymptotically, the cross section scales $\sim 1/s$.

The angular distribution of the Z/H bosons in the bremsstrahl process is sensitive to the spin–zero of the Higgs particle. For high energies, the Z boson is produced in a state of longitudinal polarization so that – according to the equivalence theorem – the production amplitude becomes equal to the amplitude $A(e^+e^- \to \phi^0 H)$, with ϕ^0 being the neutral Goldstone boson which is absorbed to give mass to the vector boson. The angular distribution,

$$\frac{\mathrm{d}\sigma}{\mathrm{d}\cos\theta} \sim \lambda \sin^2\theta + 8M_Z^2/s$$

therefore approaches the spin–zero angular distribution, $\to \sin^2\theta$ asymptotically. The distribution is shown in Fig. 21 for $M_H = 120$ GeV and two energy values. The prediction for the ZH final state is compared with the distribution for ZZ final states which is maximal for forward/backward production. The Z-bosons in ZZ final states are predominantly transversely polarized, but longitudinally polarized in ZH final states.

The recoiling Z boson in the two–body reaction $e^+e^- \to ZH$ is mono–energetic, $E_Z = (s - M_H^2 + M_Z^2)/2\sqrt{s}$, and the mass of the Higgs boson can be derived from the energy of the Z boson,

$$M_H^2 = s - 2\sqrt{s}E_Z + M_Z^2$$

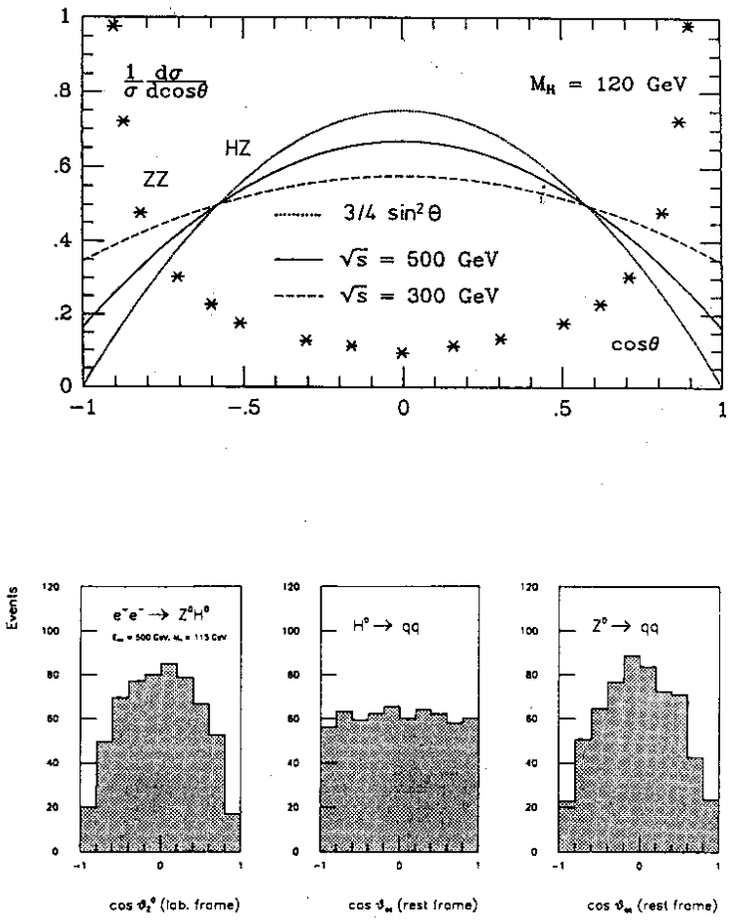

Fig. 21: *Angular distributions of the bremsstrahl process $e^+e^- \to ZH$ confronted with $e^+e^- \to ZZ$ final states; distribution of the jets in Higgs decays and Z decays (ZH final states). From Ref.[83].*

if the initial e^+ and e^- beam energies are sharp. Beamstrahlung however smears out the c.m. energy and the system moves along the beam axes. The intensity of the beamstrahlung depends on the machine design. It must be suppressed as strongly as possible for a given luminosity in order to allow for the high quality experimental analyses which are based on the powerful kinematical constraints familiar from low–energy e^+e^- physics. Favorable examples in this context are the DESY–Darmstadt and the TESLA design studies. For these designs the smearing of the missing mass is of the same magnitude as the experimental uncertainties in the reconstruction of the Z boson in the leptonic decay channels, Fig. 22.

Since the recoiling Z boson remains approximately mono–energetic, even if the beamstrahlung is taken into account in these cases, it is easy to separate the signal from the background. Four mass regions must be considered:

(*i*) For Higgs masses close to the Z mass, double Z–production $e^+e^- \to ZZ$ is the main background source. The cross section is large but can be reduced by cutting out the forward production and by selecting $b\bar{b}$ final jets by means of flavor tagging through vertex detection. While the Higgs particle decays almost exclusively to $b\bar{b}$ final states, the branching ratio of the decay $Z \to b\bar{b}$ is small, $\sim 15\%$.

(*ii*) For masses between 100 and 140 GeV, the background comes from single Z–production in $e^+e^- \to ZZ^*(\to q\bar{q})$. The cross section is suppressed by one order of the electroweak coupling compared to the signal. Further reductions of the background can be achieved through flavor tagging.

(*iii*) In the mass range above $\sim$ 140 GeV where gauge boson decays become dominant, the most important background is due to $e^+e^- \to Z + WW^*(\to q\bar{q}')$. The cross section of this reaction is suppressed by two powers of the electroweak coupling relative to the signal.

(*iv*) Beyond 160 GeV and 180 GeV, the reactions with three gauge bosons in the final state, $e^+e^- \to Z + WW$ and $e^+e^- \to Z + ZZ$, are the main background channels. In the background the invariant mass distribution of the WW or ZZ final states is broad as opposed to the resonance structure of the signal. The background under the signal is therefore small.

(c) Fusion Processes

The cross section for the fusion processes can be cast into a compact form [84]

$$\sigma = \frac{G_F^3 M_V^4}{64\sqrt{2}\pi^3} \int_{\kappa_H}^1 \mathrm{d}x \int_x^1 \frac{\mathrm{d}y}{[1+(y-x)/\kappa_V]^2} \left[(v^2+a^2)^2 f(x,y) + 4v^2a^2 g(x,y)\right]$$

$$f(x,y) = \left(\frac{2x}{y^3} - \frac{1+2x}{y^2} + \frac{2+x}{2y} - \frac{1}{2}\right)\left[\frac{z}{1+z} - \log(1+z)\right] + \frac{x}{y^3}\frac{z^2(1-y)}{1+z}$$

$$g(x,y) = \left(-\frac{x}{y^2} + \frac{2+x}{2y} - \frac{1}{2}\right)\left[\frac{z}{1+z} - \log(1+z)\right]$$

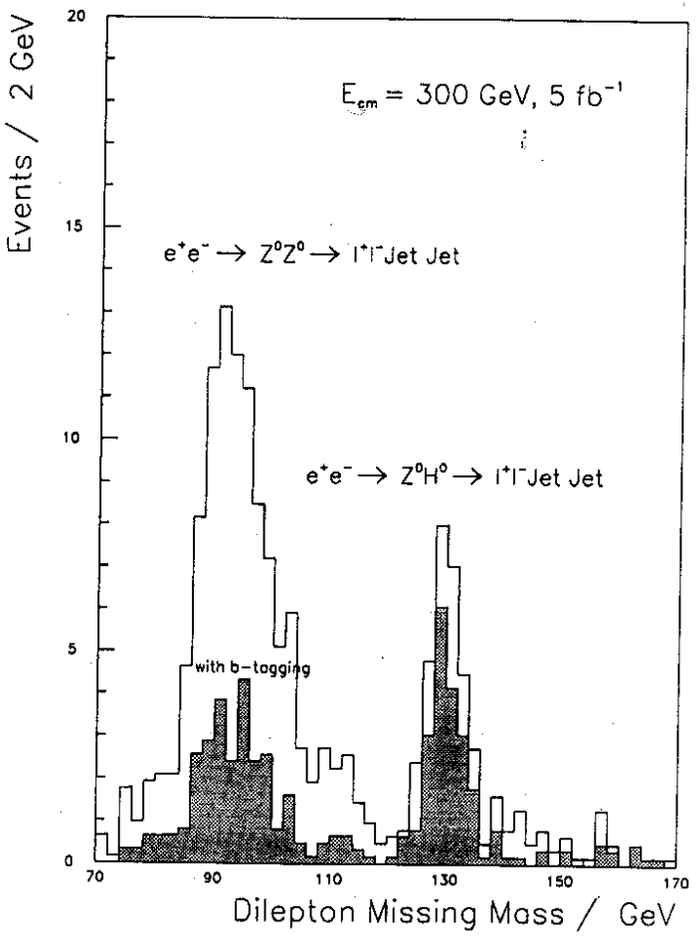

Fig. 22: *Missing mass distribution in bremsstrahl production of Higgs bosons; from Ref.[84].*

with $\kappa_H = M_H^2/s$, $\kappa_V = M_V^2/s$, $z = y(x-h)/(\kappa_V x)$ and v, a the electron couplings to the gauge bosons [$v = -1 + 4s_W^2, a = -1$ for the Z and $v = a = \sqrt{2}$ for the W boson].

For a total energy $\sqrt{s} = 500$ GeV and a Higgs mass in the intermediate range, the WW fusion cross section is of about the same magnitude as the bremsstrahl cross section, for lower energies it is smaller, for higher energies larger [see Fig. 20]. Asymptotically it keeps growing logarithmically $\sim M_W^{-2} \log s/M_H^2$ in contrast to the bremsstrahl cross section which falls $\sim s^{-1}$. The cross section for ZZ fusion is about an order of magnitude smaller than the cross section for WW fusion; this is a mere consequence of the fact that the NC couplings are smaller than the CC couplings. The lower rate however is, at least partly, compensated by the clean signature of the e^+e^- final state that allows for a missing-mass analysis to tag the Higgs particle. The production of the Higgs particle in the fusion processes is central with a spread in the rapidity Δy of about one unit; the energy distribution peaks at about 30 GeV above the mass value. The transverse momentum of the Higgs particle has a broad maximum at $P_T \sim 60$ GeV.

For a light Higgs mass, the dominant background is the process $e^+e^- \rightarrow e^+W^-\nu_e$. This cross section exceeds the signal for jet–jet final states by about a factor of 60. Another background arises from WW fusion into a Z boson which is three times larger than the signal. All other backgrounds can be efficiently reduced. The single $W(Z)$ boson production behaves similarly to the Higgs boson in the signal process so that cuts enhance the signal/background ratio very little – except for three distinctive features: the resonance structure, the spin of the resonance and the flavor composition of the decays. As the Higgs mass enters the Z and W resonance region, flavor tagging is indispensable. Its application would lead to an event sample of about 240 events composed of 60 $W \rightarrow jj$, 80 $Z \rightarrow jj$ and 100 $H \rightarrow jj$ tagged as $b\bar{b}$–jets [for a luminosity of 20 fb^{-1}]. For a Higgs mass around $2M_W$, the background process with W^+W^- and WZ final states can be reduced to a negligible level.

The process $e^+e^- \rightarrow e^+e^-H$ is, for $M_H \sim M_Z$, contaminated by $e^+e^- \rightarrow e^+e^-Z$ [mainly arising from the $\gamma e \rightarrow Ze$ subprocess] which is about 10 times stronger than the signal after requiring both e^+ and e^- to be detected with $P_T > 30$ GeV but before tagging the b's in the Higgs decay. The signal to background ratio improves rapidly as M_H moves away from the Z mass.

(d) Measurements of Higgs Couplings

The fundamental particles acquire masses through the interaction with the Higgs field. The scale of the Higgs couplings to fermions and gauge bosons is therefore set by the masses of these particles. This is a necessary requirement to unitarize the theory of electroweak interactions. Once the Higgs particle has been found, it will be mandatory to measure its couplings to the fundamental particles, which are uniquely predicted by the very nature of the Higgs mechanism [85].

The Higgs couplings to massive gauge bosons can directly be determined from the measurement of the production cross sections: the HZZ coupling in the bremsstrahl and in the ZZ fusion processes; the HWW coupling in the WW fusion process. For sufficiently large Higgs masses above ~ 250 GeV, these couplings can also be determined experimentally from the decay widths $H \to ZZ, WW$.

Higgs couplings to fermions are not easy to measure directly. For Higgs bosons in the intermediate mass range where the decays into $b\bar{b}, c\bar{c}$ and $\tau^+\tau^-$ are important, the decay width is so narrow that it cannot be resolved experimentally. Nevertheless, the branching ratios into τ leptons and charm quarks reveal the couplings of these fermions relative to the coupling of the b quarks into which the Higgs boson decays predominantly. In the upper part of the intermediate mass range but below the threshold for real WW decays, the branching ratios $\mathrm{BR}(H \to WW^*/ZZ^*)$ are sizeable and can be determined experimentally. In this case, the absolute values of the b and eventually of the c, τ couplings can be derived once the HZZ/HWW couplings are fixed by the production cross sections.

The decays $H \to gg$ and $\gamma\gamma, Z\gamma$ and the fusion processes $gg, \gamma\gamma \to H$ are mediated by loop diagrams, that are proportional to the couplings of the Higgs boson to heavy particles. The number of heavy particles can be counted in these processes if their masses are generated by the Higgs mechanism and their couplings to the Higgs particles grow with the mass. [This is not the case for heavy supersymmetric particles which decouple asymptotically from the vertices introduced above.] In the Standard Model only the top quark contributes to the Hgg vertex so that the Htt coupling can be measured in the gluonic decays of the Higgs particle [and, in the same way, through the cross section for the gluon fusion $gg \to H$ at hadron colliders]. In the case of $H \to \gamma\gamma, Z\gamma$ additional contributions to the decay amplitudes come from W loops. However, these vertices may also be affected by loops of heavy particles beyond the Standard Model. A new generation of fermions, for instance, could enhance the branching ratio $\mathrm{BR}(H \to gg)$ to a level which becomes comparable to the $b\bar{b}$ mode in the intermediate mass range. [At $M_H = 120$ GeV one would have $\mathrm{BR}(H \to gg) = 0.35$ and $\mathrm{BR}(H \to b\bar{b}) = 0.45$ in this case.] This allows the measurement of the number of families with heavy neutrinos in any theory incorporating the standard Higgs mechanism. Because of the destructive interference between the W and the fermionic contributions, the partial width $\Gamma(H \to \gamma\gamma)$ is reduced in the presence of a fourth family. The difference is large enough to be measured in the fusion process $\gamma\gamma \to H$.

A direct way to determine the Yukawa coupling of the intermediate mass Higgs boson to the top quark in the range $m_H \leq 120$ GeV is provided by the bremsstrahl process $e^+e^- \to t\bar{t}H$ in high energy e^+e^- colliders [30]. For large Higgs masses above the $t\bar{t}$ threshold, the decay channel $H \to t\bar{t}$ increases the cross section of $e^+e^- \to t\bar{t}Z$ through the reaction $e^+e^- \to ZH(\to t\bar{t})$ [31]; without the Higgs decay this final state is produced mainly through virtual γ and Z bosons. These methods have been discussed extensively in the top section of this report.

4.2 The Higgs Sector of the Minimal Supersymmetric Standard Model

Supersymmetric theories are most appealing extensions of the Standard Model. They provide a theoretical framework in which the problems of hierarchy and naturalness are solved while retaining the Higgs bosons as elementary spin-zero particles. The Minimal Supersymmetric extension of the Standard Model [76] may serve as a useful guideline into this area. Though some of the phenomena will be specific to this minimal version, many of the patterns will also be valid in more general extensions [86]. The $\mathcal{MSSM}$ therefore provides an interesting example for novel Higgs phenomena which can be expected in the terrain beyond the Standard Model in general.

The Higgs sector is a most interesting field in this context. Supersymmetry requires the existence of at least two iso-doublet scalar fields Φ_1 and Φ_2, thus extending the physical spectrum of scalar particles considerably. The $\mathcal{MSSM}$ is restricted to this minimal extension. The field Φ_2 (with vacuum expectation value v_2) couples only to up-type quarks while Φ_1 (with vacuum expectation value v_1) couples to down-type quarks and charged leptons. Five physical Higgs bosons are introduced in this extension: two $\mathcal{CP}$-even neutral bosons h and H (where h will be considered to be the lightest particle), a $\mathcal{CP}$-odd neutral boson A (usually called pseudoscalar) and two charged Higgs bosons $H^\pm$. Besides the four masses M_h, M_H, M_A and $M_{H^\pm}$, two additional parameters define the properties of the scalar particles and their interactions with gauge bosons and fermions the ratio of the two vacuum expectation values $\mathrm{tg}\beta = v_2/v_1$ and a mixing angle α in the neutral $\mathcal{CP}$-even sector. Supersymmetry leads to several relations among these parameters and, in fact, only two of them are independent. These relations impose a strong hierarchical structure on the mass spectrum [$M_h < M_Z, M_A < M_H$ and $M_W < M_{H^\pm}$] which however is broken by radiative corrections if the top quark mass is large [73]. The parameter $\mathrm{tg}\beta$ will in general be assumed in the range $1 < \mathrm{tg}\beta < \mathrm{m_t/m_b}$ [$\pi/4 < \beta < \pi/2$], consistent with GUT restrictions on the model [87].

(a) Parameters and Decay Modes

Since the lightest $\mathcal{CP}$-even Higgs boson h is likely to be the particle which will be discovered first, an attractive choice of the two input parameters is the set $[M_h, \mathrm{tg}\beta]$, with $\mathrm{tg}\beta$ parametrizing the production cross sections. Once these two parameters [as well as the top quark mass and the associated squark masses which enter through radiative corrections] are specified, all other masses $M_H, M_A, M_{H^\pm}$ and the angle α can be derived.

The radiative corrections grow as the fourth power of the top quark mass m_t and logarithmically with the squark mass M_S. They are positive and they shift the mass of the light neutral Higgs boson h upward with increasing top mass. The variation of the upper limit of M_h with the top quark mass is shown in Fig. 23a for $M_S = 1$ TeV and three representative values of $\mathrm{tg}\beta = 2.5, 5$ and 20. The upper bound on M_h is shifted from the tree level value M_Z up to ~ 130 GeV for $m_t = 180$ GeV. Assuming [from now on] that

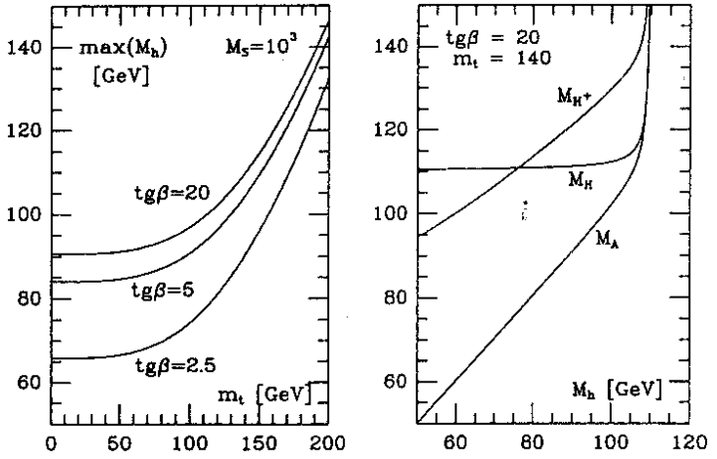

Fig. 23: *Masses of the SUSY Higgs bosons. (a) Max(M_h) as a function of m_t and (b) M_H, M_A and $M_{H^\pm}$ as functions of M_h for $m_t = 140$ GeV. The squark masses M_S are fixed to 1 TeV.*

$m_t = 140$ GeV and $M_S = 1$ TeV, the masses M_A, M_H and $M_{H^\pm}$ are depicted in Fig. 23b as a function of the light neutral Higgs mass for $\mathrm{tg}\beta = 20$. Apart from the range near the upper limit of M_h for fixed $\mathrm{tg}\beta$, the mass values cluster in characteristic bands of 100 to 150 GeV for M_H and $M_{H^\pm}$, and up to $\sim$ 100 GeV for M_A. On general grounds, the masses of the heavy neutral and charged Higgs bosons are expected to be of the order of the electroweak symmetry breaking scale so that a large part of the Higgs mass spectrum can be explored in e^+e^- colliders with a total energy of 500 GeV [75,89,90].

The couplings of the various neutral Higgs bosons to fermions and gauge bosons will in general depend on the angles α and β. Normalized to the $\mathcal{SM}$ Higgs couplings, they are summarized in the table and Fig. 24. The pseudoscalar boson A does not have tree–level couplings to gauge bosons, and its couplings to down (up) type fermions are (inversely) proportional to $\mathrm{tg}\beta$. The couplings depend in general strongly on the input parameters $\mathrm{tg}\beta$ and M_h. The couplings to down (up) type fermions are enhanced (suppressed) compared to the $\mathcal{SM}$ Higgs couplings. If M_h is very close to its upper limit for a given value of $\mathrm{tg}\beta$, the couplings to fermions and gauge bosons are $\mathcal{SM}$ like. If all other Higgs bosons are very heavy, it is very difficult to distinguish the Higgs sector of the $\mathcal{MSSM}$ from the $\mathcal{SM}$.

The lightest neutral Higgs boson will decay mainly into fermion pairs since its mass is smaller than $\sim$ 130 GeV, Fig. 25. This is also the dominant decay mode of the pseudoscalar boson A which has no tree–level couplings to gauge bosons. For values of $\mathrm{tg}\beta$ larger than unity and for masses less than $\sim$ 140 GeV, the main decay modes of the neutral Higgs bosons are decays into $b\bar{b}$ and $\tau^+\tau^-$ pairs; the branching ratios being always larger than $\sim$ 90% and 8%, respectively. The decays into $c\bar{c}$ pairs and gluons [proceeding through t

Φ	$g_{\Phi\bar{u}u}$	$g_{\Phi\bar{d}d}$	$g_{\Phi VV}$
h	$\cos\alpha/\sin\beta$	$-\sin\alpha/\cos\beta$	$\sin(\beta-\alpha)$
H	$\sin\alpha/\sin\beta$	$\cos\alpha/\cos\beta$	$\cos(\beta-\alpha)$
A	$1/\mathrm{tg}\beta$	$\mathrm{tg}\beta$	0

Table 2: *Higgs couplings in the $\mathcal{MSSM}$ to fermions and gauge bosons relative to $\mathcal{SM}$ couplings.*

and b quark loops] are strongly suppressed especially for large $\mathrm{tg}\beta$. For large masses, the top decay channels $H, A \to t\bar{t}$ open up; yet this mode remains suppressed for large $\mathrm{tg}\beta$. For large $\mathrm{tg}\beta$, the neutral Higgs bosons decay almost universally into $b\bar{b}$ and $\tau^+\tau^-$ pairs with ratios $\sim$ 90% and 8%, respectively.

If the mass is high enough, the heavy $\mathcal{CP}$–even Higgs boson can in principle decay into weak gauge bosons $H \to VV$, $V = W$ or Z. Since the partial widths are proportional to $\cos^2(\beta-\alpha)$, they are strongly suppressed and the gold–plated ZZ signal of the heavy $\mathcal{SM}$ Higgs boson is lost in the supersymmetric extension. [If M_H is large enough for these decay modes to be kinematically allowed, M_h is very close to its maximum value so that $\cos^2(\beta-\alpha) \to 0$.] For the same reason, the cascade decay of the $\mathcal{CP}$–odd Higgs boson, $A \to Zh$, is suppressed in general. The heavy neutral Higgs boson H can also decay into two lighter Higgs bosons. These modes, however, are restricted to very small domains in the parameter space. Decays into $\gamma\gamma$ and $Z\gamma$ final states are very rare and do not play a significant role at e^+e^- colliders.

Other possible channels are decays into supersymmetric particles [91,75]. While sfermions are likely too heavy to affect Higgs decays in the mass range considered here, Higgs boson decays into charginos and neutralinos could eventually be important since

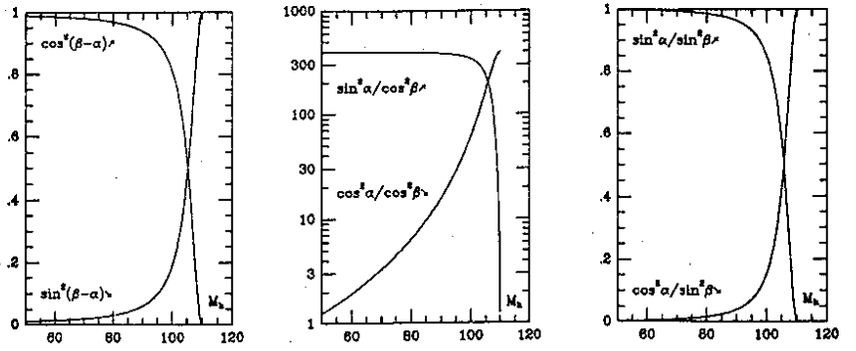

Fig. 24: *H and h couplings to fermions and gauge bosons as a function of M_h for $\mathrm{tg}\beta = 20$.*

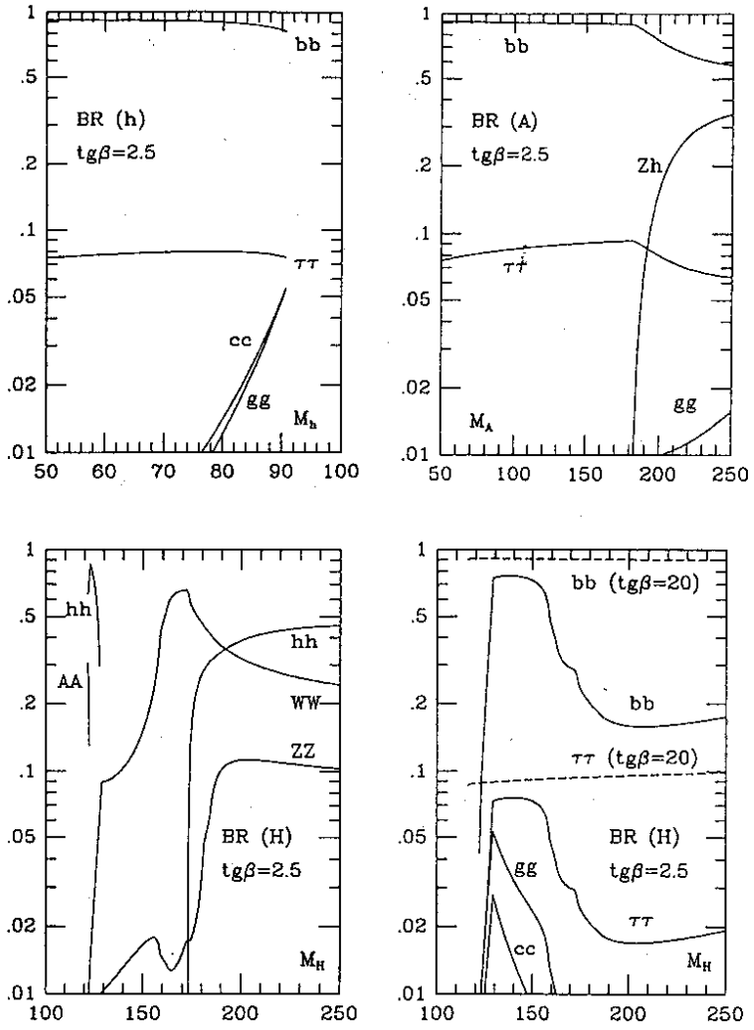

Fig. 25: **(a–c)** *Decay branching ratios of the $\mathcal{CP}$-even neutral Higgs bosons as a function of their masses for the value* $\mathrm{tg}\beta = 2.5$.

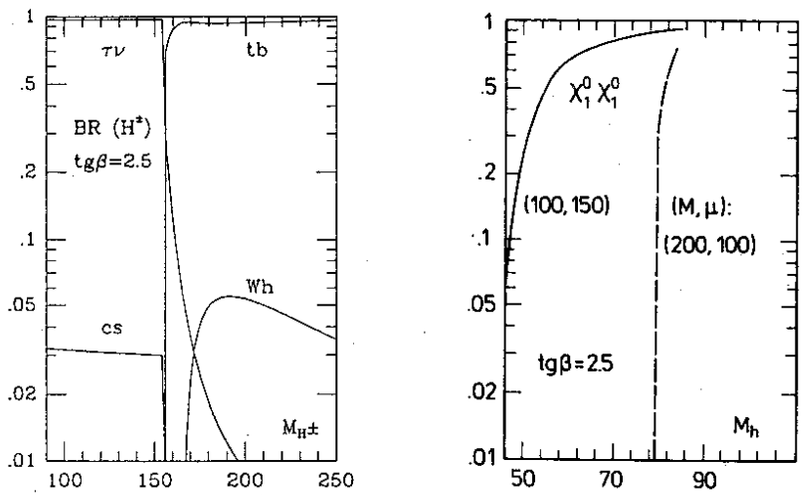

Fig. 25: **(d–e)** *Decay branching ratios of the charged Higgs boson* ($\mathrm{tg}\beta = 2.5$) *and invisible decays of the lightest Higgs boson into LSP pairs.*

some of these particles are expected to be of the order of M_Z. These new channels are kinematically accessible at least for the heavy Higgs bosons H, A and $H^\pm$; in fact, the branching fractions can be very large and they can even be dominant in some regions of the $\mathcal{MSSM}$ parameter space. Decays of h into the lightest neutralinos (LSP) and charginos are also important, exceeding 50% in some corners of the $\mathcal{SUSY}$ parameter space. These decays will affect experimental searches. In particular, neutral Higgs decays into the lightest neutralinos which would be invisible, are important and they could jeopardize the search for the Higgs particles at hadron colliders where these decays are very difficult to find. At e^+e^- colliders however, missing mass techniques allow to isolate these events easily, at least for the $\mathcal{CP}$-even Higgs bosons which can be produced in association with the Z boson.

The coupling of the charged Higgs particles to fermions is a $\mathcal{P}$ violating mixture of scalar and pseudoscalar currents. The charged Higgs particles decay into fermions but also, if allowed kinematically, into the lightest neutral Higgs and a W boson. Below the tb and Wh thresholds, the charged Higgs particles will decay mostly into $\tau\nu_\tau$ and $c\bar{s}$ pairs, the former being dominant for $\mathrm{tg}\beta > 1$. For large $M_{H^\pm}$ and $\mathrm{tg}\beta$ values, the top–bottom decay mode $H^+ \to t\bar{b}$ becomes dominant.

Adding up the various decay modes, the width of all five Higgs bosons remains very narrow, being of the order of 1 GeV even for large masses. Apart from the $\mathcal{CP}$-even heavy neutral Higgs boson H and small values of $\mathrm{tg}\beta$, the pattern of branching ratios is in general quite simple if supersymmetric decays are ignored. The neutral Higgs bosons

decay preferentially to $b\bar{b}$, and to a lesser extent to $\tau^+\tau^-$ pairs; the charged Higgs bosons to $\tau\nu_\tau$ and, preferentially, to $t\bar{b}$ pairs above the threshold. The decay patterns lead to clear signatures for the detection of these particles in e^+e^- colliders.

(b) Production

The search for the neutral $\mathcal{SUSY}$ Higgs bosons at 500 GeV e^+e^- colliders will be a direct continuation of the search to be performed at LEP200. This collider is expected to cover the mass range up to $\sim$ 85 GeV for neutral Higgs bosons. Higher energies, $\sqrt{s} \sim 240$ GeV, are required to sweep the entire parameter space of the $\mathcal{MSSM}$. The main production mechanisms of neutral Higgs bosons at e^+e^- colliders [74,75,88] are the bremsstrahl process and pair production,

$$\begin{array}{lll} (a) \text{ bremsstrahlung} & e^+e^- \to (Z) \to Z + h/H \\ (b) \text{ pair production} & e^+e^- \to (Z) \to A + h/H \end{array}$$

as well as the fusion processes,

$$\begin{array}{lll} (c) \text{ fusion processes} & e^+e^- \to \nu\,\bar{\nu}\,(WW) \to \nu\,\bar{\nu}\, + h/H \\ & e^+e^- \to e^+e^-(ZZ) \to e^+e^- + h/H \end{array}$$

The $\mathcal{CP}$-odd Higgs boson A cannot be produced in fusion processes to leading order.

The cross sections for the four bremsstrahl and pair production processes can be expressed as

$$\begin{aligned} \sigma(e^+e^- \to Zh) &= \sin^2(\beta-\alpha)\;\sigma_{SM} \\ \sigma(e^+e^- \to ZH) &= \cos^2(\beta-\alpha)\;\sigma_{SM} \\ \sigma(e^+e^- \to Ah) &= \cos^2(\beta-\alpha)\;\sigma_{SM}\;\bar{\lambda} \\ \sigma(e^+e^- \to AH) &= \sin^2(\beta-\alpha)\;\sigma_{SM}\;\bar{\lambda} \end{aligned}$$

where σ_{SM} is the $\mathcal{SM}$ cross section for Higgs bremsstrahlung and the factor $\bar{\lambda} \sim \lambda_{Aj}^{3/2}/\lambda_{Zj}^{1/2}$ accounts for the correct suppression of the P-wave cross sections near the threshold. The cross sections for the bremsstrahlung and for the pair production as well as the cross sections for the production of the light and the heavy neutral Higgs bosons h and H are mutually complementary to each other, coming either with a coefficient $\sin^2(\beta-\alpha)$ or $\cos^2(\beta-\alpha)$. Since σ_{SM} is large, at least the lightest $\mathcal{CP}$-even Higgs boson can be detected [88,89]. Depending on the values of M_h and tgβ, the following final states will be observed [Fig. 26]:

$$\begin{array}{llllllll} M_h \text{ "small"} , & \text{tg}\beta \text{ small} : & hZ , & HZ , & hA , & HA \\ & \text{tg}\beta \text{ large} : & & HZ , & hA , & \\ M_h \text{ "large"} , & \text{tg}\beta \text{ small} : & hZ , & & & [HA] \\ & \text{tg}\beta \text{ large} : & hZ , & & & [HA] \end{array}$$

where "M_h small" and "large" are synonymous for "considerably below" and "close to the upper limit of the light $\mathcal{CP}$-even Higgs boson" for a given value of tgβ. If M_h is "large" the H, A masses can exceed the kinematical limit for HA pair production. In the part of the $\mathcal{MSSM}$ parameter space in which invisible h decays into neutralinos are important, the bremstrahl cross section is large so that missing mass techniques can be applied.

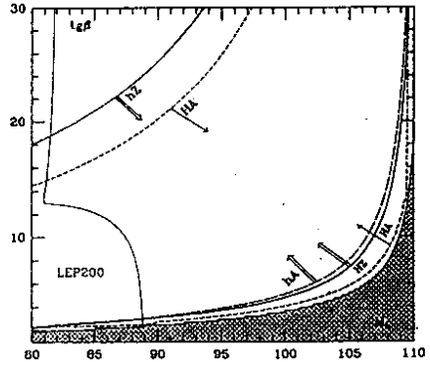

Fig. 26: *Regions of the (M_h, tgβ) plane where the four cross sections are larger than 2.5 fb [50 events for $\int \mathcal{L} = 20\ fb^{-1}$]. The dashed area is the theoretically forbidden region. The thin lines are the regions which can be probed at LEP200 [25 events at $\sqrt{s} = 180$ GeV and $\int \mathcal{L} = 500\ pb^{-1}$.]*

The cross sections for the various production mechanisms of the neutral Higgs bosons are shown as functions of the Higgs mass in Fig. 27, for tgβ = 20; Ref. [89]. The cross section for hZ is large for large values of M_h where it is of the order of $\sim$ 50 fb, corresponding to $\sim$ 500 events for an integrated luminosity of 10 fb^{-1}. By contrast, the cross section for HZ is large for light h [implying small M_H]. In the case of h [and also for H in most of the parameter space] the signal consists of a Z boson accompanied by a $b\bar{b}$ or a $\tau^+\tau^-$ pair. The signal is easy to separate from the background which comes mainly from ZZ production if the Higgs mass is close to M_Z. For the associated channels $e^+e^- \to Ah$ and AH, the situation is opposite to the previous case: the cross section for Ah is large for light h whereas AH production is preferred in the complementary region. The sum of the two cross sections decreases from $\sim$ 50 to 10 fb if M_A increases from $\sim$ 50 to 200 GeV. In major parts of the parameter space, the signals consist of four b quarks in the final state, requiring facilities for efficient b quark tagging. Mass constraints will help to eliminate the backgrounds from QCD jets as well as ZZ final states. For the WW fusion mechanism, the cross sections are larger than for the bremsstrahl process if the Higgs mass is moderately small – less than 160 GeV at $\sqrt{s}$ = 500 GeV. However, since the final state cannot be fully reconstructed, the signal is more difficult to extract. As in the case of the bremsstrahl process, the production of light h and heavy H Higgs bosons are complementary. The cross sections for the ZZ fusion mechanism are about an order of magnitude smaller than for the WW fusion process. ZZ fusion will nevertheless be useful since the final state can be fully reconstructed.

The preceding discussion of the neutral $\mathcal{MSSM}$ Higgs sector at e^+e^- linear colliders can be summarized in the following points:

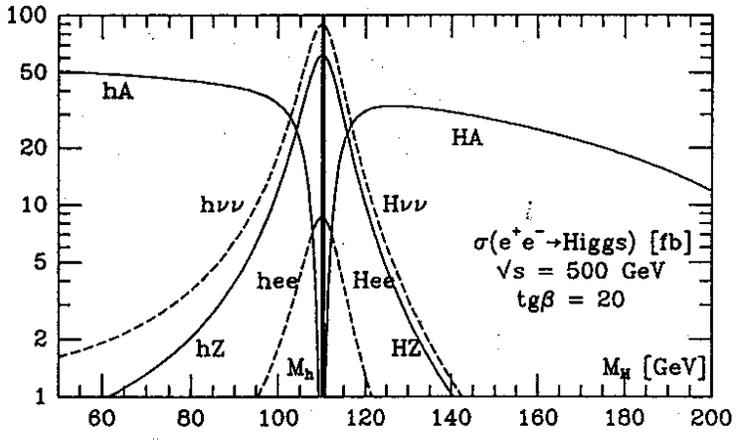

Fig. 27: *Production cross sections of the $\mathcal{SUSY}$ neutral Higgs bosons in e^+e^- collisions as a function of the masses [in GeV] for* $\mathrm{tg}\beta = 20$.

(*i*) The lightest $\mathcal{CP}$–even Higgs particle h can be detected in the entire range of the $\mathcal{MSSM}$ parameter space, either through the bremsstrahl process $e^+e^- \to hZ$ or through pair production $e^+e^- \to hA$. In fact, this conclusion holds true even at a c.m. energy of 300 GeV, independently of the top and squark mass values, and also if invisible neutralino decays are allowed for.

(*ii*) There is a substantial area of the $[M_h, \mathrm{tg}\beta]$ parameter space where *all* neutral $\mathcal{SUSY}$ Higgs bosons can be discovered at a 500 GeV collider. This is possible if the masses of the heavy scalar H and the pseudoscalar A boson are less than ~ 230 GeV.

(*iii*) In some part of the $\mathcal{MSSM}$ parameter space, the lightest Higgs particle h can be detected, but it cannot be distinguished from the $\mathcal{SM}$ Higgs boson. This happens if, for a given value of $\mathrm{tg}\beta$, M_h is very close to its maximum and H and A are too heavy to be produced in association. In this case, the couplings of h to gauge bosons and fermions are $\mathcal{SM}$ like. As long as this ambiguity cannot be resolved by proceeding to higher collider energies, the only way to distinguish h from the $\mathcal{SM}$ Higgs particle is provided by Higgs production in $\gamma\gamma$ fusion. While this process is built-up by W and top quark loops in the $\mathcal{SM}$, additional contributions in $\mathcal{SUSY}$ models are provided by supersymmetric particle loops, such as charginos, which alter the $\mathcal{SM}$ production rates.

Some of these features are not specific to the minimal extension but they are expected to be realized also in more general $\mathcal{SUSY}$ models. For example, a light Higgs boson with a mass in the intermediate range is predicted in supersymmetric theories quite generally.

In the $\mathcal{MSSM}$, the mass of the charged Higgs bosons $H^\pm$ is constrained to be larger than that of the W boson. More precisely, the lower limit $M_h > 60$ GeV obtained at LEP100 implies $M_{H^\pm} > 100$ GeV. In e^+e^- collisions,

$$\sigma(e^+e^- \to H^+H^-) = \frac{\pi\alpha^2}{3s}\left[1 - \frac{\hat{v}_e\hat{v}_H}{1 - M_Z^2/s} + \frac{(\hat{a}_e^2 + \hat{v}_e^2)\hat{v}_H^2}{(1 - M_Z^2/s)^2}\right]\beta^3$$

[with Z charges $\hat{v}_e(\hat{a}_e) = v_e(a_e)/4c_W s_W$ and $\hat{v}_H = (-1 + 2s_W^2)/c_W s_W$] the production of a pair of charged Higgs bosons proceeds through virtual photon and Z boson exchange. The cross section depends only on the charged Higgs mass [and does not depend on any extra parameter]. For small Higgs masses the cross section is of order 100 fb, but it drops very quickly due to the P–wave suppression $\sim \beta^3$ near the threshold; Fig. 28. For $M_{H^\pm} = 220$ GeV, the cross section has fallen to a level of $\simeq 5$ fb, which for an integrated luminosity of 10 fb^{-1} corresponds to 50 events. [Search strategies have been investigated in Ref.[92].] The angular distribution of the charged Higgs bosons follows the $\sin^2\theta$ law typical for spin–zero particle production. Charged Higgs particles can also be created in $\gamma\gamma$ collisions. Generating the γ beams through back–scattering of laser light, the total energy of the $\gamma\gamma$ collider can go up to $\sim 80\%$ of the original e^+e^- energy, which corresponds to $\sqrt{s_{\gamma\gamma}} \simeq 400$ GeV for a 500 GeV e^+e^- collider. Due to the reduced energy, the maximum Higgs mass which can be probed in $\gamma\gamma$ collisions, is smaller than the limit at the original e^+e^- collider; the cross section however is enhanced by a factor ~ 3 in the low mass range [Fig. 28].

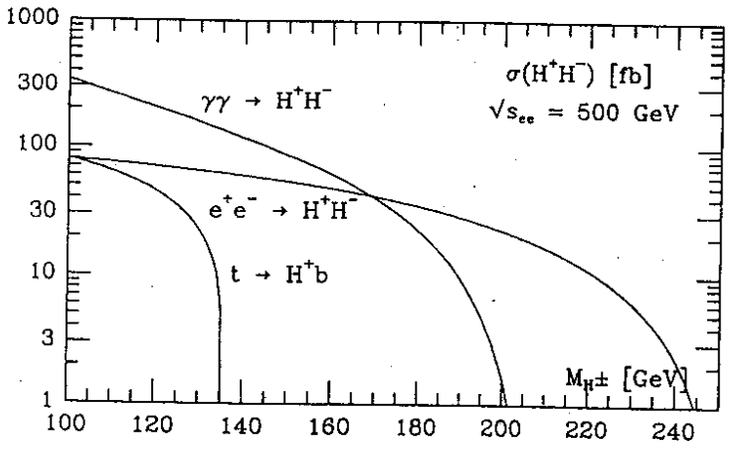

Fig. 28: *Production cross sections of the charged Higgs bosons in e^+e^- and $\gamma\gamma$ collisions as well as from top decays [for $m_t = 140$ GeV and $\mathrm{tg}\beta = 20$].*

The charged Higgs boson, if lighter than the top quark, can also be produced in top decays as discussed above. In the range $1 < \mathrm{tg}\beta < m_t/m_b$ favored by $\mathcal{SUSY}$ models,

the branching ratio varies between $\sim 2\%$ and 20%. Since the cross section for top pair production is of order 0.5 pb at $\sqrt{s} = 500$ GeV, this corresponds to 200 and 2000 charged Higgs bosons at a luminosity $\int \mathcal{L} = 10$ fb^{-1}. If $M_{H^\pm} < m_t + m_b$, the charged Higgs boson will decay mainly into $\tau\nu_\tau$ and $c\bar{s}$ pairs, the $\tau\nu_\tau$ mode dominating for tgβ larger than unity. This results in a surplus of τ final states over e, μ final states in t decays, an apparent breaking of τ *vs.* e, μ universality. For large Higgs masses the dominant decay mode is the top decay $H^+ \to t\bar{b}$. In some part of the parameter space also the decay $H^+ \to W^+h$ is allowed, leading to cascades with heavy τ and b particles in the final state.

5. Supersymmetric Particles

Even though there is no experimental evidence so far for the realization of supersymmetry in nature, this concept has so many attractive features that it may be considered as one of the prime targets of experimental particle research at the present time and in the future [72,87]. Arguments in favor of supersymmetry are deeply rooted in particle physics. Supersymmetry is the most general symmetry of the S matrix in quantum field theory and it may play an important role in a quantum theory of gravity. In relating particles of different spins to each other, fermions and bosons, low–energy supersymmetry, broken at the electroweak scale, stabilizes the masses of fundamental Higgs scalars in the background of very high energy scales associated with grand unification. Besides solving this hierarchy problem, supersymmetry may even be closely related to the physical origin of the Higgs phenomenon itself. In a simple GUT realization with universal scalar masses at the GUT scale, the evolution of one of the Higgs masses squared can become negative and thus lead to spontaneous symmetry breaking if the top mass has a value between about 100 to 200 GeV while all other masses squared of squarks and sleptons remain positive.

The minimal supersymmetric extension of the Standard Model is based on the $\mathcal{SM}$ group $SU(3) \times SU(2) \times U(1)$. The gauginos are the supersymmetric spin–$\frac{1}{2}$ partners of the gauge bosons. The quark and lepton matter particles are associated with scalar supersymmetric particles, squarks and sleptons. To preserve supersymmetry, two Higgs doublets are needed, the supersymmetric partners of which are spin–$\frac{1}{2}$ higgsinos. Supersymmetric partners carry a multiplicative quantum number $R = -1$ ($R = +1$ for ordinary particles) which is conserved in this model. Supersymmetric particles are therefore generated in pairs and the lightest state (LSP) is stable.

In the GUT related formulation of the theory, four parameters specify basically the supersymmetric particle sector. The scalar mass parameter m_0, the $SU(2)$ gaugino mass M, the coupling μ of the Higgs doublets in the superpotential, and $\tan\beta$, the ratio of the vacuum expectation value v_2/v_1. M is related to the gluino mass by $M/m_{\tilde{g}} \approx \alpha_2/\alpha_3 \approx 0.3$. The Higgs sector requires another parameter which in the theoretical literature is in general identified with the mass of the pseudoscalar Higgs boson m_A. Evolving the scalar masses from the GUT scale down to low energies, it turns out that non–colored particles are significantly lighter than colored particles. A range of mass values, compatible with present low–energy high–precision data and the requirement of no unnatural fine–tuning, is shown in the following table [92] (in which no radiative corrections are included). The non–colored Winos and charged Higgsinos mix in general to form the chargino mass eigenstates $\tilde{\chi}_i^\pm (i = 1, 2)$ while the Zinos and neutral Higgsinos form the neutralinos $\tilde{\chi}_i^0 (i = 1, \ldots, 4)$.

Positive support for a spectrum of the $\mathcal{MSSM}$ in the several hundred GeV mass range follows from the measurement of the electroweak mixing angle $\sin^2\vartheta_W$ [93]. The value $\sin^2\vartheta_W = 0.2334 \pm 0.0026$ predicted by the $\mathcal{MSSM}$ is matched surprisingly well by the present experimental value $\sin^2\vartheta_W = 0.2324 \pm 0.0006$.

Parameters	$m_{1/2}$	140	230
	m_0	190	120
	μ_0	190	—120
	m_t	160	100
	$\tan\beta$	21	5
Gauginos	$\tilde{\gamma}$	57	83
	$\tilde{Z}$; $\tilde{W}$	99; 99	120; 112
	$\tilde{g}$	354	559
Sleptons	$\tilde{l}_L$	220	206
	$\tilde{l}_R$	195	146
Squarks	$\tilde{u}_L$, $\tilde{c}_L$; $\tilde{d}_L$, $\tilde{s}_L$	365; 373	511; 517
	$\tilde{u}^c_L$, $\tilde{c}^c_R$	359	495
	$\tilde{d}^c_R$, $\tilde{s}^c_R$, $\tilde{b}_R$	358	491
	$\tilde{t}_L$; $\tilde{b}_L$	325; 335	491; 497
	$\tilde{t}^c_R$	273	452
Higgs & Higgsinos	H^0	91, 264	84, 221
	$H^\pm$; A^0	276; 264	232; 218
	$\widetilde{H}^0$	205, 225	139, 226
	$\widetilde{H}^\pm$	229	227

Table 3: *Estimate of possible mass ranges of supersymmetric particles [92] based on present high-precision data and the requirement of no fine-tuning; masses in GeV.*

5.1 Gauginos and Higgsinos

The two charginos $\tilde{\chi}^+_i$ and the four neutralinos $\tilde{\chi}^0_i$, mixtures of the [non–colored] gauginos and Higgsinos, are expected to be the lightest supersymmetric particles. In the $\mathcal{MSSM}$ with conserved R–parity, the neutralino $\tilde{\chi}^0_1$ with the smallest mass, assumed to be the lightest supersymmetric particle altogether, is stable. The heavier neutralinos and the charginos decay into (possibly virtual) gauge and Higgs bosons plus $\tilde{\chi}^0_1$,

$$\tilde{\chi}^0_i \longrightarrow \tilde{\chi}^0_1 + Z \ ; \ \tilde{\chi}^0_1 + h, H \text{ or } A$$
$$\tilde{\chi}^+_i \longrightarrow \tilde{\chi}^0_1 + W \ ; \ \tilde{\chi}^0_1 + H^+$$

or, if they are heavy enough, into cascades of neutralinos/charginos plus gauge and Higgs bosons. In the same way the heavy charginos decay into $\tilde{\chi}^0_1$ and $W^\pm$ or $H^\pm$ bosons *etc.*

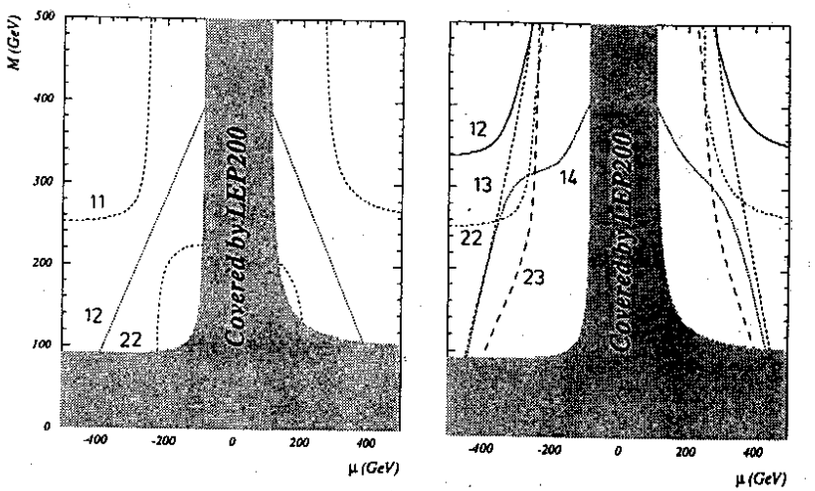

Fig. 29: *Regions of the $[\mu, M]$ plane for $\mathrm{tg}\beta = 4$ where the processes $e^+e^- \to \tilde{\chi}^+_i\tilde{\chi}^-_j$ and $e^+e^- \to \tilde{\chi}^0_i\tilde{\chi}^0_j$ are kinematically accessible at $\sqrt{s} = 500$ GeV. The numbers ij correspond to $\tilde{\chi}_i\tilde{\chi}_j$ combinations; from Ref.[96].*

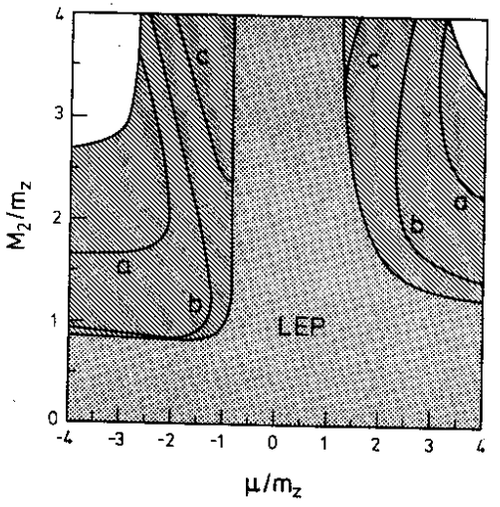

Fig. 30: *Area covered by the search for charginos at 500 GeV, dashed area; the shaded area can be covered by LEP. The boundaries a, b, c correspond to $m_{\tilde{\chi}^+_1} - m_{\tilde{\chi}^0_1} < m_W$, 50, 20 GeV respectively. From Ref.[96].*

Neutralinos and charginos are difficult to observe at hadron colliders, but they are easy to detect at e^+e^- colliders [94,95]. They are produced in pairs

$$e^+e^- \longrightarrow \tilde{\chi}_i^+ + \tilde{\chi}_j^- \qquad [i,j = 1,2]$$
$$e^+e^- \longrightarrow \tilde{\chi}_i^0 + \tilde{\chi}_j^0 \qquad [i,j = 1,..,4]$$

through s–channel γ, Z exchange and t–channel selectron or sneutrino exchange. The kinematically accessible $\mathcal{SUSY}$ parameter range in the $[M, \mu]$ plane for various chargino and neutralino pairs is shown in Fig. 29, for the different chargino and neutralino production processes at a 500 GeV e^+e^- collider [96]. Compared to the region which can be explored by LEP200, a substantial extension can be expected. Since the cross sections are as large as $\mathcal{O}$(100 fb), enough events will be produced to discover these particles and to study their properties, for masses nearly up to the kinematical limit. It has been demonstrated, in fact, by detailed experimental simulations [95] that these particles can be found with masses up to the beam energy if the mass difference $m(\tilde{\chi}) - m(\tilde{\chi}_1^0)$ is not less than about 20 GeV. The region in the $[\mu, M]$ plane that can be covered in the search for charginos is indicated in Fig. 30 by dashed lines while the shaded area will be explored by LEP.

5.2 Sleptons

Left or right–handed scalar particles $\tilde{f}_L$ or $\tilde{f}_R$ correspond to each chiral $\mathcal{SM}$ fermion. Starting with a universal scalar mass m_0^2 at the GUT scale, squark and slepton masses evolve differently down to low energies. Slepton masses are expected to be significantly smaller than squark masses, and they may have values near the scale of the electroweak symmetry breaking.

The superpartners of the right–handed leptons decay into the associated $\mathcal{SM}$ partners and neutralinos/charginos. In major parts of the $\mathcal{SUSY}$ parameter space the dominant decay mode is

$$\tilde{\mu}_R \rightarrow \mu + \tilde{\chi}_1^0$$

For the superpartners of the left–handed sleptons, the decay pattern is slightly more complicated since besides the $\tilde{\chi}_1^0$ channels, decays into leptons and charginos are also possible [96], Fig. 31. In e^+e^- collisions, sleptons are produced in pairs

$$e^+e^- \longrightarrow \tilde{e}_L^+\tilde{e}_L^- \ , \ \tilde{e}_R^+\tilde{e}_R^- \ , \ \tilde{e}_L^+\tilde{e}_R^- \ , \ \tilde{e}_R^+\tilde{e}_L^-$$
$$e^+e^- \longrightarrow \tilde{\nu}_L\bar{\tilde{\nu}}_L$$
$$e^+e^- \longrightarrow \tilde{\mu}_L^+\tilde{\mu}_L^- \ , \ \tilde{\mu}_R^+\tilde{\mu}_R^- \ , \ \tilde{\tau}_L^+\tilde{\tau}_L^- \ , \ \tilde{\tau}_R^+\tilde{\tau}_R^-$$

For charged sleptons, the production proceeds via γ, Z exchange in the s–channel. In the case of selectrons, an additional t–channel neutralino exchange, which is also responsible for the creation of the mixed left and right–handed selectron states, is present. For sneutrinos, the process is mediated by s–channel Z–exchange and in the case of electron–sneutrinos also by t–channel exchange of charginos.

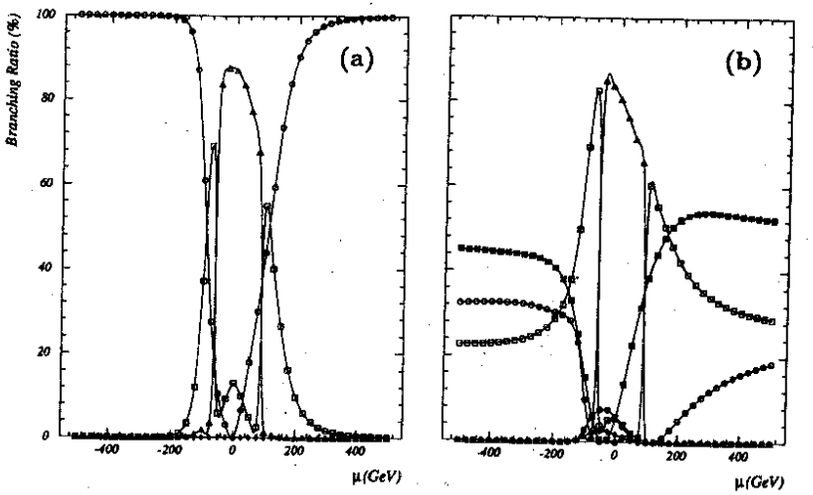

Fig. 31: *Branching ratios for smuon decays into neutralinos and charginos, as a function of μ, for $m(\tilde{\mu}_{L,R}) = 200$ GeV, $M = 150$ GeV and $\tan\beta = 4$; Ref. [97].*

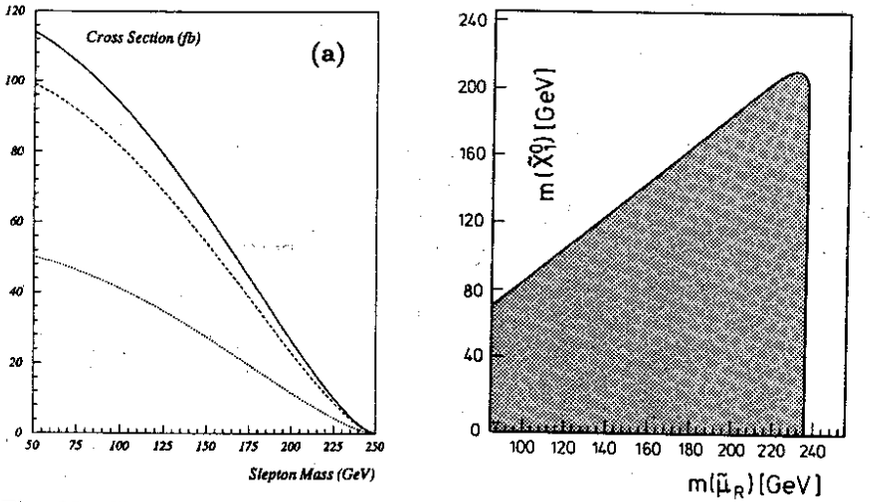

Fig. 32: *The total cross section [in fb] for slepton pair production at $\sqrt{s} = 500$ GeV as a function of the mass, Ref.[97]; and the detection range of $\tilde{\mu}_R$ in the $[m(\tilde{\mu}_R), m(\tilde{\chi}_1^0)]$ plane, Ref.[98].*

The cross sections for the pair production of smuons (stau's) and their neutral partners are shown in Fig. 32. Again, smuons can be discovered up to the kinematical limit if the mass difference $m(\tilde{\mu}) - m(\tilde{\chi}_1^0)$ is not smaller than a few tens of GeV [97]. Similar results have been obtained for selectrons for which the cross sections are larger because of additional contributions from t–channel neutralino exchange [98]. Though not investigated in detail yet, sneutrinos should also be found readily at e^+e^- colliders.

Selectrons can also be produced in association with photinos [$\sim \tilde{\chi}_1^0$] in $e\gamma$ collisions, $e\gamma \to \tilde{e}\tilde{\chi}_1^0$ [99]. For small photino masses, the kinematic range of the selectron mass extends beyond the $e^\pm$ beam energy. However, it seems difficult to exploit this window in practice, since for masses beyond the $e^\pm$ beam energies the rates are quite low.

While colored squarks [and gluinos] can be detected up to masses of $\mathcal{O}(1$ TeV), the slepton search at proton colliders, on the other hand, is very difficult due to the low production rates and the large backgrounds so that e^+e^- linear colliders are unique facilities in this sector.

ACKNOWLEDGEMENTS

Thanks go first of all to A. Djouadi with whom part of the material on extended gauge theories and Higgs particles presented in this report has been elaborated jointly. R. Altmeyer's help in LaTeXing this report is also gratefully acknowledged.

REFERENCES

[1] Proceedings, e^+e^- *Collisions at 500 GeV: The Physics Potential*, Munich–Annecy–Hamburg 1991, P.M. Zerwas ed., DESY 92–123A+B.

[2] Proceedings, *Physics and Experiments with* e^+e^- *Linear Colliders*, Saariselkä 1991, R. Orava, P. Eerola and M. Nordberg eds., World Scientific, Singapore 1992.

[3] T. Barklow, P. Chen and W. Kozanecki in Ref. [1] / SLAC–PUB–5718.

[4] J. Rossbach, Talk at *The 1992 Linear Accelerator Conference*, Ottawa, Internal Report DESY M-93-01.

[5] D. Schaile and P.M. Zerwas, Phys. Rev. D45 (1992) 3262;
update by D. Schaile, private communication.

[6] W. Albrecht et al. [ARGUS Coll.], Phys. Lett. 192B (1987) 245;
M. Artuso et al. [CLEO Coll.], Phys. Rev. Lett. 62 (1989) 2233.

[7] F. Abe et al., [CDF Coll.], Phys. Rev. Lett. 68 (1992) 447.

[8] R. Rolandi, *XXVI Int. Conference on High Energy Physics*, Dallas 1992; Report CERN–PPE-93-175.

[9] E. Reya and P.M. Zerwas [*conv.*], *LHC Workshop Aachen* 1990, G. Jarlskog and D. Rein eds., CERN 90–10.

[10] I. Bigi, Yu. Dokshitzer, V. Khoze, J. Kühn and P.M. Zerwas, Phys. Lett. 181B (1986) 157.

[11] M. Jezabek and J.H. Kühn, Nucl. Phys. B314 (1989) 1.

[12] A. Denner and T. Sack, Nucl. Phys. B358 (1991) 46;

[13] P. Igo–Kemenes and J.H. Kühn [*conv.*] et al., in Ref. [1].

[14] K. Fujii in Ref. [2] / KEK–92–6.

[15] G. Jikia, Phys. Lett. 257B (1991) 196;
V.A. Khoze, W.J. Stirling and L.H. Orr, Nucl. Phys. B378 (1982) 413;
Yu.L. Dokshitzer, V.A. Khoze, L.H. Orr and W.J. Stirling, Durham, Preprint DTP/92/88.

[16] T. Sjöstrand and P.M. Zerwas in Ref. [1] / CERN–TH–6313/91.

[17] See e.g. S. Bertolini, F. Borzumati and A. Masiero, in "*B Decays*", S. Stone ed.,World Scientific, Singapore 1992;
V. Barger, M.S. Berger and R.J.N. Phillips, Wisconsin Preprint MAD/PH/730;
J.L. Hewett, Argonne Preprint ANL–HEP–CP–92–125;
F. Borzumati, Talk at the Hamburg 1993 Workshop on "*Physics with* e^+e^- *Linear Colliders*".

[18] K. Hikasa and M. Kobayashi, Phys. Rev. D36 (1987) 724;
H. Baer, M. Drees, R. Godbole, J.F. Gunion and X. Tata, Phys. Rev. D44 (1991) 725.

[19] H. Fritzsch, Phys. Lett. 224B (1989) 423.

[20] W. Buchmüller and M. Gronau, Phys. Lett. 220B (1989) 641.

[21] J. Jersak, E. Laermann and P.M. Zerwas, Phys. Rev. D25 (1982) 363.

[22] S. Güsken, J.H. Kühn and P.M. Zerwas, Phys. Lett. 155B (1985) 185.

[23] W. Beenakker, S.C. van der Marck and W. Hollik, Nucl. Phys. B365 (1991) 24.

[24] C. Peterson, D. Schlatter, I. Schmitt and P.M. Zerwas, Phys. Rev. D27 (1983) 105.

[25] G.L. Kane, G.A. Ladinsky and C.–P. Yuan, SSCL Report 486 (1991).

[26] C. Schmidt and M.E. Peskin, Talk at the Workshop on "*Physics and Experiments with e^+e^- Linear Colliders*", Saariselkä 1991.

[27] T. Arens and L. Sehgal, Aachen Preprint PITHA 92/18.

[28] W. Bernreuther et al. in Ref.[13].

[29] W. Bernreuther, T. Schröder and T.N. Pham, Phys. Lett. 279B (1992) 389;
W. Bernreuther, O. Nachtmann, P. Overmann and T. Schröder, Nucl. Phys. B388 (1992) 53;
C.-P. Yuan, Phys. Rev. D45 (1992) 439;
D. Atwood and A. Soni, Phys. Rev. D45 (1992) 2405;
A. Soni amd R.M. Xu. Phys. Rev. Lett. 69 (1992) 33;
D. Chang, W.-Y. Keung and I. Phillips, Preprint CERN–TH–6658/92;
G.A. Ladinsky and C.-P. Yuan, Michigan Preprint MSUTH 92/07;
B. Grzadkowski and J.F. Gunion, Phys. Lett. 287B (1992) 237;
R. Cruz, B. Grzadkowski and J.F. Gunion, Phys. Lett. 289B (1992) 440.

[30] A. Djouadi, J. Kalinowski and P.M. Zerwas, Mod. Phys. Lett. A7 (1992) 1765 and Z. Phys. C54 (1992) 255.

[31] K. Hagiwara, H. Murayama and I. Watanabe, Nucl. Phys. B367 (1991) 257.

[32] J.H. Kühn and P.M. Zerwas, Phys. Rep. 167C (1988) 321.

[33] J.H. Kühn, Acta Phys. Austr. Suppl. 24 (1982) 203.

[34] V.S. Fadin and V.A. Khoze, JETP Lett. 46 (1987) 525 and Sov. J. Nucl. Phys. 48 (1988) 309.

[35] M.J. Strassler and M.E. Peskin, Phys. Rev. D43 (1991) 1500.

[36] D. Schaile, Z. Phys. C54 (1992) 387.

[37] H. Inazawa and T. Morii, Phys. Lett. 203B (1988) 279, (E) 207B (1988) 520;
H. Inazawa, T. Morii and S. Tanaka, Z. Phys. C43 (1989) 569.

[38] R.J. Guth and J.H. Kühn, Nucl. Phys. B368 (1992) 38;
V. Fadin and O.I. Yakovlev, Sov. J. Nucl. Phys. 53 (1991) 1053;
W. Beenakker and W. Hollik, Phys. Lett. 269B (1991) 425.

[39] Y. Sumino, K. Fujii, K. Hagiwara, M. Murayama and C.K. Ng, Phys. Rev. D47 (1993) 56;
M. Jezabek, J.H. Kühn and T. Teubner, Z. Phys. C56 (1992) 653 and Karlsruhe Preprint TTP 92–16;
M. Jezabek and T. Teubner, Karlsruhe Preprint TTP 92–38.

[40] R. Miquel, Talk at the Annecy 1993 Workshop on "*Physics with e^+e^- Linear Colliders*", to be published.

[41] S. Bethke, in Ref. [1,2] / HD–PY–92–01.

[42] For a thorough discussion see K. Hagiwara in Ref. [2] / KEK–TH 320.

[43] W. Beenakker, F.A. Berends, A. Denner [*conv.*] et al., in Ref. [1].

[44] F. Boudjema and F.M. Renard [*conv.*] et al., in Ref. [1] / ENSLAPP-A-365-92.

[45] T. Barklow in Ref. [2] / SLAC–PUB–5808.

[46] M.E. Peskin in Ref. [2] / SLAC–PUB–5798.

[47] K. Hikasa in Ref. [2] /KEK-TH 319, and references therein.

[48] O.P. Sushkov, V.V. Flambaum and I.B. Khriplovich, Sov. J. Nucl. Phys. 20 (1975) 537;
W. Alles, Ch. Boyer and A.J. Buras, Nucl. Phys. B119 (1977) 125.

[49] M. Frank, P. Mättig, R. Settles and W. Zeuner in Ref. [1] / MPI–PHE–92–02.

[50] G. Gounaris, J. L. Kneur, J. Layssac, G. Moultaka, F. M. Renard and D. Schildknecht in Ref. [1] / BI–TP–91–40.

[51] A. De Rujula, M. Gavela, P. Hernandez and E. Masso, Nucl. Phys. B384 (1992) 3;
K. Hagiwara and D. Zeppenfeld, Phys. Lett. 283B (1992) 353;
G.J. Gounaris and F.M. Renard, Montpellier Preprint PM/92–31.

[52] G. Kane, J. Vidal and C. P. Yuan, Phys. Rev. D39 (1989) 2617.

[53] S. Ambrosanio and B. Mele in Ref. [1];
G. Couture, R. Lewis and S. Godfrey, Phys. Rev. D45 (1992) 777.

[54] E. Yehudai, Phys. Rev. D44 (1991);
S. Choi and F. Schrempp in Ref. [1] and Phys. Lett. 272B (1991) 149.

[55] G. Bélanger and F. Boudjema in Ref. [1] and Phys. Lett. 288B (1992) 210.

[56] L. Okun, *Leptons and Quarks*, North Holland Pub. Comp. 1982.

[57] See e.g. the report of the BESS group in Ref. [1];
H. Veltman and M. Veltman, Acta Phys. Polon. B22 (1991) 669.

[58] A. Djouadi, D. Schaile and C. Verzegnassi [*conv.*] et al. in Ref. [1].

[59] J. Maalampi and M. Roos, Phys. Rep. C186 (1990) 53;
I. Montvay, Phys. Lett. 205B (1988) 315;
F. Csikor and I. Montvay, Phys. Lett. 231B (1990) 503.

[60] G. Bélanger and S. Godfrey, Phys. Rev. D34 (1986) 1309;
U. Amaldi et al., Phys. Rev. D36 (1987) 1385;
V. Barger et al., Phys. Rev. D37 (1987) 2893;
J. L. Hewett and T. G. Rizzo, Z. Phys. C36 (1987) 209;
G. Costa et al., Nucl. Phys. B297 (1988) 293;
A. Blondel et al., Nucl. Phys. B331 (1990) 293.

[61] A. Djouadi, A. Leike, T. Riemann, D. Schaile and C. Verzegnassi in Ref. [1] and Z. Phys. C56 (1992) 289.

[62] W. Buchmüller in Ref. [2] / DESY 92–011;
V. Barger et al., Phys. Rev. D33 (1986) 1912;
T. G. Rizzo, Phys. Rev. D34 (1986) 1438;
F. del Aguila, E. Laermann and P. M. Zerwas, Nucl. Phys. B297 (1988) 1;
W. Buchmüller and C. Greub, Nucl. Phys. B363 (1991) 345.

[63] P. Langacker and D. London, Phys. Rev. D38 (1988) 244;
W. Buchmüller, C. Greub and H. Kohrs, Nucl. Phys. B370 (1992) 3;
E. Nardi, E. Roulet and D. Tommasini, Nucl. Phys. B386 (1992) 239.

[64] A. Djouadi, M. Spira and P. M. Zerwas in Ref. [1].

[65] W. Buchmüller, C. Greub, P. Mikowski, M. Talbi and G. Tysarcszyk–Niemeyer in Ref. [1];
F. Csikor, A. Djouadi and I. Montvay in Ref. [1].

[66] B.W. Lee, C. Quigg and H.B. Thacker, Phys. Rev. D16 (1977) 1519.

[67] N. Cabibbo, L. Maiani, G. Parisi and R. Petronzio, Nucl. Phys. B158 (1979) 295;
M. Chanowitz, M. Furman and I. Hinchliffe, Phys. Lett. B78 (1978) 285;
R. A. Flores and M. Sher, Phys. Rev. D27 (1983) 1679;
M. Sher, Phys. Rep. 179 (1989) 273.

[68] M. Lindner, Z. Phys. C31 (1986) 295.

[69] H. Georgi, H. Quinn and S. Weinberg, Phys. Rev. Lett. 33 (1974) 451.

[70] J. Ellis, S. Kelley and D. V. Nanopoulos, Phys. Lett. 260B (1991) 131;
U. Amaldi, W. de Boer and H. Fürstenau, Phys. Lett. 260B (1991) 447;
P. Langacker and M. Luo, Phys. Rev. D44 (1991) 817.

[71] B. Schrempp and F. Schrempp, Preprint DESY 92–147.

[72] P. Fayet and S. Ferarra, Phys. Rep. 32 (1977) 249;
H. P. Nilles, Phys. Rep. 110 (1984) 1;
H. Haber and G. L. Kane, Phys. Rep. 117 (1985) 75;
R. Barbieri, Riv. Nuovo Cimento 11 (1988) 1.

[73] Y. Okada, M. Yamaguchi and T. Yanagida, Prog. Theor. Phys. 85 (1991) 1;
H. Haber and R. Hempfling, Phys. Rev. Lett. 66 (1991) 1815;
J. Ellis, G. Ridolfi and F. Zwirner, Phys. Lett. 257B (1991) 83;
R. Barbieri, F. Caravaglios and M. Frigeni, Phys. Lett. 258B (1991) 167;
J. Gunion and A. Turski, Phys. Rev. D39 (1989) 2701 and D40 2333;
M. Berger, Phys. Rev. D41 (1990) 225;
P. H. Chankowski, S. Pokorski and J. Rosiek, Phys. Lett. 274B (1992) 191;
A. Yamada, Phys. Lett. 263B (1991) 233;
J. R. Espinosa and M. Quiros, Phys. Lett. 266B (1991) 389;
M. Drees and M. N. Nojiri, Phys. Rev. D45 (1992) 2482;
P.H. Chankowski, S. Pokorski and J. Rosiek, Phys. Lett. 274B (1992) 191.

[74] J. F. Gunion et al., Phys. Rev. D38 (1988) 3444.

[75] A. Djouadi, J. Kalinowski and P.M. Zerwas, Report DESY 92–168.

[76] For a summary see J. Gunion, H. Haber, G. Kane and S. Dawson, "*The Higgs Hunter's Guide*", Addison–Wesley, Reading 1990.

[77] E. Braaten and J.P. Leveille, Phys. Rev. D22 (1980) 715;
N. Sakai, Phys. Rev. D22 (1980) 2220;
T. Inami and T. Kubota, Nucl. Phys. B179 (1981) 171;
M. Drees and K. Hikasa, Phys. Lett. B240 (1990) 455;
S.G. Gorishny, A. L. Kataev, S. A. Larin and L. R. Surguladze, Mod. Phys. Lett. A5 (1990) 2703.

[78] W.-Y. Keung and W.J. Marciano, Phys. Rev. D30 (1984) 248.

[79] A. Djouadi, M. Spira and P.M. Zerwas, Phys. Lett. B264 (1991) 440.

[80] J. Ellis, M.K. Gaillard and D.V. Nanopoulos, Nucl. Phys. B106 (1976) 292.

[81] J.D. Bjorken, Proceedings of Summer Institute on Particle Physics, SLAC Report 198 (1976);
B.L. Ioffe and V.A. Khoze, Sov. J. Part. Nucl. 9 (1978) 50.

[82] D.R.T. Jones and S.T. Petcov, Phys. Lett. 84B (1979) 440;
R.N. Cahn and S. Dawson, Phys. Lett. 136B (1984) 196;
K. Hikasa, Phys. Lett. 164B (1985) 341;
G. Altarelli, B. Mele and F. Pitolli, Nucl. Phys. B287 (1987) 205.

[83] P. Grosse–Wiesmann, D. Haidt and J. Schreiber in Ref. [1].

[84] A. Djouadi, D. Haidt, B. Kniehl, B. Mele and P.M. Zerwas in Ref. [1].

[85] M. Hildreth, Talk at the Workshop on "*Electroweak Symmetry Breaking at Colliding-Beam Facilities*", UC Santa Cruz 1992.

[86] J. Ellis, J. Gunion, H. Haber, L. Roszkowski and F. Zwirner, Phys. Rev. D39 (1989) 844;
M. Drees, Int. J. Mod. Phys. A4 (1989) 3635 ;
J. F. Gunion, L. Roskowski and H. Haber, Phys. Rev. D38 (1988);
J. R. Espinosa and M. Quiros, Phys. Lett. 279B (1992) 92;
U. Ellwanger and M. R. de Traubenberg, Z. Phys. C53 (1992) 531;
P. Binétruy and C. Savoy, Phys. Lett. 277B (1992) 453;
G. Kane, C. Kolda and J. Wells, Michigan Preprint UM–TH–92–24.

[87] F. Zwirner in Ref.[2] / CERN–TH.6357/91.

[88] A. Djouadi, J. Kalinowski and P. M. Zerwas in Ref. [1].

[89] P. Janot in Ref. [1] and LAL–92–27;
A. Yamada, Mod. Phys. Lett. A7 (1992) 2877;
V. Barger, K. Cheung, R. Phillips and A. Stange, MAD–PH–704 (1992).

[90] J. Gunion and H. Haber, Nucl. Phys. B307 (1988) 445.

[91] P. Eerola and J. Sirkka in Ref. [1] / CERN–PPE–92–076.

[92] G.G Ross and R.G. Roberts, Nucl. Phys. B377 (1992) 571.

[93] J. Ellis, S. Kelley and D. V. Nanopoulos, Phys. Lett. 260B (1991) 131;
U. Amaldi, W. de Boer and H. Fürstenau, Phys. Lett. 260B (1991) 447;
P. Langacker and M. Luo, Phys. Rev. D44 (1991) 817.

[94] A. Bartl and D. Treille [*conv.*] et al. in Ref. [1].

[95] J. F. Grivaz in Ref. [1].

[96] A. Bartl, W. Majerotto and B. Mösslacher in Ref. [1].

[97] R. Becker, Talk at the Annecy 1993 Workshop on "*Physics with e^+e^- Linear Colliders*", to be published.

[98] C. Vander Velde in Ref. [1].

[99] D. Borden, D. Bauer and D. Caldwell, SLAC–PUB–5715 (1992);
H. König and K. Peterson, Phys. Lett. 294BB (1992) 110;
F. Cuypers, G. van Oldenborgh and R. Rückl, Nucl. Phys. B383 (1992) 45.